

AD A078121

AFFDL-TR-79-3001

LEVEL 71

2

INVESTIGATION OF NUMERICAL TECHNIQUES FOR PREDICTING AERODYNAMIC HEATING TO FLIGHT VEHICLES

Arthur B. Lewis, Jr.
Neil J. Sliski

High Speed Aero Performance Branch
Aeromechanics Division

May 1979

TECHNICAL REPORT AFFDL-TR-79-3001

Final Report for the Period May 1975 - December 1977

Approved for Public Release; Distribution Unlimited.

DDC
RECEIVED
DEC 12 1979
RECEIVED
D

AIR FORCE FLIGHT DYNAMICS LABORATORY
AIR FORCE WRIGHT AERONAUTICAL LABORATORIES
AIR FORCE SYSTEMS COMMAND
WRIGHT-PATTERSON AIR FORCE BASE, OHIO 45433

79 12 6 085

DDC FILE COPY

NOTICE

When Government drawings, specifications, or other data are used for any purpose other than in connection with a definitely related Government procurement operation, the United States Government thereby incurs no responsibility nor any obligation whatsoever; and the fact that the government may have formulated, furnished, or in any way supplied the said drawings, specifications, or other data, is not to be regarded by implication or otherwise as in any manner licensing the holder or any other person or corporation, or conveying any rights or permission to manufacture, use, or sell any patented invention that may in any way be related thereto.

This report has been reviewed by the Information Office (OI) and is releasable to the National Technical Information Service (NTIS). At NTIS, it will be available to the general public, including foreign nations.

This technical report has been reviewed and is approved for publication.

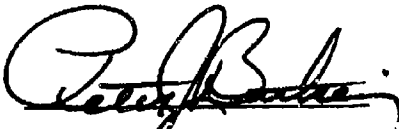


ARTHUR B. LEWIS, JR.
Project Engineer



NEIL J. SLISKI
Project Engineer

FOR THE COMMANDER



PETER J. BUTKEWICZ, Lt Col, USAF
Chief, Aeromechanics Division

"If your address has changed, if you wish to be removed from our mailing list, or if the addressee is no longer employed by your organization please notify AFFDL/FXG, W-PAFB, OH 45433 to help us maintain a current mailing list".

Copies of this report should not be returned unless return is required by security considerations, contractual obligations, or notice on a specific document.

UNCLASSIFIED

SECURITY CLASSIFICATION OF THIS PAGE (When Data Entered)

| REPORT DOCUMENTATION PAGE | | READ INSTRUCTIONS BEFORE COMPLETING FORM |
|--|---|---|
| 1. REPORT NUMBER AFFDL-TR-79-3001 | 2. GOVT ACCESSION NO. | 3. RECIPIENT'S CATALOG NUMBER |
| 4. TITLE (and Subtitle) INVESTIGATION OF NUMERICAL TECHNIQUES FOR PREDICTING AERODYNAMIC HEATING TO FLIGHT VEHICLES | 5. TYPE OF REPORT & PERIOD COVERED Final Report May 1975 to September 1977 | 6. PERFORMING ORG. REPORT NUMBER |
| 7. AUTHOR(s) Arthur B. Lewis, Jr. Neil J. Sliski | 8. CONTRACT OR GRANT NUMBER(s) | |
| 9. PERFORMING ORGANIZATION NAME AND ADDRESS Air Force Flight Dynamics Laboratory High Speed Aero Performance Branch (FX) Wright-Patterson Air Force Base, Ohio 45433 | 10. PROGRAM ELEMENT, PROJECT, TASK AREA & WORK UNIT NUMBERS Project No. 2404 Task No. 240407 Work Unit No. 24040714 | |
| 11. CONTROLLING OFFICE NAME AND ADDRESS Air Force Flight Dynamics Laboratory Aeromechanics Division (FX) Wright-Patterson Air Force Base, Ohio 45433 | 12. REPORT DATE May 1979 | 13. NUMBER OF PAGES 121 |
| 14. MONITORING AGENCY NAME & ADDRESS (if different from Controlling Office) | 15. SECURITY CLASS. (of this report) Unclassified | 15a. DECLASSIFICATION/DOWNGRADING SCHEDULE |
| 16. DISTRIBUTION STATEMENT (of this Report) Approved for public release, distribution unlimited. | | |
| 17. DISTRIBUTION STATEMENT (of the abstract entered in Block 20, if different from Report) | | |
| 18. SUPPLEMENTARY NOTES | | |
| 19. KEY WORDS (Continue on reverse side if necessary and identify by block number) Reentry vehicle, Ogive-cylinder, flow fields, three-dimensional, hypersonic, inviscid flow, boundary layers, aeroheating, streamline tracing, heat transfer | | |
| 20. ABSTRACT (Continue on reverse side if necessary and identify by block number) The development of complex lifting configurations and high speed maneuvering vehicles has emphasized the need for numerical techniques to predict aero- dynamic heating rates as a function of the vehicle trajectory. These numerical programs are not expected to eliminate the requirements for wind tunnel and flight testing, but will be an aid to more efficient use of experimentation time and improve confidence that all potential problem areas on the vehicle have been examined. Three programs, the Hypersonic Arbitrary Body Program, the MINIVER Program, | | |

DD FORM 1473 EDITION OF 1 NOV 65 IS OBSOLETE

UNCLASSIFIED

SECURITY CLASSIFICATION OF THIS PAGE (When Data Entered)

BLOCK 20.

both developed by McDonnell Douglas, and a program developed by Dr. F.R. DeJarnette were examined to determine their usefulness for vehicles with non-circular cross sections and large flat areas as exemplified by lifting reentry vehicles. The MINIVER code was found to be unsuitable for this; the Hypersonic Arbitrary Body Program was applicable to these shapes, but because of program limitations was used for only limited calculations. The DeJarnette program also had limitations in the areas of geometry description and surface pressure calculations. Efforts were made to remove these limitations and several shapes were investigated. In particular it was found that a major problem in both the Arbitrary Body Program and DeJarnette Program was the poor definition of the surface pressure distribution. To improve this, an inviscid code developed by Solomon was obtained and used to calculate an inviscid surface pressure distribution for use with the DeJarnette Program.

The ultimate goal of this effort was to extend the capabilities of one or more of the heating codes; while no effort was made to improve MINIVER or the Hypersonic Arbitrary Body Program, significant improvements were made in the DeJarnette program and Solomon's inviscid flow field program.

FOREWORD

This document presents the results of a study of improvements which could be made in aerodynamic heating programs to make them better able to handle complex high speed vehicles. The study was conducted by the High Speed Aero Performance Branch (FXG), Aeromechanics Division, Air Force Flight Dynamics Laboratory, Wright-Patterson AFB, Ohio. The work concludes an in-house program and was performed under task 240407 "Aeroperformance and Aeroheating Technology", work unit 24040714, "Development of Numerical Techniques for Predicting Aerodynamic Heating to Flight Vehicles" and covers work performed from May 1975 to September 1977.

| | |
|---------------------|-------------------------------------|
| Accession For | |
| NTIS GRA&I | <input checked="" type="checkbox"/> |
| DDC TAB | <input type="checkbox"/> |
| Unannounced | <input type="checkbox"/> |
| Justification | |
| By _____ | |
| Distribution/ _____ | |
| Availability Codes | |
| Dist. | Avail and/or special |
| A | |

DDC
 RECEIVED
 DEC 12 1979
 D

TABLE OF CONTENTS

| SECTION | | PAGE |
|---------|--|------|
| I | INTRODUCTION | 1 |
| II | MARK IV SUPERSONIC-HYPERSONIC ARBITRARY BODY PROGRAM STUDIES | 4 |
| | 1. Program Description | 4 |
| | 2. Blunt Cone Studies with the Mark IV HABP | 5 |
| | 3. X-24C-10D Studies with the Mark IV HABP | 6 |
| | 4. Summary of the Mark IV HABP Studies | 8 |
| III | STUDIES WITH THE DEJARNETTE PROGRAM | 10 |
| | 1. Program Description | 10 |
| | 2. Program Limitations and Sources of Error | 15 |
| | 3. Sample Test Cases | 18 |
| IV | THREE-DIMENSIONAL SHOCK-CAPTURING TECHNIQUE | 27 |
| | 1. Background | 27 |
| | 2. Cone Study | 29 |
| | 3. Ogive-Cylinder Study | 31 |
| | 4. Lifting Body Study | 33 |
| V | HEAT TRANSFER CALCULATIONS USING SCT PRESSURES AND DEJARNETTE PROGRAM | 39 |
| VI | CONCLUSIONS | 42 |
| | REFERENCES | 44 |
| | APPENDIX A: BODY PROGRAM FOR OGIVE-CYLINDER | 49 |
| | APPENDIX B: BODY PROGRAM FOR A GENERAL BODY | 51 |

LIST OF TABLES

| TABLE | | PAGE |
|-------|--|------|
| I | Data for Six Sample Test Cases | 58 |
| II | Comparison of Desired and Smoothed Phi Angles | 59 |
| III | Location of Circumferential Planes for X-24C-10D Cases | 59 |

LIST OF ILLUSTRATIONS

| FIGURE | TITLE | PAGE |
|--------|--|------|
| 1 | X-24C-10D Geometry | 60 |
| 2 | Comparison of Numerical and Experimental Stanton Numbers for the X-24C-10D Side Panel at Model Station 20.52 | 62 |
| 3 | Location of X-24C-10D Streamlines (HABP) | 64 |
| 4 | Plot of Streamline Angle Vs Angle of Attack | 65 |
| 5 | Orthogonal Coordinate System and Body Orientation for the DeJarnette Program | 66 |
| 6 | 25° Cone Pressure Distribution | 67 |
| 7 | 25° Cone Heat-Transfer Distribution | 68 |
| 8 | 0.7:1.0 Elliptical Cone Description | 69 |
| 9 | 0.7:1.0 Elliptical Cone Windward Streamline Heat-Transfer Distribution | 70 |
| 10 | 0.7:1.0 Elliptical Cone Circumferential Heat-Transfer Distribution | 71 |
| 11 | 80° Delta Wing Windward Streamline Heat-Transfer Distribution | 74 |
| 12 | 80° Delta Wing Spanwise Heat-Transfer Distribution | 75 |
| 13 | 10° Cone Windward Streamline Heat-Transfer Distribution | 76 |
| 14 | 10° Cone Spanwise Heat-Transfer Distribution | 77 |
| 15 | Ogive-Cylinder Geometry | 79 |
| 16 | Surface Pressures on Ogive-Cylinder at Model Station 41.7 | 80 |
| 17 | Pitot Pressure Surveys for the Ogive-Cylinder at Model Station 41.7 | 81 |
| 18 | Surface Pressures on the X24C-10D at 2° Angle of Attack | 84 |
| 19 | Surface Pressures on the X24C-10D at 6° Angle of Attack | 87 |

LIST OF ILLUSTRATIONS (Cont'd)

| Figure | Title | Page |
|--------|---|------|
| 20 | X24C-10D Inviscid Shock Location (Longitudinal Plane) | 90 |
| 21 | X24C-10D Inviscid Shock Location (Tangential Plane) | 91 |
| 22 | Longitudinal Slope of the Shock Wave at $\phi = 0^\circ$ | 93 |
| 23 | Angular Dependence of the Longitudinal Slope of the Shock at Three Body Stations | 94 |
| 24 | Tangential Slope of the Bow Shock | 95 |
| 25 | Comparison of Numerical and Experimental Stanton Numbers on the Ogive-Cylinder | 97 |
| 26 | Comparison of Numerical and Experimental Heat Transfer to the Ogive-Cylinder | 101 |
| 27 | Comparison of Numerical and Experimental Pressures and Stanton Numbers on the Ogive-Cylinder as a Function of Angle of Attack | 102 |
| A-1 | Construction Used in the Calculation of the Ogive-Cylinder Geometry | 103 |
| B-1 | Typical Cross Section of the X24C-10D | 104 |
| B-2 | Construction of the Body Radius for a Circular Bottom | 105 |
| B-3 | Construction of the Body Radius for a General Circular Segment | 106 |
| B-4 | Construction Used for a Straight Bottom Segment | 107 |
| B-5 | Construction Used for a General Straight Segment | 108 |

LIST OF SYMBOLS

| | |
|------------|---|
| A_r | See Eq B-1 |
| A_x | See Eq B-1 |
| A_y | See Eq B-1 |
| B_m | See Eq B-24 or Figure B-5 |
| B_n | See Eq B-1 |
| B_s | See Figure B-2 |
| B_x | See Eq B-1 |
| B_y | See Eq B-1 |
| B_0 | Body Radii used in four-point numerical differentiation formula. See Eqs B-31, 32, and 33 |
| B_1 | |
| B_2 | |
| B_3 | |
| c_f | Local coefficient of skin friction |
| C | Radius of the bow shockwave |
| C_n | See Eq B-1 |
| C_x | See Eq B-1 |
| C_y | See Eq B-1 |
| D_{temp} | See Eq A-5 |
| f | In the DeJarnette analysis, body radius measured normal to the longitudinal body axis. See Figure 5 |
| h | Either body scale factor or local heat-transfer coefficient in Btu/ft ² -sec-°R. In Eqs B-31, 32 and 33 the interval between B_1 and B_2 . |
| h_{o2} | Stagnation point heat-transfer coefficient (Btu/ft ² -sec-°R) |
| H | Enthalpy |
| H_w | Wall enthalpy |

| | |
|---------------|---|
| H_o | Total enthalpy |
| K | Curvature of the boundary layer edge streamline in the plane tangent to the body surface. Also used as a dummy variable in Appendix B |
| L | Body length. See Table I |
| L_{og} | Length of blunted ogive. See Figure A-1 |
| M | Mach number |
| P | Pressure |
| q | Local aerodynamic heat-transfer rate |
| r | Length in the radial direction |
| R | Radius |
| R_B | Local body radius. See Figure B-1 |
| R_{Base} | Base radius. See Page 29 |
| R_{cy} | Radius of cylinder. See Figure A-1 |
| R_n | Nose radius. See Page 29 & Table I |
| R_{og} | Radius of ogive. See Figure A-1 |
| R_{temp} | Dummy variable defined by Eq A-5 |
| R_o | Radii of circular arcs. See Figure B-1 |
| R_1 | |
| R_2 | |
| Re_{∞} | Freestream unit Reynolds number (1/ft) |
| S | In the DeJarnette analysis, S is the distance along a streamline measured from the stagnation point |
| S_{og} | Length of ogive. See Figure A-1 |
| St_{∞} | Stanton number based on freestream conditions and freestream total temperature |
| T | Temperature |
| u | In the DeJarnette analysis the velocity in the streamline direction; in the NSWC analysis, the tangential velocity |

| | |
|--------------|--|
| v | Velocity in the radial direction |
| V_{∞} | Freestream velocity |
| w | Velocity in the axial direction |
| W_f | Weighing factor. See Eq (4) |
| X | In the DeJarnette analysis, distance along the longitudinal axis of the body from the nose-tip See Figure 1 for coordinate system description |
| X_a | See Figure B-1 |
| X_n | See Eq B-1 |
| X_{ere} | In the DeJarnette analysis, the distance along the longitudinal axis of the body between the nose-tip and the end of boundary layer transition |
| X_{tre} | In the DeJarnette analysis, the distance along the longitudinal axis of the body between the nose-tip and the beginning of boundary layer transition |
| X_{vn} | In the DeJarnette analysis, the distance along the longitudinal axis of the body measured from the vertical origin |
| X_0 | Coordinates used in the construction of the X24C-10D cross section. See Figure B-1 |
| X_1 | |
| X_2 | |
| Y | In the DeJarnette analysis, the distance normal to the longitudinal axis of the body in the X-Y plane. See Figure 1 for coordinate system description |
| Y_a | See Figure B-1 |
| Y_k | See Eq B-1 |
| Y_0 | Coordinates used in the construction of the X-24C-10D cross section. See Figure B-1 |
| Y_1 | |
| Y_2 | |
| Z | In the DeJarnette analysis, the distance normal to the longitudinal axis of the body in the X-Z plane. See Figure 1 for coordinate system description. In the NSWC analysis the longitudinal coordinate in the cylindrical coordinate system |

| | |
|------------|--|
| Z_{\max} | In the DeJarnette analysis the maximum value of Z for a particular cross section |
| α | Angle of attack. See Figure 5. Also in the NSWC geometry analysis a body slope at sphere-ogive function. See Figure A-1 |
| γ | Ratio of specific heats. In the NSWC analysis a body angle. See Figure B-3 |
| δ | Boundary layer displacement thickness |
| θ | Angle used in body description. See Figures B-2 and B-4 |
| θ_m | Boundary layer momentum thickness |
| μ | In the DeJarnette analysis the viscosity. In the NSWC analysis a substitution used in the body description. See Eq B-14. |
| ρ | Density |
| σ | A substitution used in the body description See Eq B-15. Also slope of a straight line segment in X-24C-10D cross section. See Figure B-1 |
| ϕ | Circumferential body angle. See Figures 1 and B-1 |
| ϕ_m | Angle used in body description. See Figure B-3 |
| ϕ_s | Angle used in body description. See Figure B-5 |
| ψ | Angle used in body description. See Figures B-2 and B-3 |

Subscripts

| | |
|----------|--|
| AW | Adiabatic wall conditions |
| b | Body |
| cy | Cylinder |
| e | Conditions the inviscid flow at the boundary layer edge |
| o | Total or reservoir conditions, or a given value |
| og | Ogive |
| o_2 | Conditions at the stagnation point |
| W | Conditions at the wall |
| ∞ | Freestream conditions in the undisturbed flowfield upstream of the vehicle |

SECTION I

INTRODUCTION

The development of complex lifting configurations and high speed maneuvering vehicles has emphasized the need for numerical techniques to predict aerodynamic heating rates as a function of the vehicle trajectory. These numerical programs are not expected to eliminate the requirement for wind tunnel and flight testing, but are expected to result in efficient use of test time and improve confidence that all potential problem areas on the vehicle have been examined.

Large-scale numerical programs for the prediction of force and moments are available for complex shapes. One such program, the Supersonic-Hypersonic Arbitrary Body Program (HABP) (Reference 1), also includes routines to trace streamlines and calculate viscous effects including heat transfer rates to the body. An earlier version, the Mark III Hypersonic Arbitrary Body Program (HABP) (Reference 2), contained a simplified skin friction option to calculate viscous effects. The Mark III version of the program has been modified and used extensively at NASA Langley to predict heating rates on shuttle-type vehicles at many points along the reentry trajectory (Reference 3). While the Mark IV HABP still contains the simplified skin friction option, it also has an option to treat viscous effects with an integral boundary layer method. Very little experience has been documented with the integral boundary layer option in the Mark IV HABP.

A second program to predict the aerodynamic heating to shuttle-type vehicles has been developed by DeJarnette in cooperation with NASA Langley

(Reference 4). This program is based on the axisymmetric analog and has been modified to include entropy swallowing, input pressure distributions and a more general body geometry. Although basically an ideal gas program, it does offer an equilibrium air option.

A third program, named MINIVER, was developed by the McDonnell Douglas Company (Reference 5). MINIVER is a smaller version of a more complex heating program and differs significantly from the HABP and DeJarnette programs in that it is a point-calculation program. In such a program, the local pressure is found and a running length from the stagnation point to the point in question is approximated in some manner; a flat plate analogy is used in the present code. One major advantage of this code is that the heat transfer rates can be obtained at a set of points which are input by the user. This advantage is off-set by the need to know the origin and length of the streamline crossing that point.

The HABP was used to calculate heat transfer rates on the X-24C-10D configuration; the DeJarnette code was used with the ogive-cylinder. The MINIVER code was not used, except to demonstrate proper operation on the local computer system, due to the lack of streamline information for complex vehicles. The MINIVER program may prove to be very useful in the future for use on wings, fins and possibly the side panels of an X-24C type configuration.

During this study it became apparent that an improvement in program accuracy could be obtained with a better inviscid surface pressure calculation. At about the same time, the Three-Dimensional Shock-Capturing Technique (SCT) based on work by Kutler and developed by Solomon

(Reference 6) became available. This code proved to be fast and reliable, but lacked an adequate geometry routine for the type of bodies of interest. New geometry routines were developed for the SCT and one case was run using the SCT pressure distribution in the DeJarnette heat transfer program.

During the period these numerical methods were being studied, experimental investigations of some configurations of interest were also being conducted at the Arnold Engineering Development Center by AFFDL. The experimental results were intended for comparison with the numerical results. There is never enough experimental data to really satisfy the comparison requirements of the numerical program; in this case, hindsight indicates more pitot pressure surveys, flow angularity studies and better knowledge of the location of both bow and imbedded shocks would have increased confidence in the numerical technique. A follow-on study will address these problems.

Some of the comparisons are adequately covered in other reports and are only referenced here. The purpose of this report is not to detail all of the results developed by this study, but to indicate the present capabilities of the various numerical techniques and indicate areas in which improvements have been or can be made.

The ultimate goal of this effort was to extend the aero heating prediction capabilities of HABP, the DeJarnette code and the inviscid pressure methods to practical bodies. No improvements were possible with the HABP at this time, but significant improvements were made in the DeJarnette program and the inviscid pressure program.

SECTION II

MARK IV SUPERSONIC-HYPERSONIC ARBITRARY BODY PROGRAM STUDIES

1. PROGRAM DESCRIPTION

The Mark IV HABP was developed by Gentry et al. at the Douglas Aircraft Division of the McDonnell Douglas Corporation under contract to the AF Flight Dynamics Laboratory (Reference 1). Earlier versions of the program were developed with support from Douglas Independent Research and Development funds and Air Force contracts (Reference 2). One goal of the program was to supply design engineers with a flexible engineering tool to provide realistic modeling of the flow about complex aerodynamic shapes. While designed primarily to supply first-order aerodynamic data, the program also includes viscous two-dimensional boundary layer calculations. A wide choice of empirical pressure techniques is available for selection by the user; the resultant pressure distribution is used to obtain the inviscid flow field.

The Mark III HABP contains a simplified skin friction option. The Mark IV HABP, in addition to this skin friction option, contains an integral boundary layer technique based on McNally (Reference 7) which was the option used in this study. To use this option, the program is first required to locate the streamline trajectory along the body surface. The calculation, although carried out on a three-dimensional body, is basically a two-dimensional calculation; that is, cross-flow pressure gradients are neglected. The integral boundary layer method uses Cohen and Reshotko's (Reference 40) method for laminar boundary layer calculations, Sasman and Cresci's (Reference 41) method for turbulent boundary layers and the Schlichting-Wrigh-Granville method for predicting the transition point. The present version does not calculate transitional flow; it switches from laminar to turbulent at the transition point.

The Mark IV HABP obtains its geometry flexibility by allowing the user to construct the body as a family of flat elements. Surface elements are combined to form a section of the vehicle, sections are combined into panels, and panels combined into vehicle components. Regardless of what type of geometry input is used, eventually a set of plane, quadrilateral surface elements are generated and their centroids stored. All surface data are calculated based on these centroids. Each streamline calculation begins at the centroid of a surface element and continues to the centroid of the last element of the panel on which it started. There is no calculation of streamlines from one panel to another.

2. BLUNT CONE STUDIES WITH THE MARK IV HABP

The first cases attempted with the Mark IV HABP were blunted cones. In addition to the obvious analytic advantages of studying a cone first, the cone is a particularly easy body to input into the program. The two cones selected were a 10° cone with a 1-inch nose radius at $M_\infty = 7.98$ and a 25° cone with a 0.5-inch nose radius at $M_\infty = 7.95$. Successful solutions were not obtained for either cone at any angle of attack. Several factors contributed to problems with the cone solutions, but the most important problem was the inability of the program to obtain a successful surface fit of the pressure distribution.

To understand this failure, it is necessary to know that the pressure at each element centroid is fit with a surface spline. While the cone is an easy analytic problem, the resultant pressure distribution is not simple if the entire cone is to be treated as one panel. Successful fits could be obtained by dividing the cone into several panels and fitting the pressure

on each panel individually, but, of course, if this were done, the streamlines could not be traced along the cone. Further efforts with a cone were discontinued. In closing this portion of the work, it should be noted the Mark IV HABP was never intended to perform this type of calculation.

3. X-24C-10D STUDIES WITH THE MARK IV HABP

When experimental pressure data became available from the X-24C-10D this configuration was programmed into the Mark IV HABP. Figure 1a* shows the model configuration; Figure 1b the simplified side view used in the HABP. Initial efforts resulted in problems similar to those encountered with the cone. The problem was resolved by making the flat bottom surface on the vehicle one panel and the upper surface a second panel. Not all details were included in the numerical model. Because the surface pressures in the HABP are predicted using empirical methods (i.e. the surface pressure is predicted as a function of the turning angle and freestream mach number), the bottom panel was a constant pressure surface and did not even approximate proper streamline locations or viscous effects. The HABP does permit the input of surface pressures at the centroids of each panel, but adequate surface pressures were not available. If the surface pressures were known, empirical methods, for example DeJarnette, are available for calculating the viscous effects on such a surface with the same accuracy of the HABP.

However, an extensive series of computer runs was made on the side of the X-24C-10D. Experimental Stanton Numbers were available (Reference 8) at station 20.52 on the model. In the HABP, streamline calculations must

*Figures and tables are located at end of report, pages 58 through 108.

start at the centroid of an element. As none of the streamlines starting at centroids near the nose remained on the model side at this station, it was necessary to start streamlines at centroids on the leading edge of the model. Different centroids were selected for each angle of attack calculated, moving further back with increasing angle. In general, good agreement was obtained with experimental results as shown in Figure 2. There were however, several problems which should be noted by future users. The Mark IV HABP locates the streamlines by an integration of the Euler equations. These steps may be quite small (relative to the length of the panel) particularly in regions of steep pressure gradients. As storage locations are available for only 100 streamline points, the user may choose to save only every n^{th} point. This resulted in the saving of only every 5^{th} point on many streamlines and occasionally only every 10^{th} point on long streamlines passing through regions of steep pressure gradients. This restriction resulted in warnings from the integral boundary layer program that the pressure change between data points exceeded the values allowed by the tables used in the program. Although there was no incidence of program failure due to this, and the resultant heat transfer rates compare favorably with experimental data, such warning can not be ignored and all such solutions must be treated with suspicion.

Three changes might be made to correct this problem. New tables should be included in the integral boundary layer routine to permit steeper pressure gradients, the code could be changed to permit an input value to change the points saved in a particular region of the body, or more storage could be set aside to store streamline data. While the additional storage would appear to be the easiest solution, the elaborate mass storage file

built by the Mark IV HABP discouraged any attempt at restructuring. While the other two are possible modifications to the code, a decision was made not to change the program at this time.

Because the empirically predicted pressure is constant on a flat surface, the streamlines calculated by the Mark IV HABP are parallel straight lines (Figure 3) on the flat side of the vehicle. Some curvature can be seen on the crown. To determine how representative these streamlines really are, approximate flow angularity was obtained from oil flow experiments and compared with the numerical results. As seen in Figure 4, the results are acceptable. A single streamline angle from Powers' method of characteristics program (Reference 31) is also shown.

4. SUMMARY OF THE MARK IV HABP STUDIES

The Mark IV HABP was found to be a reasonably accurate program for the prediction of viscous effects on general shapes. If the program is to be used on a wide variety of shapes, tables used in the integral boundary layer routine should be extended to handle a wider range of pressure gradients, the number of streamline points saved should be increased or the number of points saved should be a function of pressure gradient. The major advantage of this program is its very flexible geometry package; this advantage is off-set, however, by the current restriction on saving streamline data and the inability to continue streamlines across panel boundaries.

It is important to realize the selection of panels on the vehicle may be governed by the behavior of the surface spline used in the program. For a surface spline to result in acceptable fits the region fit must be

normalized in a manner consistent with the behavior of the flow. Thus, for example, on the X-24C-10D the side and bottom of the vehicle had to be handled as separate panels with separate surface splines to obtain satisfactory results.

Streamlines do not now cross panel boundaries because data must be extrapolated from the centroid of the last element in the panel to the panel edge, then as the first centroid in the new panel in general does not fall on a continuation of the streamline, the data must be interpolated in the circumferential direction and, finally, matched with the data saved on the next set of centroids. While the problem is not insurmountable, the risk of error is great.

Finally, a flat windward surface will have to be supplied with a pressure distribution from some other source. It is recommended the Mark IV HABP be retained to estimate heating on strakes and fins where other codes have proven unsuccessful.

SECTION III

STUDIES WITH THE DEJARNETTE PROGRAM

1. PROGRAM DESCRIPTION

The aerodynamic heating program developed by Fred R. DeJarnette (References 4 and 9 through 14) and subsequently modified by the AFFDL (Reference 44) is described in this section. The program applies the small cross-flow approximation to three-dimensional boundary-layer equations and utilizes the axisymmetric analog technique to predict laminar, transitional and turbulent heating rates to arbitrary, blunt nosed, three dimensional bodies at angle of attack in supersonic and hypersonic flow.

Body geometry is generated by a bivariate, cubic spline fit of the surface coordinates. For simple geometries the coordinates are calculated by the program. For complex shapes the body coordinates can be read into the program. Inviscid streamlines are calculated by either the method of steepest descent or Euler's momentum equation. The surface pressure is either calculated by the modified Newtonian technique or read into the program from an external source. Laminar heating rates are based on the locally similar boundary layer analysis of Cohen (Reference 15) and Beckwith and Cohen (Reference 16). Turbulent heating rates are predicted by applying the von Karman form of the Reynolds analogy to the semi-empirical correlation of Spalding and Chi (Reference 17) using the momentum thickness calculated by the integral method of Reshotko and Tucker (Reference 18). The beginning and end of boundary layer transition is specified either by geometric location, momentum thickness Reynolds number or integrated, local unit Reynolds number along a streamline.

Transitional heating rates are a weighted average of local laminar and turbulent values following the approach of Dhawan and Narasimha (Reference 19). Entropy layer swallowing effects are accounted for by a modified form of Maslen's method (Reference 20) for inviscid, axisymmetric flows. Either perfect or equilibrium air properties may be used.

Better understanding of the program can be achieved if its various functions are described separately.

a. Body Description - Incorporated in the program is a bivariate, cubic spline fit of the body radius as a function of the longitudinal and circumferential coordinates X and ϕ . Body coordinates are either calculated by or read into the program.

A special provision for handling body data originally intended for the Supersonic-Hypersonic Arbitrary Body Program (Reference 1) is also included.

b. Inviscid Flow Field Calculations

1. Surface Pressure - Surface pressures are either computed by modified Newtonian theory or read into the program. For 80-degree swept delta wing configurations, a pressure correlation formula from Reference 21 is also available. Pressures around the body circumference at several axial stations are used to generate a bivariate cubic spline function for the pressure distribution at any point on the body. The technique is similar to that used to describe the body geometry. In "shadowed" regions, $P = P_\infty$ is used.

2. Boundary-Layer-Edge Gas Properties - The flow field calculation is based on the entropy and pressure at the boundary layer edge. The entropy can be determined by either of two different techniques. The first method simply assumes that the boundary-layer-edge entropy is equal to the entropy just downstream of the normal shockwave. This assumption is

invalidated once the boundary layer has swallowed a significant portion of the entropy layer. The second method incorporates an entropy layer swallowing technique (described in detail in References 4 and 14) to determine the local entropy. The usual thin boundary layer assumption sets the pressure at the boundary layer edge equal to the surface pressure.

For ideal gases surface pressure and entropy are sufficient to determine all the other gas properties using isentropic flow relations. For equilibrium air properties the correlation formulas of Cohen (Reference 22) are used.

3. Streamline and Scale Factor Calculations - In order to apply the axisymmetric analog technique, described in Section III-C, to three-dimensional boundary-layer equations, it is necessary to compute the effective body radius (scale factor). This requires a knowledge of streamline direction and curvature. Two different streamline techniques are available in the program. The first one depends on the body orientation and geometry only and is referred to as the method of steepest descent in Reference 23 (and throughout the remainder of this report) and Newtonian streamlines in Reference 24. The other streamline method is based on Euler's equation written in streamline coordinates. This latter method uses both body geometry and pressure distribution to determine the streamline geometry (Reference 11 and 13).

c. Viscous Boundary-Layer Calculations - The general, three-dimensional boundary-layer equations are reduced to equivalent axisymmetric equations by using the small-cross-flow assumption of Vaglio-Laurin (Reference 25). The constraint necessary to assure that the three-dimensional equations

can be reduced to axisymmetric form in that

$$k \left[\left(\frac{u}{u_e} \right)^2 - \frac{\rho_e}{\rho} \right] \rightarrow 0 \quad (1)$$

where k is the curvature of the boundary layer edge streamline in the plane tangent to the body surface. The condition $\left[(u/u_e)^2 - \rho_e/\rho \right] \rightarrow 0$ is closely approximated when the wall is highly cooled and $u_e^2/(H_0 - H_w) \ll 1$. Experience has shown that this last constraint may be overly restrictive.

The axisymmetric equations that are obtained can be solved by any method applicable to a body of revolution at zero incidence. The distance along the streamline is interpreted as the distance along an equivalent axisymmetric body. The scale factor for the surface coordinate normal to the streamline is interpreted as the radius of an equivalent axisymmetric body at zero incidence. This method is commonly referred to as the axisymmetric analog technique.

d. Heat Transfer Rate Predictions

1. Stagnation Region Heat Transfer Rate - Using the small cross flow approximation, the heating rate along an inviscid surface streamline is obtained from Lees' heat transfer equation for a cold wall (Reference 26) on an equivalent, axisymmetric body at zero incidence by replacing the body radius by the scale factor and the distance along the body surface by the distance along the streamline. The limit of this equation is taken as the stagnation point is approached. Finally, the resulting equation is modified so that it produces results compatible with experimental results in the limit of two-dimensional and axisymmetric stagnation points (Reference 11).

2. Surface Heating Rates

(1) Laminar Boundary Layers

Laminar heating rate ratios are determined by applying the axisymmetric analog to solutions of the locally similar boundary layer equations for relatively cold walls given by Beckwith and Cohen in Reference 16.

(2) Turbulent Boundary Layers

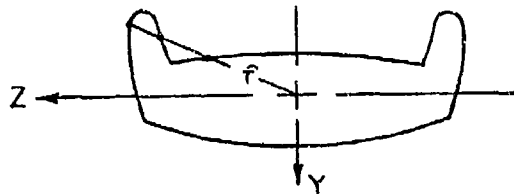
The axisymmetric analog is applied to a modified form of the integral method of Reshotko and Tucker (Reference 18) to obtain the turbulent momentum thickness. Then the momentum thickness is used to calculate the local skin friction coefficient from the semi-empirical correlation of Spalding and Chi (Reference 17). Finally, skin friction coefficients are converted to turbulent heating rates through the von Karman form of Reynolds analogy.

(3) Transition Region Heating Rates

The transition region heating rates are based on a weighted average of the local laminar and turbulent heating rates. The method (based on the results of Dhawan and Narasimha in Reference 19) uses a Gaussian distribution for the weighting function which is based on the geometric locations of the beginning and end of transition. The analysis does not predict transition onset or extent. Instead, the beginning and end of transition is specified in the input data by one of three options which are: geometric location, value of the local momentum thickness Reynolds number, or value of the integrated local unit Reynolds number.

2. PROGRAM LIMITATIONS AND SOURCES OF ERROR

Since the body geometry is approximated by a bivariate cubic spline fit, there exist certain restrictions that pertain to the input geometry. One restriction is that the body radius must be single valued. This means that a cross section such as shown in the sketch below cannot be computed because the body radius, f , is multi-valued on certain portions of the body.



In addition, the program is restricted to relatively smooth aerodynamic configurations such as shown in Figure 5. In general, only blunt nose configurations can be computed although there is an input option that sets the inviscid streamline pressure equal to the input surface pressure. With this option and the Euler streamline option, reasonably good results can be obtained for sharp nose bodies.

In theory, the bivariate cubic spline function can be used to describe very general body shapes. However, when a cylindrical coordinate system is used, as in the present program, computations are inaccurate on planar type bodies. This is due to the non-linearity of the second derivative of the square of the body radius with respect to the circumferential angle. The result is that, on the flat section, oscillations in the body surface slope occur that induce errors in the streamline solution.

When reading body geometry data into the program, the axial stations are not required to be equally spaced. However, the spline fit in the axial direction is generally more accurate when the axial stations are spaced approximately equal. Although the circumferential body points do not have

to be equally spaced, it is required that the first body point be on the windward streamline ($\phi = 0^\circ$) followed by other points located at monotonically increasing values of ϕ until the final body point is reached on the leeward streamline ($\phi = 180^\circ$).

Computer storage restrictions limit the number of body points that can be input to the program. Only a maximum of 20 cross sections, each having a maximum of 20 circumferential body points, is allowed. In addition, no restart capability exists. Therefore, the size and shape of aerodynamic configurations that can be considered is somewhat restricted.

The inviscid flow field properties at the edge of the boundary layer are computed from the local entropy and pressure. Therefore, the flow-field accuracy is dependent on the accuracy of the surface pressure distribution and the validity of the entropy swallowing technique. Pressure data can either be read into the program or be calculated from modified Newtonian theory. In general, pressures on blunt slender bodies are not adequately described by the Newtonian assumption nor are pressures over locally flat portions of a three-dimensional body. In addition, leeside pressures are usually quite different from those obtained from a Newtonian calculation. If accurate pressure distributions are available, the calculated inviscid flow field characteristics and streamline orientation should closely approximate the physical situation.

Another source of error can develop whenever a non-monotonic pressure distribution (in either the X or ϕ coordinate directions) is used. It has been observed that whenever a non-monotonic pressure distribution is used,

the scale factor behaves strangely downstream of the pressure distribution inflection point.

Streamlines computed from the method of steepest descent are based solely on a geometric concept and cannot be expected to be physically representative when overriding aerodynamic forces are present. Since the steepest descent streamline calculation is independent of surface pressures, its accuracy for axisymmetric bodies at zero degrees angle of attack cannot be degraded by an inaccurate pressure distribution. However, heating rates along these streamlines on axisymmetric bodies at zero degrees angle of attack can be in error due to inaccurate inviscid flow conditions calculated from an inaccurate pressure distribution.

Streamlines determined from Euler's equation are dependent on the pressure distribution as well as the body geometry. Consequently, any error in the pressure field will affect streamline direction and curvature. Because the equivalent body radius (scale factor) is dependent solely on the position and curvature of the streamline, an accurate streamline pattern is essential for the success of the program.

The accuracy of the axisymmetric analog method depends on the degree to which the governing assumptions of small cross flow and/or cool wall temperatures are satisfied.

While the program accounts for the effect of an adverse surface-pressure gradient, no provision is made to account for the effect of a wall temperature gradient for either laminar or turbulent boundary layers.

The turbulent boundary layer analysis is expressed in terms of the boundary layer form factor and momentum thickness. Development of the analysis along these lines is due solely to the need for obtaining a reasonably compact engineering technique for solving the boundary layer equations.

3. SAMPLE TEST CASES

In this section experimental heat transfer data are compared with theoretical predictions for four different test models. Program accuracy and some of its limitations are noted where appropriate. A summary of each body geometry, its attitude and the corresponding flow conditions is given in Table I.

1. 25° Half-Angle Cone at $\alpha = 0^\circ$

This is a very simple case intended to demonstrate the accuracy of the program for the zero cross-flow situation. It has a spherically blunted nose with a 1/2-inch nose radius. Freestream Mach number was 7.95 and the freestream unit Reynolds number was 3.96×10^6 per foot. Detailed freestream flow conditions are given in Table I. The experimental heat transfer coefficients are based on a recovery factor of 0.85, where the recovery factor is defined as $(T_{aw} - T_e)/(T_o - T_e)$. For the calculation of local flow conditions, an isentropic expansion from the model stagnation point to the local experimental pressure level was assumed. Test data were reported by Bushnell et al. in Reference 27. Both analytical and experimental heat-transfer coefficients were ratioed to the stagnation point value given in Reference 27 which is $h_{o2} = 34 \times 10^{-3}$ (Btu/ft²-sec-°R).

In Figure 6, a comparison of experimental surface pressures ratioed to stagnation point pressure is made with a spline fit of the modified

Newtonian pressure distribution. Clearly, the modified Newtonian result is in considerable error as is to be expected. Also shown in Figure 6 are pressures determined analytically by the method described in Reference 28. The spline fit of both pressure distributions produces a pressure dip near $S/R = 1.5$. This is due to limitations inherent in the bivariate cubic spline fitting technique.

Using the fitted Newtonian pressure distribution, the calculated heating rates are essentially identical for streamlines calculated either by the steepest descent method or by the Euler equation method. Results of both methods are shown as the broken line in Figure 7. Because the Newtonian pressure approximation does not account for the over expansion region just downstream of the sphere-cone junction, the predicted heating rates between $S/R = 1.2$ and $S/R = 7.0$ are noticeably higher than the data. Using the spline fit of the pressures from Reference 28, somewhat different heating rates, shown in Figure 7 as the dashed line, result. The accuracy of the predicted heat transfer distribution is contingent on the accuracy of the surface pressure distribution. Consequently, use of the more accurate pressure field results in improved agreement between the experimental and calculated heating rate distribution as can be seen in Figure 7. However, results given by the present program differ somewhat from the results of Bushnell, et al. in Reference 27. This is due to the inaccuracy of the spline fit of the pressure distribution between $S/R = 1.0$ and $S/R = 2.8$, shown in Figure 6 as a dotted line.

2. 0.7:1.0 Elliptic Cone

The second test case considered is that of a blunt, elliptical cone having a semi-minor to semi-major axis ratio of 0.7. Data for this case were taken from experimental results reported by Hillsamer and Rhudy in Reference 29. A description of the geometric properties of the test vehicle is given in Figure 8. Nominal freestream flow conditions are given in Table I. Experimental and analytical heat-transfer coefficients, h , are based on total temperature,

$$h = \dot{q}_w / (T_o - T_w). \quad (2)$$

Nominal values are $T_o = 1910$ ($^{\circ}\text{R}$) and $T_w = 470$ ($^{\circ}\text{R}$). Local flow field calculations utilize the entropy layer swallowing process in conjunction with a modified Newtonian pressure distribution.

Heating rates on the windward streamline ($\phi = 0^{\circ}$) are shown in Figure 9 for $\alpha = 0^{\circ}$ and $\alpha = 30^{\circ}$ angle of attack. At $\alpha = 0^{\circ}$ it can be seen that neither the steepest descent nor the Euler streamline computations give very accurate heating rates when compared with experimental data. As in the 25° cone case, the inaccuracy is due primarily to limitations of the modified Newtonian pressure distribution at small inclination angles. However, the steepest descent method provides more accurate heating rates than the Euler equation method. This is because the effect of an inaccurate pressure field is compounded when using the Euler equation to determine streamline orientation and body scale factor. In the heat-transfer calculation not only are the inviscid flow values in error, but so is the integration of the Euler equation which is dependent on the inaccurate pressure distribution. By comparison, inaccuracy in the steepest descent method (for this case at $\phi = 0^{\circ}$) is due entirely to

erroneous flow field values calculated from the spline fit of the modified Newtonian pressure distribution.

The circumferential calculations at $\alpha = 0^\circ$ are shown in Figure 10. It can be seen that the heating distribution approaches the experimental values near $\phi = 90^\circ$ where the body surface is more steeply inclined to the freestream flow direction. Agreement between data and the steepest descent theory is seen to improve with increasing distance downstream of the stagnation point. At station 14.5 the agreement is seen to be quite good especially near $\phi = 90^\circ$. As for heating distributions calculated from the Euler equation, the agreement with data is uniformly poor.

At $\alpha = 30^\circ$ angle of attack, both heating rate prediction techniques give values that agree quite well with experiment. In Figure 9 the agreement between data and the method of steepest descent is seen to be slightly better than the method based on Euler's equation. The same results can also be seen in Figure 10. The agreement between data and theory on the leeside of the model is seen to be relatively poor as would be expected.

3. Blunt, 80° Delta Wing

This test case is a blunt, 80° delta wing at $\alpha = 40^\circ$ angle of attack, $M_\infty = 7.97$ and unit freestream Reynolds number $Re_\infty = 1.94 \times 10^6$ per foot (Reference 21). Detailed freestream flow conditions are given in Table I. The model is 29.4 inches long and has a $1/8$ inch nose radius. This test case demonstrates the deleterious effect that a flat surface has on heat-transfer calculations.

The experimental heat-transfer coefficients shown in Figures 11 and 12 were determined from the semi-infinite flat plate heat conduction equation.

Since all heat transfer data were taken at $X/R > 40$, it was assumed that the blunt nose induced entropy layer had been completely swallowed by the boundary layer upstream of the $S/R = 40$ location. Consequently, experimental heat-transfer coefficients were based on local flow conditions calculated from experimental surface pressures in conjunction with oblique shockwave theory.

Numerical heat-transfer calculations were made using the entropy layer swallowing analysis and the experimentally determined pressure distribution. All calculations used a perfect gas with $\gamma = 1.4$.

In Figure 11 it can be seen that on the windward streamline at $\alpha = 40^\circ$ there is fairly good agreement between analysis and experiment. However, in Figure 12 the agreement between theory and data at spanwise locations is quite poor in some instances. The worst agreement occurs between $Z/Z_{\max} = 0.12$ and $Z/Z_{\max} = 0.4$ at $X_{vn} = 12$. In this region the body radius and its first and second derivatives with respect to X and ϕ were consistently more in error than in nearby regions where the agreement between fitted and exact results was better. Therefore, it is suspected that the poor agreement between data and the calculated results is due to the inaccurate surface fit. The primary drawback regarding cubic splines is that the second derivative of the function being fitted must vary linearly with respect to the independent variable. When describing a flat section using a cylindrical coordinate system, the second derivative of the square of the body radius varies non-linearly with ϕ , the circumferential angle. Thus, the program is limited to non-planar type bodies. On the flat section, oscillations in the body surface slope occur that induce errors in the streamline solution for the scale factor.

4. 10° Half-Angle Cone

The last test case is a blunt, 10° half-angle cone at $\alpha = 50^\circ$ angle of attack, $M_\infty = 8.0$ and unit freestream Reynolds number, Re_∞ of 3.7×10^6 per foot (Reference 30). Detailed freestream flow conditions are given in Table I. The nose is a 1.0-inch-radius sphere, and the model is 25.24 inches long.

This test case was chosen to demonstrate the transition region heating rate prediction capabilities of the program for a simple body shape. The experimental heat-transfer coefficients shown in Figures 13 and 14 (Reference 30) were determined from the semi-infinite flat-plate heat conduction equation with the simplifying assumption that $T_{aw} = T_o$. Theoretical results were adjusted for an adiabatic wall temperature equal to the total temperature. Theoretical stagnation-point heating rates were set equal to experimental results so that a comparison with data could be made. A perfect gas with $\gamma = 1.4$ was used for both the analytical and experimental calculations.

In the program transitional heat-transfer rates are calculated as a weighted average of the local laminar and turbulent heating rates. The transition region heating rate is defined as

$$\dot{q}_w = \dot{q}_{w_{lam}} + W_f (\dot{q}_{w_{turb}} - \dot{q}_{w_{lam}}). \quad (3)$$

Calculations for the weighting factor, W_f , are based on the flat-plate, low-speed, semi-empirical analysis of Dhawan and Narasimha (Reference 19).

This analysis uses a Gaussian distribution for W_f , which is given by

$$W_f = 1 - 1/\exp \left[9.257 \left(\frac{X - X_{tri}}{X_{tre} - X_{tri}} \right)^2 \right] \quad (4)$$

DeJarnette (Reference 11) assumes that this distribution can be applied directly to compressible flows having streamline divergence. This is tantamount to assuming that the inviscid flow conditions at the boundary layer edge do not vary from the beginning to end of transition, and that the streamline divergence is constant over the transition region.

DeJarnette further assumes that the distribution for W_f can also be accurately determined if either local momentum thickness Reynolds number, $\rho_e u_e \theta_m / \mu_e$, or local integrated unit Reynolds number, $\int_0^s \frac{\rho_e u_e}{\mu_e} ds$, are substituted for the physical X-locations in Equation (4). For such a substitution to be valid, both momentum thickness and integrated unit Reynolds number must vary linearly with X.

All three program options for predicting transition region heating rates were used for this case. Results using the geometric location option and the integrated local unit Reynolds number option were essentially identical and are shown in Figure 13. Reasonably good agreement between theory and experiment can be seen. Results from the momentum thickness Reynolds number option, also shown in Figure 13, differed considerably from data and results from the other two options. The reason for this is that program calculations for the local momentum thickness Reynolds number showed a very non-linear variation with X. By comparison, the local integrated unit Reynolds number varied (in this case at least) linearly with X. Examination of the momentum integral equation for high-speed flow over axisymmetric bodies, Equation (5) below,

$$\frac{d\theta_m}{ds} + \left(2 + \frac{\delta^*}{\theta_m} - M_e^2 \right) \frac{\theta_m}{u_e} \frac{du_e}{ds} + \frac{\theta_m}{f} \frac{df}{ds} = \frac{c_f}{2} \quad (5)$$

reveals that momentum thickness, θ_m , is a complicated function of flow conditions and body geometry. Even for the simple case of laminar flow over a flat plate, where

$$\frac{d\theta_m}{dx} \sim 1/\sqrt{X}, \quad (6)$$

the momentum thickness does not vary linearly with X . Within the transition region the relation between momentum thickness and X is certainly not linear. We can conclude then, that the momentum thickness Reynolds number option is a poor choice to use for predicting heating rates in the transition region.

Calculated spanwise heating rates, shown in Figure 14, agree quite well with experimental data taken in the transition region. The local integrated unit Reynolds number option was used to define the beginning and end of transition. End-point values were based on windward streamline data. At spanwise locations laminar theory compares less favorably with data than do transition region results. In turbulent flow the effects of streamline divergence are much less than for laminar flow. This effect is carried over into the transition region to give good agreement between analytical and experimental results at $X/L = 0.7$ and $X/L = 0.9$ as shown in Figure 14.

One of the inherent drawbacks of a boundary layer integration along a streamline is that streamlines tend to spread or converge depending on body shape and pressure distribution. There is no way of knowing beforehand just which stagnation region streamlines should be chosen in order to provide a uniform circumferential streamline distribution at a

certain body cross section downstream of the stagnation region. Also, any set of stagnation region streamlines that produce a uniform circumferential distribution of streamlines at one body station will probably not produce a very good circumferential streamline distribution at a significantly different body station if sizeable spanwise surface or pressure gradients are present.

SECTION IV

THREE-DIMENSIONAL SHOCK-CAPTURING TECHNIQUE

1. BACKGROUND

While empirical techniques have been very successful in predicting the surface pressure on large areas, the increased emphasis on heating rates requires better streamline definition which, in turn, requires better pressure detail. Some more nearly "exact" program is required to supply such pressure detail. It should be noted that this is not quite as difficult as might appear, because surface pressure is relatively insensitive to errors in the flow-field calculation (one of the reasons for the success of empirical approximations). The Northrop Three-Dimensional Method of Characteristics (Reference 31) has been used for this purpose, although there are geometry limits and the development of a strong cross-flow shock will result in failure of the characteristic code. A three-dimensional time-dependent solution is much too costly and the Grumman STEIN code (a three-dimensional shock-tracking technique) (Reference 32) was not locally available and was reported to be very large and slow (Reference 33). The Three Dimensional Shock Capturing Technique (SCT) developed by Solomon (Reference 6) is available. The SCT calculates the flow in a supersonic region by solving the steady, inviscid equations written in a weak conservation form. With the equations in this form, imbedded shocks are located in an approximate manner; the bow shock is explicitly located and tracked by the program. The SCT code is able to handle steep entropy gradients near the body, vehicles which are not symmetric about the pitch plane and perform real-gas as well as perfect-gas calculations.

Because the program employs an explicit finite differencing scheme which advances the solution along the longitudinal axis, the storage requirements are minimized. As each surface is completed, it becomes the initial value surface for the next step, thus the program may be halted at any station, the surface saved and the program restarted from that location.

All geometry calculations are carried out in a subroutine "BODY" which computes body radius as a function of meridional angle; the first and second derivatives of body radius with respect to meridional angle; the first and second derivatives with respect to the longitudinal direction and the cross derivative with respect to longitudinal direction and meridional angle. All other required manipulation of geometry data is in a separate, permanent subroutine. Thus, if a body is required which cannot be described by the existing routine, a new BODY subroutine can be used in place of the original routine.

As delivered, the BODY routine was designed to calculate a multiconic body with cuts, flaps, and flares. This routine was used for the blunt and sharp biconic studies described in the next section.

For the type aerodynamic study of interest here, however, different bodies were required. The first non-conical shape attempted was a blunted ogive-cylinder for which extensive experimental data was available (References 34 and 36). The new subroutine is described in Appendix A. Some results of these calculations are discussed later in this section.

More complex lifting configurations required a more elaborate program. Details of this code are included in Appendix B of this report. This

subroutine calculates the body geometry for any body which can be described by a set of circular arcs and straight lines. Elliptic arcs could also be included but have not been as yet. The subroutine assumes the slope is continuous at the junction of each segment in the meridional direction; the body may be discontinuous in the longitudinal direction.

The SCT is a fast, efficient code and the comparisons with experimental data are excellent. The code is not completely automatic; some knowledge of the flow behavior and behavior of the equations is necessary to tailor the run set up, but it has failed only when a compression forced the axial flow to go subsonic or downstream of large expansions in either the longitudinal or circumferential directions which caused numerical instabilities in the solution. Angles of attack in excess of 30° for 15° half-angle cones have been calculated and a few demonstration cases with a small yaw angle were completed.

2. CONE STUDY

The SCT Program was developed primarily to study three-dimensional flow over conical bodies with flats, flaps and flares. Therefore, a series of biconic shapes were selected as the initial cases to gain some experience with the program before attempting to extend the program's capabilities. This study used a $5^\circ/10^\circ$ biconic with nose bluntness ratios (R_n/R_{Base}) from 2% to 20% and angles of attack up to 25° . The experimental study was on stability and no heat transfer comparisons were available. Results of this study were presented at the AIAA 4th Atmospheric Flight Mechanics Conference (Reference 35).

One computational problem is worth discussing. At small angles of attack (less than 3°), it was possible to complete the full solution on

the computer without intervention; for larger angles it was necessary to stop calculation about three nose radii beyond the biconic junction and restart the solution at that point. The reason for this is the manner in which the program computes wall boundary conditions.

It is possible to derive two equivalent equations for the derivative of pressure in the axial direction depending on which substitutions are made in the basic equation. These two equations, however, may result in significant differences in the computed pressures. More significantly, one may give a solution in regions where the other will not. The two solutions are referred to as "MOD 3" and "MOD 0" solutions; the MOD 3 solution has proven to be the most dependable for bodies of revolution except in regions of surface discontinuity in the axial direction. In this case, the MOD 3 solution often fails; the MOD 0 solution gives good solutions in this case. However, the MOD 0 solution does not, in general, compute the leeside of cones at large angles of attack successfully. Because of the behavior of these two solutions, the default value of the program is MOD 3 until an axial discontinuity is reached, i.e., Subroutine JUMP is called, at which time MOD 0 is selected. There is no logic to permit the user to control the selection of these two solutions.

In his report, Solomon (Reference 6) makes no effort to explain why one boundary condition works when the other does not; the complexity of the equation is too great to make any definitive statements here. However, some clarifying generalities can be made. In the primary pressure method, MOD 3, numerical differences are required for

$$p, \frac{v^2}{R_B}, \frac{uv}{R_B}, \frac{vw}{R_B}, \text{ and } \frac{v}{R_B}$$

while in the alternate boundary condition, MOD 0, numerical differences are required only for

$$p, \frac{v}{w}.$$

In regions of sudden large expansion MOD 3 breaks down, probably because the products v^2 , uv , vw display very steep gradients in such a region. Dividing the circumferential velocity by the longitudinal velocity results in a parameter which is not changing rapidly, permitting successful differences to be taken in the tangential direction. On the leeside of cones at large incidence the ratio of v/w tends toward unity because of the very high cross flow velocity resulting in poor differences in the tangential direction.

Using the above guidelines, it would seem wise to force a MOD 0 type solution any time the ratio v/w is small (cross flow is small compared to the axial flow velocity), and p , u and v show high gradients and force MOD 3 solutions any time the cross flow approaches the axial velocity (v/w tends toward unity).

3. OGIVE-CYLINDER STUDY

AFFDL has conducted an extensive series of tests at AEDC on a modular missile configuration (Reference 34) to study fin interactions. Phase III of the series (Reference 36) was planned to supply data for comparison with the SCT Program. A surface oil flow study was conducted in an effort to determine streamline locations along the body. Oil flow data was taken at angles of attack of 4° , 6° , 8° and 10° . The fins shown in Figure 15

were removed and a pitot pressure rake and a total temperature probe were installed 180° apart and the run sequence was repeated. Static pressures on the surface of the model at body station 41 were also taken during this phase of the test.

A series of ogive-cylinder computer runs using the NSWC code with the subroutine described in Appendix A was made at angles of attack of 0°, 2°, 4°, 5°, 6°, 7°, 8°, 9°, 10° and 12°. Computer runs using the DeJarnette heat transfer code were made for comparison with heat transfer measurements taken in other phases of the study. No effort was made to calculate flow in the fin region.

Surface static pressures, normalized by freestream static pressure, are shown in Figure 16. The SCT pressures compare well with the experimental values on the windward portion of the model; the leeward pressures are not well matched, nor should they have been expected to match due to the reasons cited in Section IV-2.

Figure 17 shows the results of the pitot rake survey of the inviscid shock layer. The program predicts the pitot pressure successfully in the $\phi=0$ and 90° planes; however, viscous effects at $\phi = 180^\circ$ are responsible for the large discrepancies between experimental and calculated pressures close to the body. There are, however, very favorable comparisons near the shock, even on the leeward. The inviscid stream angles predicted by the SCT were consistently lower than the stream angles indicated by the oil flow experiment as expected. Consequently, the inviscid stream angles were used in the correlation theory for which this study was conducted and showed better correlation than the oil flow angles. Additional details

of the study were presented at the AIAA 15th Aerospace Science Meeting (Reference 37).

4. LIFTING BODY STUDY

The original body geometry portion of the SCT permitted only axisymmetric bodies with cuts and flaps. The extension to ogive-cylinder bodies required a new subroutine to describe the geometry, but the shape was still axisymmetric. However, a large class of vehicles, such as lifting bodies, have only one plane of symmetry and are distinguished by large, flat, or nearly flat surfaces. To utilize the SCT for these bodies a new geometry subroutine was required.

This new geometry subroutine must permit the input of shapes which vary in both the circumferential and longitudinal directions. The data required by the new subroutine should be as compatible with the information supplied on engineering drawings as possible. The subroutine described in Appendix B was developed with reference to the X-24C-10 model drawings which supply lofting type information.

There are at least two approaches to producing the required body information. The obvious one is an analytic description of the geometry in an appropriate coordinate system, the other involves surface fitting the geometry with polynomials. The latter approach is the one taken by Marconi (Reference 32). In such a scheme, the physical body must be mapped into a "mapped space" to define the body, then into the computational space.

Although there is a great deal of merit to the surface fitting approach, the purely analytic one was chosen for this program. The basic reason for this selection was the ease of taking loft-line information from engineering drawings and using them in a computer code. In the pure sense of the term,

this code also maps from cartesian coordinates to cylindrical coordinates to a rectangular computational coordinate system; the most significant difference is that in this scheme a 1:1 mapping from cartesian to cylindrical coordinates is always used. If surface fitting is the objective, the mapping is, in general, not a 1:1 mapping. Although the present analytic scheme has proved successful, changes in engineering practice in the aircraft industry may make surface fitting a more attractive approach in the future.

It should be noted that as the SCT program is presently structured, a surface spline would be very difficult. The main computational program is expecting to map body data in a cylindrical coordinate system into the computational coordinate system. The surface fitting of a shape, such as the lifting body, with a surface spline in a cylindrical coordinate system is very difficult as experience with the DeJarnette code, which uses a surface fit, has pointed up (Section III-3 and Reference 7). As a general rule, if surface splines are desired for fitting, the user should select a coordinate system based on the type of surface to be fitted. This, of course, can be done if the mapping is not 1:1. However, Solomon (Reference 6) has observed computational difficulties in this program with nonuniformly distributed body points. Points which are uniformly distributed in the mapped space to meet this requirement, may not be appropriately spaced in the physical space. These problems may be resolved in the future.

A program to develop a design for a new high-speed flight vehicle for flight test experiments has resulted in a large amount of experimental data (Reference 38) about one candidate shape, the X-24C-10D (Figure 1).

Although some care was necessary to accomplish them, successful flow fields were calculated for angles of attack from 0° to 6° in 2° increments at a freestream Mach number of 5.95. The model shape was approximated by the shape shown in Figure 1b. Results of these studies were presented by Neumann at the AIAA 16th Aerospace Science Meeting (Reference 39).

Great care was exercised in the selection of body points. As the angle of attack increases, the low pressure on the upper surface causes the velocity in the circumferential direction to increase, resulting, eventually, in the axial velocity component becoming subsonic along the leading edge. To avoid this region points were permitted in the region $75^\circ < \phi < 90^\circ$. Solomon (Reference 6) states that, as a minimum, when nonuniform spacing is used, the second differences must be fairly uniform and a preprocessor is supplied to accomplish this arrangement of the points. Table II shows the comparison of a desired ϕ -spacing and the ϕ -spacing after smoothing. Because of this smoothing, a redistribution of points with increased spacing in some region usually required a point be dropped. It should also be noted that, if strong shocks are forming, both the radial and circumferential spacing must be increased to permit the pressure rise to be spread over a larger area. The presence of the strong shock structure caused numerical instabilities which forced selection of first-order accuracy rather than second-order accuracy for the body point calculations. It might be suspected that entropy smoothing would help in this case, but this was not observed. All runs for the X-24C-10D study were made with 7 radial points informally spaced between the shock and body; the 6° angle of attack case used only 13 circumferential points

instead of the 15 circumferential points used at the lower angles of attack. The actual circumferential values used for these runs are shown in Table III.

The default value of MOD 3 for the calculation of the body points was used (see Section IV-2). The body description caused the program to see a longitudinal discontinuity which resulted in the automatic selection of MOD 0. On some of the runs, this selection resulted in program failure some 10 to 15 nose radii downstream of the discontinuity, even though the highest angle of attack was only 6° . However, stopping the calculation about 4 nose radii downstream from the discontinuity and restarting with the MOD 3 option again permitted the solution to continue.

Even with these limitations, the comparisons of numerical surface pressures and experimental values as shown in Figures 18 and 19 are good. Even on the leeside of the model, where we would not expect good agreement at angles of attack, the agreement is reasonable. The leading edges show the least agreement as might be expected.

Surface pressure is not an adequate standard on which to base the validity of a flow field program. Unfortunately, pitot pressure surveys, flow angularity measurements, and shock-shape studies were not available. There is a need to use a simpler shape displaying the basic characteristics of the X-24C-10D model with more flow-field probing to validate the results of this program. Such a study is being initiated.

The results of the SCT with the general body description must be examined with a critical eye. For example, note the bow shock shown in Figures 20 and 21. Model Station (MS) 5.55 appears quite reasonable, but notice the "dimple" at $\phi = 110^{\circ}$ at MS 9.85. This is probably the inter-

section of an imbedded shock from the leeside of the leading edge of the model and the bow shock. In the same manner, the "dimple" at $\phi = 75^\circ$ on MS 14.25 is probably an imbedded windward shock intersection. But what about the behavior of the windward shock at MS 20.52? Is this caused by program instability or shock structure? Additional experimental information and a more detailed examination of the computed flow field will be required to resolve this question.

Although it is not easy to see in Figure 20, there is an inflection of the windward shock in the symmetry plane. In Figure 22 the slope of the shock in the axial direction is plotted and a strong inflection at MS 5.86 can be seen as well as a weaker one at MS 12.51. The first inflection had a significant effect on the program, resulting in clearly observable instabilities in the flow which eventually resulted in negative entropies being calculated, a clear warning of danger. No failures were observed in this region, however.

The first inflection is easily visible in Schlieren photographs taken during the X-24C-10D wind tunnel tests at AEDC (Reference 38). The second inflection is not apparent.

In Figure 23 the slope of the shock in the axial direction is plotted as a function of circumferential angle for three model stations. The slopes from $\phi = 50^\circ$ to $\phi = 120^\circ$ are certainly suspect at MS 9.85, but the behavior damps out at MS 20.52.

Figure 24 shows the slope of the shock in the circumferential direction. The slopes support the "dimples" shown in Figure 21, but offer few clues as to the validity of the technique.

The foregoing plots (Figures 20-24) are presented as examples of program parameters which must be considered in validating the results of the program. They are not an exclusive set; such questions as Mach number behavior, entropy, and flow angle must be examined also. It should also be noted that disturbances in the flow field do not necessarily cause problems on the surface of the body. The disturbance must propagate within the Mach cone toward the body, striking it far downstream of the original disturbance. By this time, the numerical differencing may well have damped the disturbance to a point where it is negligible.

SECTION V

HEAT TRANSFER CALCULATIONS USING SCT PRESSURES AND THE DEJARNETTE PROGRAM

A major goal of this effort has been to show numerically generated surface pressures can be used in the heat transfer code by DeJarnette (Reference 4) to produce reliable heat transfer rates. We have found two serious limitations to this approach; there is a limit on the generality of the geometry the DeJarnette code will accept (the X-24C-10D has not been programmed in the DeJarnette code because of this difficulty) and the calculated pressures must be surface fit in a manner that permits the first and second derivatives of the pressure with respect to the axial and circumferential coordinates to be obtained. These pressures do not constitute a well-posed problem mathematically and the resultant derivatives are not necessarily accurate. It is therefore necessary to examine the results of the surface fit and the derivatives with some care to insure they are physically realistic. No pressure problems were encountered with the shape selected for this study, an ogive-cylinder.

The ogive-cylinder used for this study is shown in Figure 15. Surface pressure data computed by the SCT Program was saved and punched into cards in the format used by the DeJarnette code. Comparisons between the numerical and experimental values were made for model station (MS) 47.5 at angles of attack of 0° , 4° , 8° and 12° at a freestream Mach number of 5.95. The wind tunnel model contained 75 thermocouples in one quadrant of the model at MS 47.5. The model was injected into the tunnel, pitched to the desired angle of attack, and rolled 180° in 30° increments with a set of heat transfer data taken at each condition for a total of 525 bits of experimental data. The experimental Stanton numbers were calculated for

each of these bits of data using freestream velocity, density, and total temperature rather than the adiabatic wall temperature and boundary layer edge conditions which are unknown.

Pressure data were also taken at MS 47.5 at 18 points around the body. Neumann (Reference 37) found that if the surface pressure was normalized by the freestream static pressure and plotted against the tunnel-based Stanton number on a log-log plot, the result was a straight line of the form

$$\log St_{\infty} = 1.081 \log(p/p_{\infty}) + 0.5922. \quad (7)$$

Figure 25 shows the experimentally obtained Stanton numbers, the Stanton numbers based on the linear relationship above and the Stanton numbers predicted by the DeJarnette Program. As expected, in the regions of flow separation on the leeside of the model, the Stanton numbers are not well matched by the DeJarnette values. On the windward surface, where good agreement was expected, the DeJarnette values are consistently lower than the experimental values. It should be noted that the numerical pressures obtained by the SCT, and on which the DeJarnette values are based, are also lower than experimental.

To insure the observed differences are not due to the manner in which the Stanton number is calculated, the heat transfer rates were compared directly in Figure 26. Only the 4° angle of attack case was examined and not all available experimental data points were plotted, but it is clear the pattern is the same as that observed for the Stanton numbers. In Figure 27 the experimental and numerical Stanton numbers on the windward centerline are compared as a function of angle of attack. Also shown in

Figure 27 are the numerical surface pressures and the experimental surface pressures for angles of attack of 4° , 8° and 10° (no surface pressure data was taken experimentally at 12°). The pressures at 0° angle of attack are not shown, but are almost identical, 0.85 for the numerical case and 0.86 for the experimental. The differences in pressure are not sufficient to explain the resultant Stanton number differences, but they are in the correct direction.

A better geometry and pressure fitting program must be developed for the DeJarnette code to permit heat transfer studies on more complex shapes such as the X-24C-10D. A program with McDonnell Douglas Astronautics, East has been started to meet this requirement.

SECTION VI

CONCLUSIONS

The original objective of this study was to demonstrate that the heat transfer portion of the HABP is useful for lifting reentry shapes. This objective was realized only in a limited manner, as the restrictions imposed on streamline tracking limit the usefulness of the technique. Heat transfer rates obtained with this method for the flat portion of the X-24C-10D side panel compare well with data.

Within the restrictions and limitations of the DeJarnette program it represents a fairly simple, relatively accurate computer program to calculate aerodynamic heating rates over fairly general three-dimensional bodies and is available to AFFDL. The program is fast, requiring on the order of seven seconds to complete a streamline for typical cases described in this report. In general, it requires that the surface pressure distribution be obtained independently; however, it has the capability of computing a modified Newtonian pressure distribution.

An improved description of the inviscid flow field was required to obtain the improved pressure distribution. The NSWC Shock-Capturing Technique was obtained and made operational to meet this requirement. The code was used to calculate the inviscid flow about biconics, ogive-cylinders and a lifting body. Because of limits in the existing DeJarnette code, it was not possible to use the DeJarnette code with the lifting body; however, pressures calculated by the inviscid program for the ogive-cylinder were put in the DeJarnette code. The resultant heat transfer rates compared well with experiment.

In summary, techniques are available to calculate the surface pressure distribution, streamline pattern and heat transfer rate to a large class of axisymmetric bodies at angle of attack. More limited capabilities have been demonstrated for bodies with a single plane of symmetry at angle of attack.

REFERENCES

1. Gentry, A.E., Smyth, D.N., and Oliver, W.R., The Mark IV Supersonic-Hypersonic Arbitrary-Body Program, Volume I User's Manual, Volume II Program Formulation, AFFDL-TR-73-159, November 1973.
2. Gentry, A.E., and Smyth, D.N., Hypersonic Arbitrary-Body Aerodynamic Computer Program, Mark III Version, Volume I User's Manual, Volume II Program Formulation and Listing, Douglas Report DAC 61552, April 1968.
3. Edwards, L., Private Communication, NASA Langley Research Center.
4. DeJarnette, F.R., "Calculation of Heat Transfer on Shuttle-Type Configurations Including the Effects of Variable Entropy at Boundary Layer Edge", NASA CR-112180, October 1972.
5. Hender, D.R., A Miniature Version of the JA70 Aerodynamic Heating Computer Program, H800 (MINIVER), McDonnell Douglas Report MDC G0462, June 1972.
6. Solomon, J.M., Ciment, M., Ferguson, R.E., Bell, J.B., Warlaw, A.B., A Program for Computing Steady Inviscid Three-Dimensional Supersonic Flow on Reentry Vehicles, Volume I Analysis and Programming, Volume II User's Manual, NSWC/NOL/TR 77-28, February 1977.
7. McNally, W.D., FORTRAN Program for Calculating Compressible Laminar and Turbulent Boundary Layers in Arbitrary Pressure Gradients, NASA TN D-5681, May 1970.
8. Stallings, D.W., and Morrison, M.W., Heat Transfer Tests on the AFFDL X-24C-10D Model at Mach Numbers from 5.0 to 8.0, AEDC-DR-76-70, August 1976.
9. DeJarnette, F.R., and Tai, T.C., "A Method for Calculating Laminar and Turbulent Convective Heat Transfer over Bodies at an Angle of Attack", NASA CR-101678, March 1969.
10. DeJarnette, F.R., and Davis, R.M., "A Simplified Method for Calculating Laminar Heat Transfer over Bodies at an Angle of Attack", NASA TN D-4720, August 1968.
11. DeJarnette, F.R., "Calculation of Inviscid Surface Streamlines and Heat Transfer on Shuttle Type Configurations, Part I - Description of Basic Method", NASA CR-111921, August 1971.
12. DeJarnette, F.R., and Jones, M.H., "Calculation of Inviscid Surface Streamlines and Heat Transfer on Shuttle Type Configurations, Part II - Description of Computer Program", NASA CR-111922, August 1971.

13. DeJarnette, F.R., and Hamilton, H.H., "Inviscid Surface Streamlines and Heat Transfer on Shuttle-Type Configurations", J. Spacecraft, Volume 10, No. 5, May 1973, pp. 314-321. Also In AIAA Paper No. 72-703, June 26-28, 1972.
14. DeJarnette, F.R., and Hamilton, H.H., "Aerodynamic Heating on 3-D Bodies Including the Effects of Entropy-Layer Swallowing", J. Spacecraft, Volume 12, No. 1, January 1975, pp. 5-12.
15. Cohen, N.B., "Boundary-Layer Similar Solutions and Correlation Equations for Laminar Heat-Transfer Distribution in Equilibrium Air at Velocities up to 41,000 Feet per Second", NASA TR R-118, 1961.
16. Beckwith, I.E., and Cohen, N.B., "Application of Similar Solutions to Calculation of Laminar Heat Transfer on Bodies with Yaw and Large Adverse Pressure Gradient in High-Speed Flow", NASA TN D-625, 1961.
17. Spalding, D.B., and Chi, S.W., "The Drag of a Compressible Turbulent Boundary-Layer on a Smooth Flat Plate with and without Heat Transfer", J. Fluid Mech., Volume 18, Part 1, January 1964, pp. 117-143.
18. Reshotko, E., and Tucker, M., "Approximate Calculation of the Compressible Turbulent Boundary-Layer with Heat Transfer and Arbitrary Pressure Gradient", NACA TN 4154, 1957.
19. Dhawan, S., and Narasimha, R., "Some Properties of Boundary-Layer Flow During the Transition from Laminar to Turbulent Motion", J. Fluid Mech., Volume 3, No. 4, April 1958, pp. 418-436.
20. Maslen, S.H., "Inviscid Hypersonic Flow Past Smooth Symmetric Bodies", AIAA J., Volume 2, No. 6, June 1964, pp. 1055-1061.
21. Sliski, N.J., "An Investigation of Aerodynamic Heating Distributions and Boundary-Layer Transition on an 80° Swept Delta Wing Planform at Mach=8 and Angles of Attack 0°-60°", AFFDL-TM-74-98-FXG, Air Force Flight Dynamics Laboratory, Wright-Patterson Air Force Base, Ohio, March 1974.
22. Cohen, N.B., "Correlation Formulas and Tables of Density and Some Transport Properties of Equilibrium Dissociating Air for Use in Solutions of the Boundary-Layer Equations", NASA TN D-194, 1960.
23. Leigh, D.C., and Ross, B.B., "Surface Geometry of Three-Dimensional Inviscid Hypersonic Flows", AIAA J., Volume 7, No. 1, January 1969, pp. 123-129.
24. Timmer, H.G., "Determination of Hypersonic, Inviscid, Surface Streamlines for General Convex Bodies", Douglas Paper 10005, McDonnell Douglas Astronautics Company, September 1969.

25. Vaglio-Laurin, R., "Laminar Heat Transfer on Three-Dimensional Blunt Nosed Bodies in Hypersonic Flow", ARS Journal, Volume 29, No. 2, February 1959, pp. 123-129.
26. Lees, L., "Laminar Heat Transfer over Blunt-Nosed Bodies at Hypersonic Flight Speeds", ARS Journal, Volume 26, No. 4, April 1956, pp. 259-269, 274.
27. Bushnell, D.M., Jones, R.A., and Huffman, J.K., "Heat Transfer and Pressure Distributions on Spherically Blunted 25° Half-Angle Cone at Mach 8 and Angles of Attack up to 90°", NASA TN D-4792, 1968.
28. Lomax, H., and Inouye, M., "Numerical Analysis of Flow Properties About Blunt Bodies Moving at Supersonic Speeds in an Equilibrium Gas", NASA TR R-204, 1964.
29. Hillsamer, M.E., and Rhudy, J.P., "Heat Transfer and Shadow Graph Tests of Several Elliptical Lifting Bodies at Mach 10", AEDC-TDR-64-19, Arnold Engineering Development Center, Arnold Air Force Station, Tennessee 37389, February 1964.
30. Unpublished Data Obtained at AEDC in the VKF Tunnel "B" Test Facility under Project No. VA020-27BA, 26 July 1972.
31. Powers, S.A., and Chu, C.W., "The Calculation of Three-Dimensional Supersonic Flows Around Spherically-Capped Smooth Bodies and Wings", AFFDL-TR-72-91, September 1972.
32. Marconi, F., Salas, M., Yager, L., "Development of a Computer Code for Calculating the Steady Super/Hypersonic Inviscid Flow Around Real Configurations", NASA CR-2675, April 1976.
33. Adams, R., Private Communication, Aerodynamics Project Branch, Arnold Engineering Development Center.
34. Hayes, J.R., "An Overview of the Test Program and Representative Data Taken on the Modular Missile Configuration", AFFDL-TM-77-90, October 1977.
35. Stetson, K.F., and Lewis, A.B., "Aerodynamic Comparison of a Conical and Biconic Reentry Vehicle", AIAA 4th Atmospheric Flight Mechanics Conference, Paper 77-1161, 8-10 August 1977.
36. Baker, S.S., "Test Results from the AFFDL Modular Missile (Phase III) Test Conducted in the AEDC VKF Tunnel B at Mach Number 6", AEDC-DR-76-68, August 1976.
37. Neumann, R.D., and Hayes, J.R., "Prediction Techniques for the Characteristics of the Three-Dimensional Shock Wave/Turbulent Boundary Layer Interaction", AIAA 14th Aerospace Sciences Meeting, AIAA Paper 77-46, 24-26 January 1977.

38. Wannenwetsch, G.D., "Pressure Tests of the AFFDL X-24C-10D Model at Mach Numbers of 1.5, 3.0, 5.0, and 6.0", AEDC-DR-76-92, Volumes 1-13, November 1976.
39. Neumann, R.D., Patterson, J.L., and Sliski, N.J., "Aerodynamic Heating to the Hypersonic Research Aircraft, X24C", AIAA 16th Aerospace Science Meeting, AIAA Paper 78-37, January 1978.
40. Cohen, N.B., and Reshotko, E., "The Compressible Laminar Boundary Layer with Heat Transfer and Arbitrary Pressure Gradient", NACA Report 1294, 1956.
41. Sasman, P.K., and Cresci, R.J., "Compressible Turbulent Boundary Layer with Pressure Gradient and Heat Transfer", AIAA J., Volume 4, No. 1, January 1966, pp. 19-25.
42. Schlichting, H., Boundary Layer Theory, 6th Ed., McGraw-Hill, 1968.
43. Granville, P.S., "The Calculation of the Viscous Drag of Bodies of Revolution", Report 849, David Taylor Model Basili, July 1953.
44. Sliski, N.J., "A Description of the AFFDL Version of the Streamline and Heat Transfer Program Developed by DeJarnette", AFFDL-TM-77-9-FXG, January 1977.
45. Milne, W.E., Numerical Calculus, Princeton University Press, Princeton, New Jersey, 1949.

APPENDIX A

BODY PROGRAM FOR OGIVE-CYLINDER

In the three dimensional shock capturing technique, the body radius and derivatives required by the main program are calculated in a subroutine called BODY and transmitted back to the calling program through a common block. The values of ϕ -angle for which calculations are required and the value of the longitudinal station are also transmitted through common. Thus, only one calling argument, the index number of the cross sectional plane being calculated, is needed. The original BODY subroutine can be replaced by any new subroutine meeting these requirements.

An ogive-cylinder may be described by giving a radius for the ogive portion or the length of the ogive portion plus the radius of the cylinder as shown in Figure A-1. The BODY program must calculate the local body radius normal to the longitudinal axis along with the first and second derivatives with respect to circumferential angle and longitudinal distance plus the cross derivative. The calculated shape must have a blunt nose and all lengths must be normalized by the nose radius.

The subroutine written for this purpose expects the length of the ogive portion and the radius of the cylinder portion, both normalized by the nose radius, to be given as input. Then, by Figure A-1, the radius of the ogive is given by

$$R_{og} = 0.5(S_{og}^2 + R_{cy}^2)/R_{cy} \quad (A-1)$$

and the slope at the sphere-ogive junction is given by

$$\alpha = \arccos (R_{og} - R_{cy})/(R_{og} - 1) \quad (A-2)$$

and the length of the blunted ogive is given by

$$L_{og} = (R_{og} - 1.) \sin \alpha + 1. \quad (A-3)$$

At any value of z the body radius is given by

$$R_B = R_{cy} - (R_{og} - R_{temp}) \quad (A-4)$$

where

$$R_{temp} = \sqrt{R_{og}^2 - D_{temp}^2} \quad (A-5)$$

$$D_{temp} = L_{og} - z$$

The derivatives are given by

$$dR_B/d\phi = d^2R_B/d\phi^2 = d^2R_B/dz d\phi = 0 \quad (A-6)$$

$$dR_E/dz = D_{temp}/R_{temp}$$

$$d^2R_B/dz^2 = -(R_{temp} + D_{temp}) (dR_B/dz)/R_{temp}^2 \quad (A-7)$$

These values are calculated once for each body station when z is less than L_{og} . Subsequent calls to BODY result in an immediate return to the calling program. When z is greater than L_{og} , the cylinder radius is returned with all derivatives set equal to zero.

APPENDIX B

BODY PROGRAM FOR A GENERAL BODY

In the three-dimensional shock-capturing technique the body radius and derivatives required by the main program are calculated in a subroutine called BODY and transmitted back to the calling program through a common block. The values of ϕ -angle for which calculations are required and the value of the longitudinal station are also transmitted through common. Thus, only one calling argument, the index number of the cross-sectional plane being calculated, is needed. The original BODY subroutine can be replaced by any new subroutine meeting these requirements.

The initial shape considered for the new body routine is shown in Figure B-1. The body may also have flat surfaces on the top and bottom. While the present version of this BODY program is more general than the original routine and the ogive-cylinder routine, there are some specific restrictions.

The shape may be divided into any number of longitudinal sections, but each section may have no more than five segments in the circumferential direction. These segments may be arcs of circles or straight lines and may have longitudinal dependence.

Prior to starting each new segment of the body, the program computes the maximum ϕ -angle for that segment. Simple geometry is used to locate this angle; for example, if the current segment and the next segment are both arcs of circles, then the current segment will end when its radius passes through the center of the next arc. Going from a circular arc to a straight line, the arc ends when the slope of the arc equals the slope of the straight segment. As can be seen, this and similar procedures used

for the other possible cases greatly simplifies the body description. Because not all bodies have continuous slopes, it may be wise to supply the maximum ϕ angle for each segment.

A circle is described by giving the coefficients to specify the locus of the center and the radius, thus

$$\begin{aligned}x_h &= A_x Z^2 + B_x Z + C_x \\y_k &= A_y Z^2 + B_y Z + C_y \\R_o &= A_r Z^2 + B_r Z + C_r\end{aligned}\tag{B-1}$$

A straight line intersecting the plane of symmetry is uniquely described by the slope relative to the horizontal axis and its intercept point on the vertical axis

$$x_h = A_x Z^2 + B_x Z + C_x$$

A general straight line, not intersecting the plane of symmetry, is uniquely defined by its adjacent segments assuming slopes are continuous about the body. However, to simplify calculations, the program expects the slope to be given.

The first segment at each station may be either a straight line or a circular arc. If the first segment is a straight line, the second segment must be a general circular arc. The body must have a plane of symmetry and no logic is included to handle angles greater than 180° .

Having decided to use an analytic approach to the body geometry, the problem to be solved is: Given a body described in a cartesian system and given an angle ϕ in the circumferential direction, find the body radius and its first and second derivatives with respect to Z and ϕ plus the

cross derivative. The body radius can be quickly calculated by the Law of Sines using Figure B-2 for a circular arc crossing the plane of symmetry.

$$R_B = R_O \sin \theta / \sin \psi$$

where

$$\theta = 180 - \psi - \gamma$$

$$\gamma = \arcsin (B_s \sin \psi / R_O)$$

$R_O = R(Z)$, $B_s = B(Z)$, which makes $\gamma = \gamma(Z)$, $\psi = \psi(\phi)$, and $R_B = f(\phi, Z)$.

The derivatives of R_B with respect to Z and ϕ are straight forward, but long. They are listed here with some intermediate derivatives left unstated.

$$\frac{dR_B}{d\phi} = \frac{R_O \sin \psi \cos \theta \frac{d\theta}{d\phi} + \cos \psi \sin \theta}{\sin^2 \psi} \quad (B-3)$$

$$\begin{aligned} \frac{d^2 R_B}{d\phi^2} = \frac{R_O}{\sin^4 \psi} & \left[\sin^2 \psi \left(-\sin \psi \sin \theta \left(\frac{d\theta}{d\phi} \right)^2 + \sin \psi \cos \theta \frac{d^2 \theta}{d\phi^2} \right) \right. \\ & \left. + \sin \psi \sin \theta \right] - \left(\sin \psi \cos \theta \frac{d\theta}{d\phi} + \cos \psi \sin \theta \right) (-2 \sin \psi \cos \psi) \end{aligned} \quad (B-4)$$

$$\frac{dR_B}{dZ} = \frac{\sin \theta \frac{dR_O}{dZ} - R_O \cos \theta \frac{d\gamma}{dZ}}{\sin \psi} \quad (B-5)$$

$$\begin{aligned} \frac{d^2 R_B}{dZ^2} = & \left(\frac{d^2 R_O}{dZ^2} \sin \theta - 2 \frac{dR_O}{dZ} \cos \theta \frac{d\gamma}{dZ} - R_O \sin \theta \left(\frac{d\gamma}{dZ} \right)^2 \right. \\ & \left. - 2 R_O \cos \theta \frac{d^2 \gamma}{dZ^2} \right) / \sin \psi \end{aligned} \quad (B-6)$$

$$\begin{aligned} \frac{d^2 R_B}{dZ d\phi} = & \left(\cos \theta \frac{d\theta}{d\phi} \frac{dR_O}{dZ} + R_O \sin \theta \frac{d\theta}{d\phi} \frac{d\gamma}{dZ} - R_O \cos \theta \frac{d^2 \gamma}{dZ d\phi} \right) / \quad (B-7) \\ & \sin \psi + \left(\sin \theta \frac{dR_O}{dZ} - R_O \cos \theta \frac{d\gamma}{dZ} \right) \cos \psi / \sin^2 \psi \end{aligned}$$

Note all derivatives become undefined at $\phi = 0^\circ$ and 180° . A check of the numerators shows these forms are all indefinite (0/0) and by L'Hospital's Rule we find

$$R_B = R_O - B_s \quad (B-8)$$

$$\frac{dR_B}{d\phi} = \frac{d^2 R_B}{d\phi^2} = \frac{d^2 R_B}{dZ d\phi} = 0 \quad (B-9)$$

$$\frac{dR_B}{dZ} = \frac{dR_O}{dZ} - \frac{dB_s}{dZ} \quad (B-10)$$

$$\frac{d^2 R_B}{dZ^2} = \frac{d^2 R_O}{dZ^2} - \frac{d^2 B_s}{dZ^2} \quad (B-11)$$

When calculating for a general circular arc as shown in Figure B-3, we let B_s be the distance to the center of the circular arc and ϕ_m be the angle of B_s relative to the axis of symmetry, then ψ can be defined as shown. The derivatives for ϕ are the same as above, but the Z-derivatives are now given by

$$\frac{dR_B}{dZ} = \frac{\sin \psi \left(\sin \theta \frac{dR_O}{dZ} + R_O \cos \theta \frac{d\theta}{dZ} \right) - R_O \sin \theta \cos \psi \frac{d\phi_m}{dZ}}{\sin^2 \psi} \quad (B-12)$$

$$\frac{d^2 R_B}{dZ^2} = \frac{d\mu}{dZ} - \frac{d\sigma}{dZ} - \frac{dR_B}{dZ} \cos \psi \frac{d\phi_m}{dZ} \quad (B-13)$$

where

$$\frac{d\mu}{dZ} = R_O \cos \theta \frac{d\theta}{dZ} \frac{dR_O}{dZ} + \sin \theta \frac{d^2 R_O}{dZ^2} - R_O \left(\sin \theta \left(\frac{d\theta}{dZ} \right)^2 - \cos \theta \frac{d^2 \theta}{dZ^2} \right) \quad (B-14)$$

$$\frac{d\sigma}{dZ} = \frac{dR_B}{dZ} \cos \psi \frac{d\phi_m}{dZ} - R_B \left(\sin \psi \left(\frac{d\phi_m}{dZ} \right)^2 - \cos \psi \frac{d^2 \phi_m}{dZ^2} \right) \quad (B-15)$$

Again the question of limits as $\phi \rightarrow 0^0$ must be addressed. The first derivative with respect to ϕ remains equal to zero, but the second derivative is an analytic singularity not equal to zero and, at the present time, not properly defined in the program. The Z-derivatives limits are now given by

$$\frac{dR_B}{dZ} = \frac{dB_s}{dZ} + \frac{dR_o}{dZ} \quad (B-16)$$

$$\frac{d^2R_B}{dZ^2} = \frac{d^2B_s}{dZ^2} + \frac{d^2R_o}{dZ^2} \quad (B-17)$$

To calculate the required values on a straight bottom (a straight top uses the same logic), the construction shown in Figure B-4 is used. Note that the length along the x-axis is given and the slope of the bottom relative to the horizontal is known. The radius and derivatives are given by

$$R_B = B_s \sin \theta / \sin \psi$$

$$\theta = \pi/2 - \text{slope} \quad (B-18)$$

$$\psi = \pi/2 + \text{slope} - \phi$$

$$\frac{dR_B}{d\phi} = B_s \sin \theta \cos \psi \frac{d\theta}{d\phi} / \sin^2 \psi \quad (B-19)$$

$$\frac{d^2R_B}{d\phi^2} = B_s \frac{\sin \theta}{\sin \psi} + \frac{2B_s \sin \theta \cos^2 \psi}{\sin^3 \psi} \quad (B-20)$$

$$\frac{dR_B}{dZ} = \frac{\sin \theta}{\sin \psi} \frac{dB_s}{dZ} \quad (B-21)$$

$$\frac{d^2R_B}{dZ^2} = \frac{\sin \theta}{\sin \psi} \frac{d^2B_s}{dZ^2} \quad (B-22)$$

$$\frac{d^2R_B}{d\phi dZ} = - \frac{\sin \theta \cos \psi}{\sin^2 \psi} \frac{dB_s}{dZ} \frac{d\theta}{d\phi} \quad (B-23)$$

The last general case is a general straight line whose slope is measured from the vertical as shown in Figure B-5. For this case B_s is a known length and makes an angle ϕ_s relative to the plane of symmetry. Then θ is ϕ_s - Slope and

$$B_m = B_s \sin \theta \quad (B-24)$$

$$\psi = \pi/2 + \text{slope} - \phi$$

From these values we have

$$R_B = B_m / \cos \psi \quad (B-25)$$

$$\frac{dR_B}{d\phi} = - \frac{B_m \sin \psi}{\cos^2 \psi} \quad (B-26)$$

$$\frac{d^2 R_B}{d\phi^2} = \frac{B_m}{\cos \psi} (1 + 2 \tan^2 \psi) \quad (B-27)$$

$$\frac{dR_B}{dZ} = \frac{1}{\cos \psi} \frac{dB_m}{dZ} \quad (B-28)$$

$$\frac{d^2 R_B}{dZ^2} = \frac{1}{\cos \psi} \frac{d^2 B_m}{dZ^2} \quad (B-29)$$

$$\frac{d^2 R_B}{dZ d\phi} = - \frac{\sin \psi}{\cos^2 \psi} \frac{dB_m}{dZ} \quad (B-30)$$

In the case of the ogive-cylinder, all body radii and derivatives were easily obtained to check the computer code. In this case, the derivatives were not easily computed. To check the values computed by the new body code a test routine was used to calculate the required values at 2° intervals around the body and any desired number of body stations. For each section of the body, four stations 0.5 nose radii apart were computed. A small number of body radii were hand-calculated, then these and the radii computed by the test program were carefully plotted.

Once the body radii were validated, they were used in a four-point numerical differentiating formula to calculate the ϕ and Z derivatives. The differentiating formula used was (Reference 45)

$$dB_1/dK = (1/h) (-2B_0 - 3B_1 + 6B_2 - B_3) \quad (B-31)$$

where K was ϕ or Z and h the interval between B_1 and B_1 . End points were checked with

$$dB_0/dK = (1/h) (-11B_0 + 18B_1 - 9B_2 + 2B_3) \quad (B-32)$$

and

$$dB_3/dK = (1/h) (-2B_0 + 9B_1 - 18B_2 + 11B_3). \quad (B-33)$$

When the first derivatives had been checked, the same pattern was repeated to check the second derivatives and cross derivative. It is recommended that each new shape be tested in this manner prior to use in the SCT.

TABLE I
DATA FOR SIX SAMPLE TEST CASES

| Configuration | P_{∞} (PSF) | T_{∞} (°R) | V_{∞} (FPS) | T_w (°R) | M_{∞} | $Re_{\infty} \times 10^{-6}$ | h_{02} (Btu/ft ² -sec-°R) | α (DEG) | R_n (in) | L (in) | Fig No |
|--------------------------------|--------------------|-------------------|--------------------|------------|--------------|------------------------------|---|----------------|------------|--------|-------------------------------|
| 25° cone | 14.0076 | 103.369 | 3961.72 | 540. | 7.95 | 3.96 | 0.034 | 0 | 0.5 | 4.68 | 6,7 |
| 0.7:1.0 Blunt Elliptic Cone | 2.28591 | 87.3098 | 4639.42 | 470. | 10.13 | 1.007 | ----- | 0 and 30 | 1.0 | 11.47 | 9,10 |
| 80° Delta Wing | 6.3648 | 95.2 | 3810. | 810. | 7.9668 | 1.94 | ----- | 40 | 0.125 | 29.405 | 11,12 |
| 10° Cone | 12.672 | 98.2 | 3885. | 910. | 7.9986 | 3.695 | 0.023 | 50 | 1.0 | 25.241 | 13,14 |
| Ogive Cylinder | 24.3 | 102.75 | 2956. | 550. | 5.95 | 5.20 | ----- | ALL | 0.1 | 47.5 | 16,17 25,26 27 |
| X24C-10D | 25.8 | 105.1 | 2989. | 530. | 5.95 | 5.04 | ----- | ALL | 0.19 | 30.45 | 18,19 20,21 22,23 24 |

TABLE II

COMPARISON OF DESIRED AND SMOOTHED PHI ANGLES

| Desired | Smoothed | Desired | Smoothed |
|---------|----------|---------|----------|
| 0.0 | 0. | 115.0 | 111.05 |
| 23.0 | 22.97 | 135.0 | 130.46 |
| 46.0 | 45.81 | 155.0 | 148.24 |
| 69.0 | 68.33 | 170.0 | 164.56 |
| 93.0 | 90.21 | 180.0 | 180.0 |

TABLE III

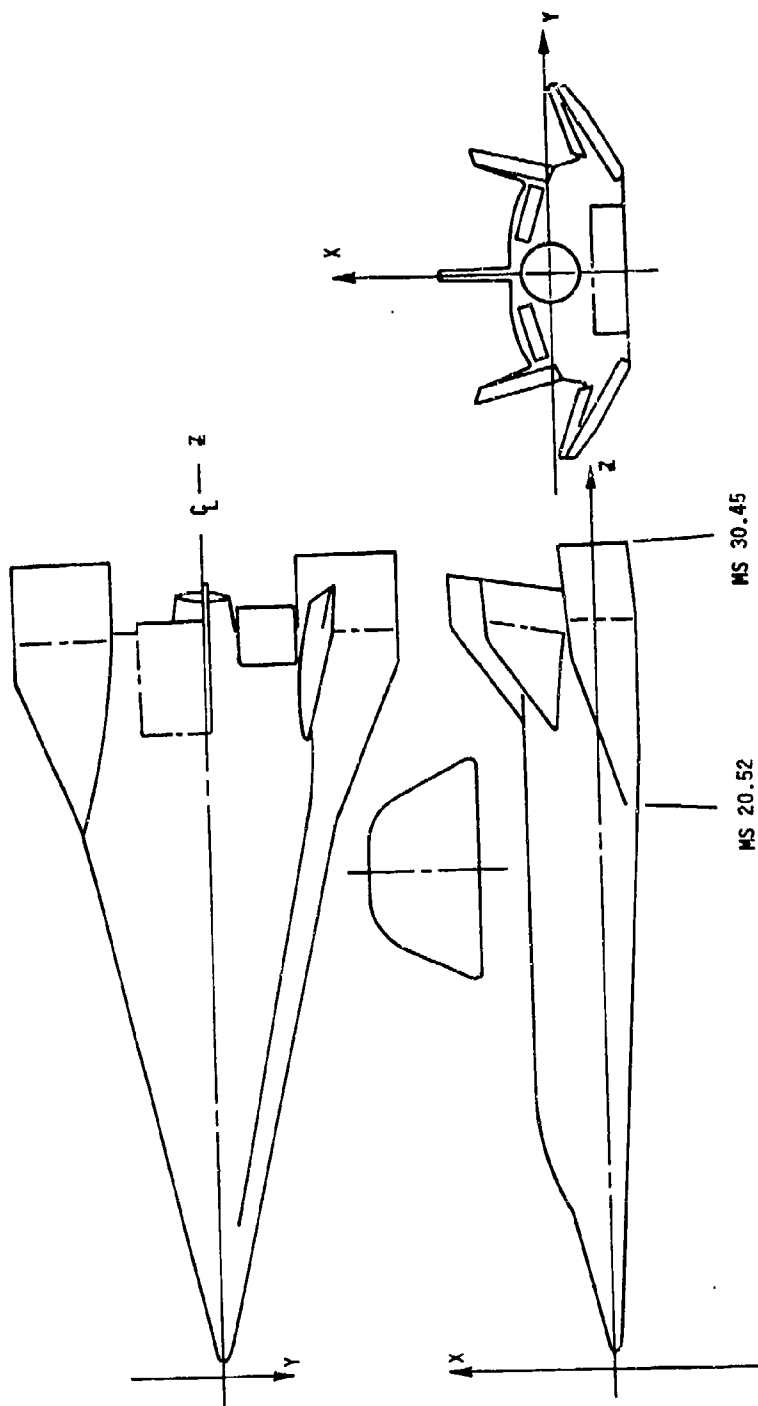
LOCATION OF CIRCUMFERENTIAL PLANES FOR X-24C-10D CASES

Values of ϕ for Angles of Attack of 0° , 2° , 4°

| | | | | |
|-------|-------|-------|--------|--------|
| 0.00 | 30.44 | 64.85 | 107.63 | 151.89 |
| 10.04 | 41.14 | 78.27 | 122.70 | 166.01 |
| 20.14 | 52.52 | 92.66 | 137.49 | 180.00 |

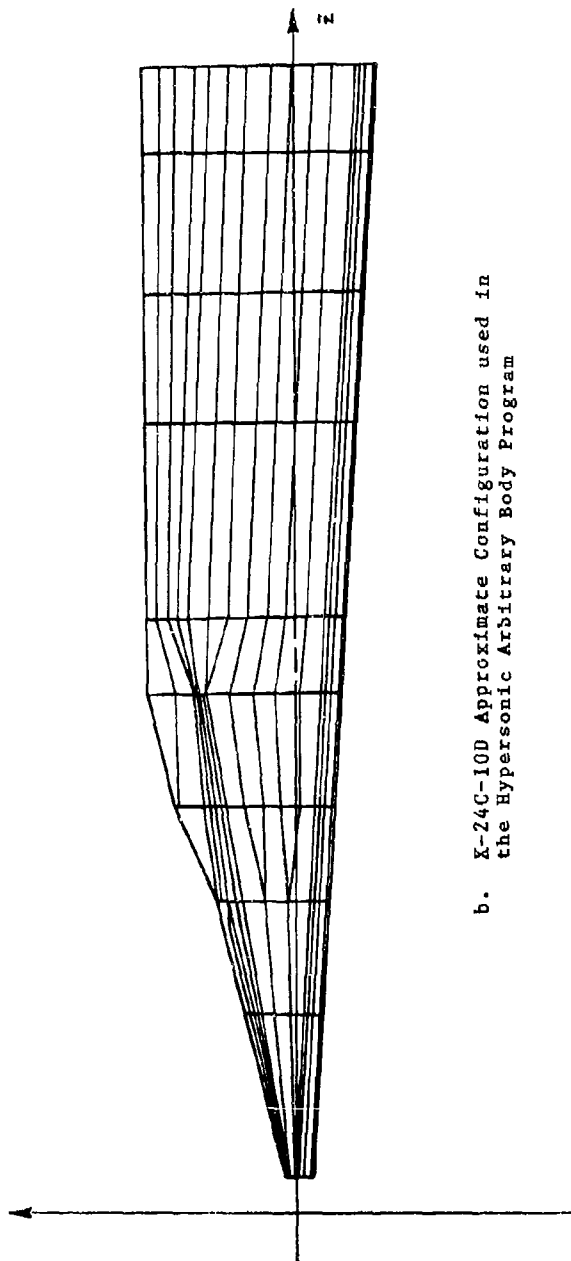
Values of ϕ for Angles of Attack of 6°

| | | | | |
|-------|-------|--------|--------|--------|
| 0.00 | 42.42 | 90.07 | 136.66 | 180.00 |
| 13.61 | 57.91 | 106.93 | 151.33 | |
| 27.66 | 73.92 | 121.58 | 165.73 | |



a. X-24C-10D Wind Tunnel Model Configuration

Figure 1. X-24C-10D Geometry



b. X-24C-10D Approximate Configuration used in
the Hypersonic Arbitrary Body Program

Figure 1. Concluded

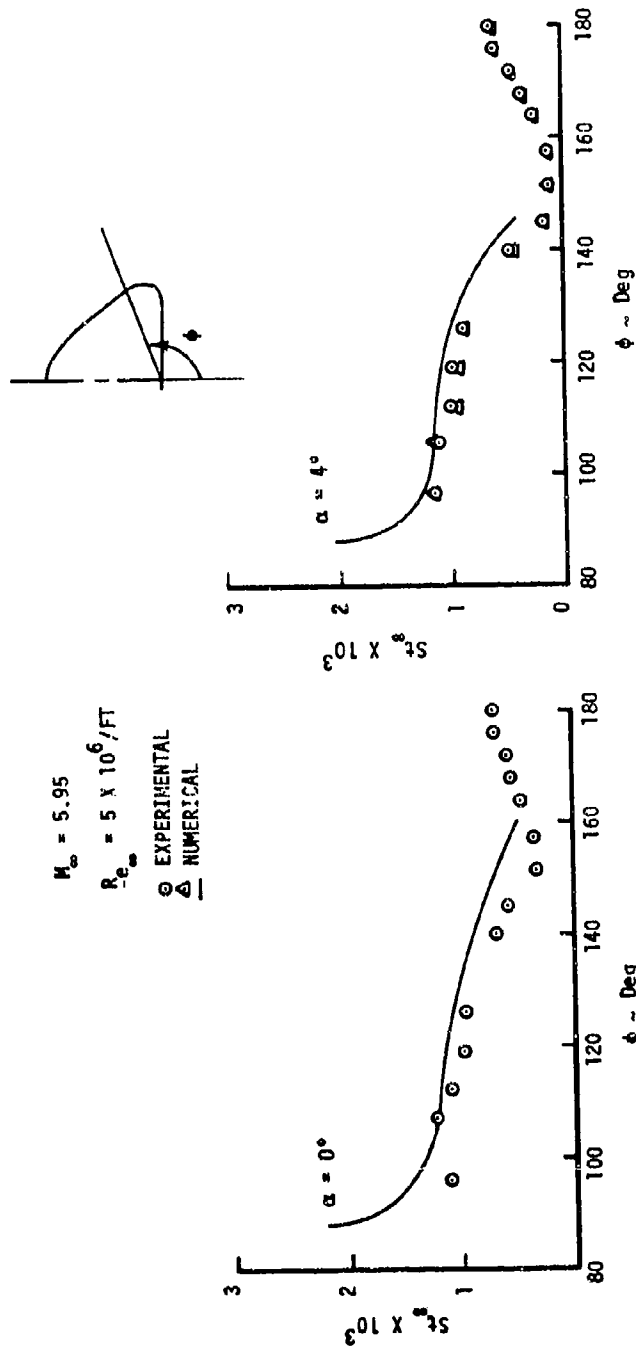


Figure 2. Comparison of Numerical and Experimental Stanton Numbers for the X-24C-10D Side Panel at Model Station 20.52

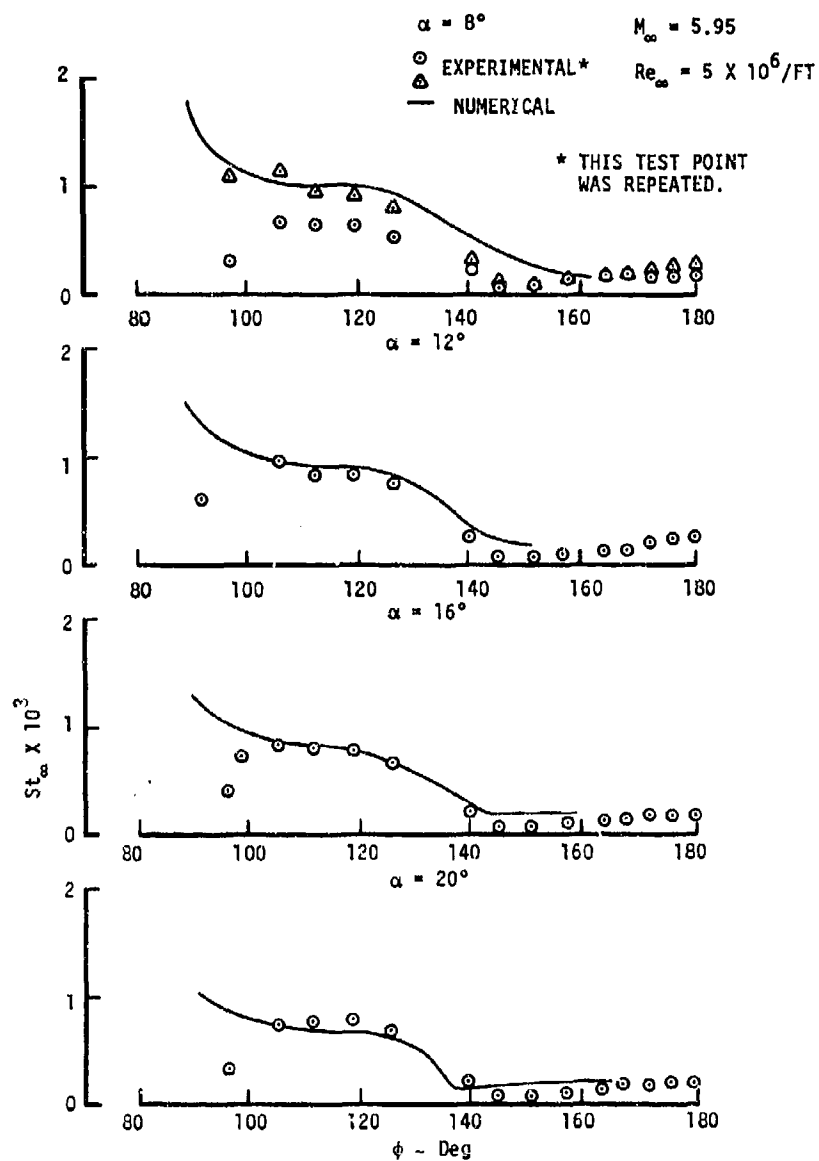


Figure 2. Concluded

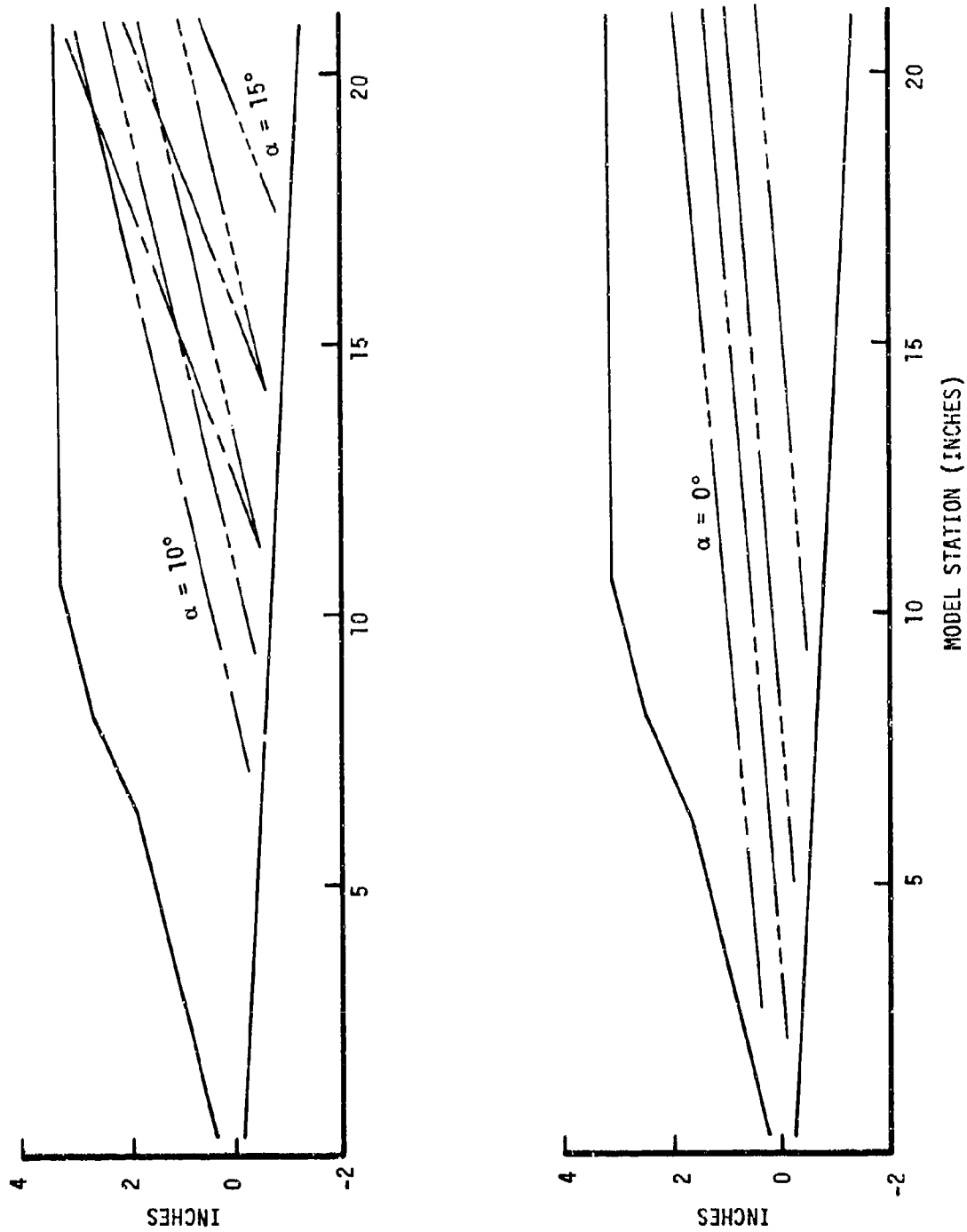


Figure 3. Location of X-24C-10D Streamlines (HABP)

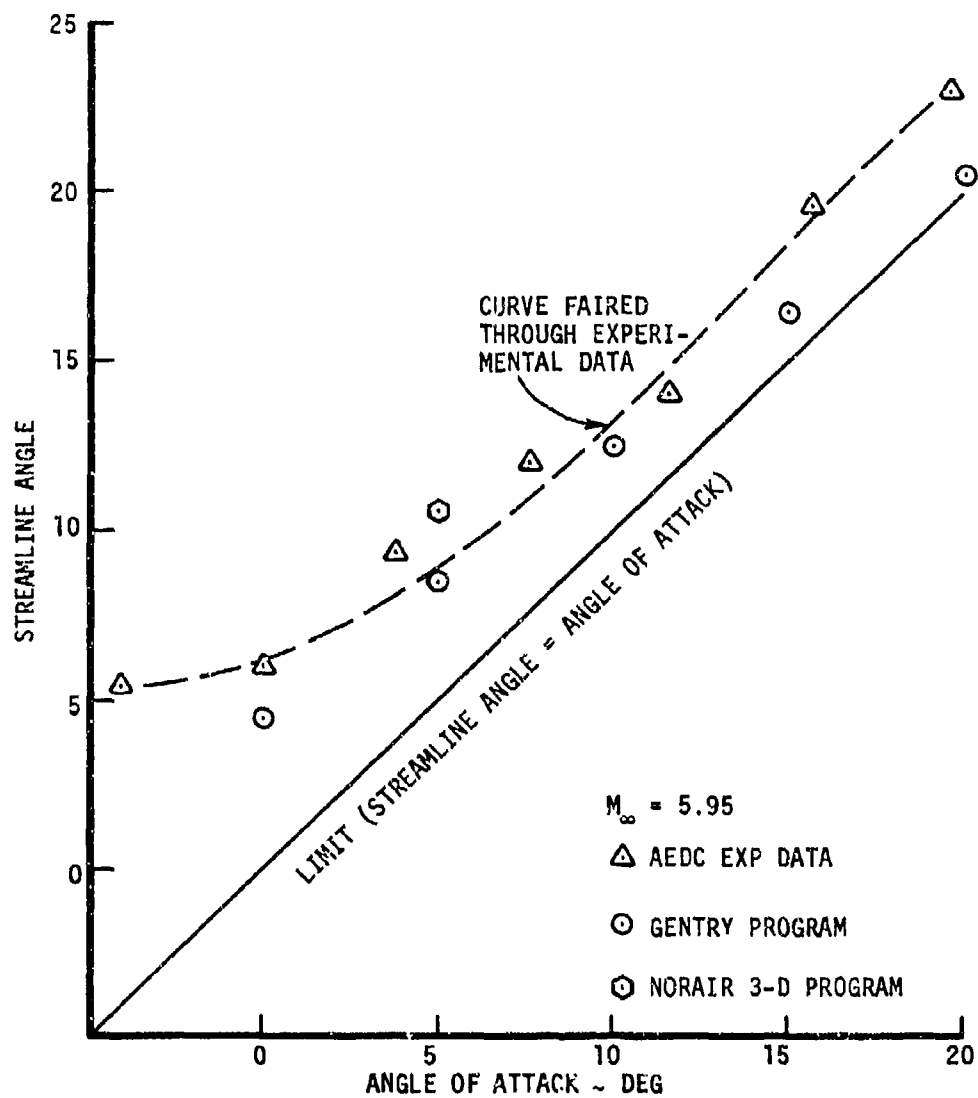


Figure 4. Plot of Streamline Angle Vs Angle of Attack

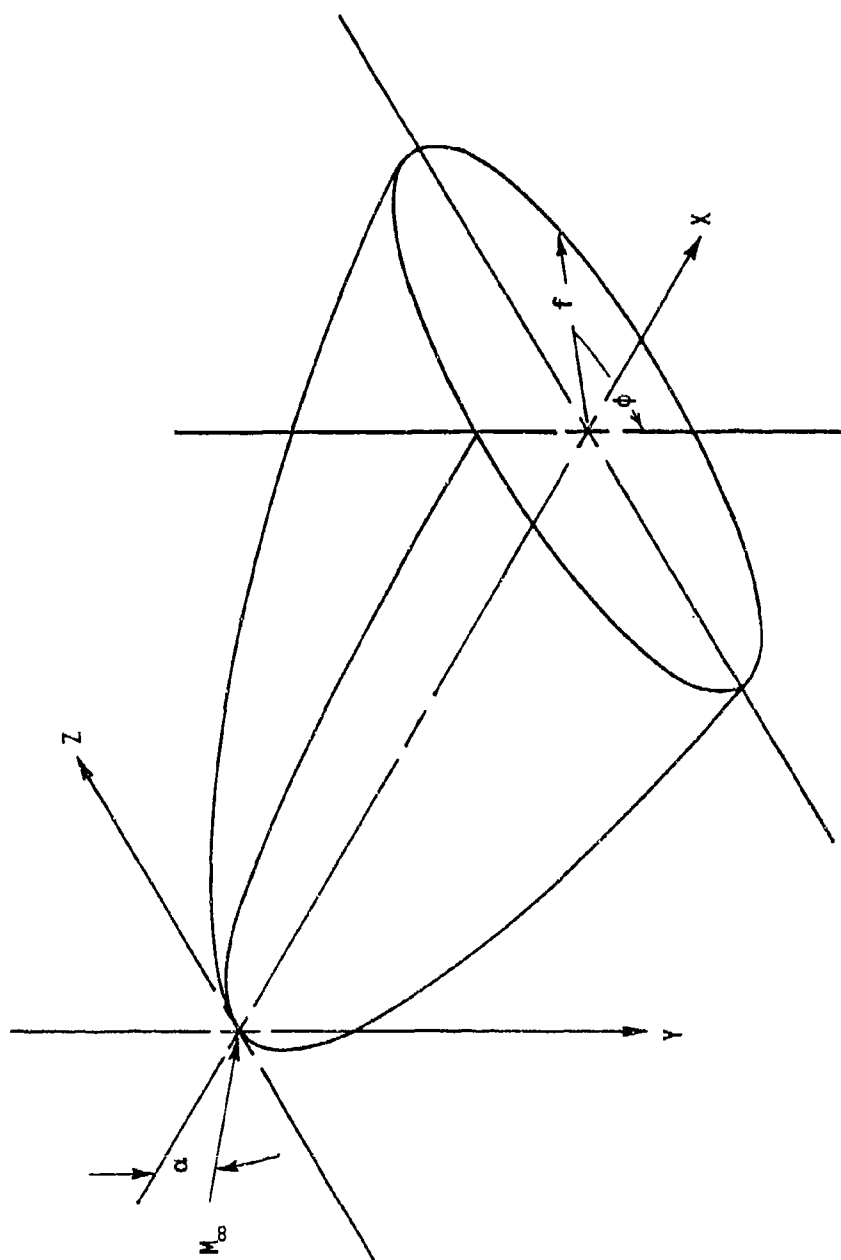


Figure 5. Orthogonal Coordinate System and Body Orientation for the DeJarnette Program

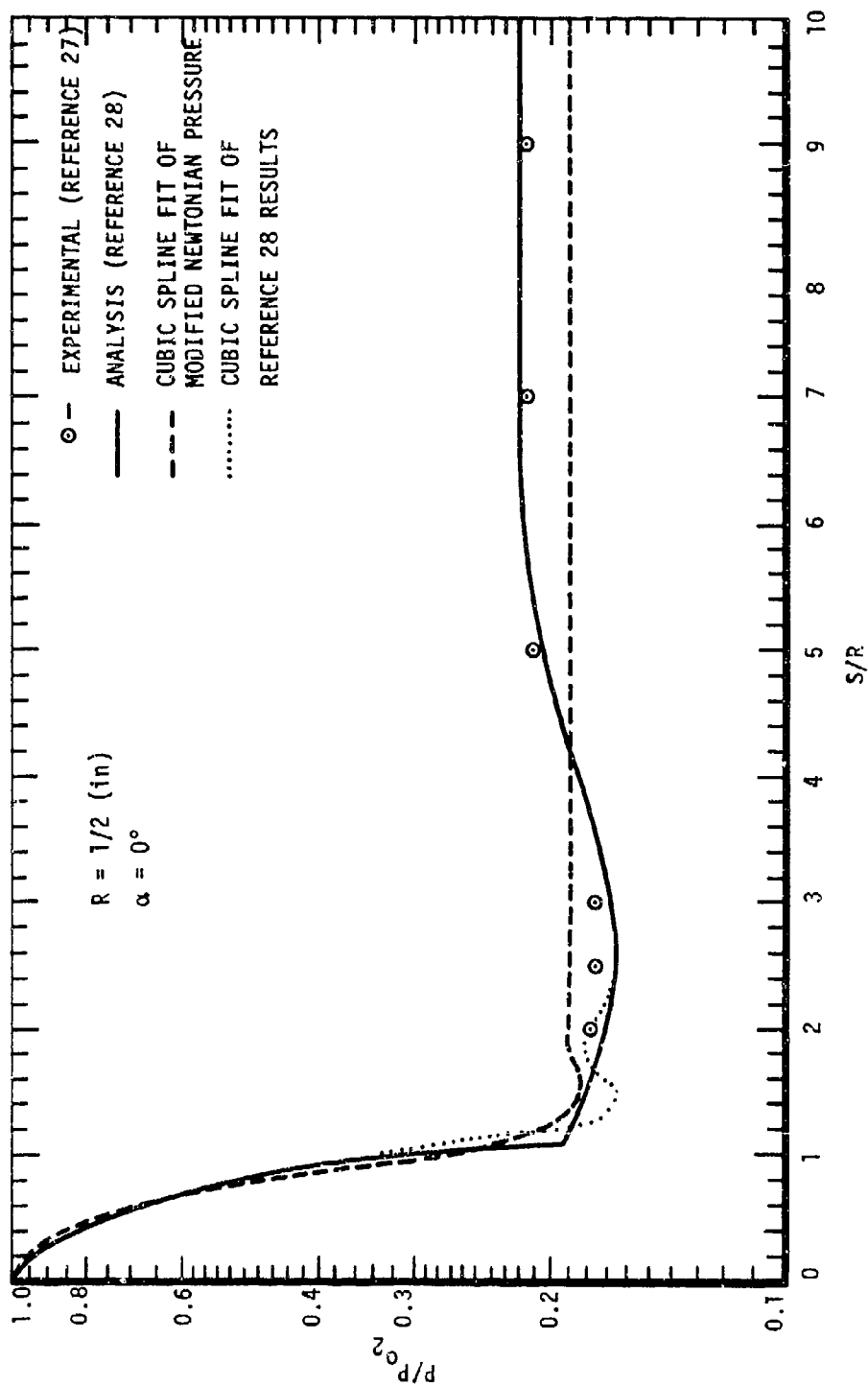


Figure 6. 25° Cone Pressure Distribution

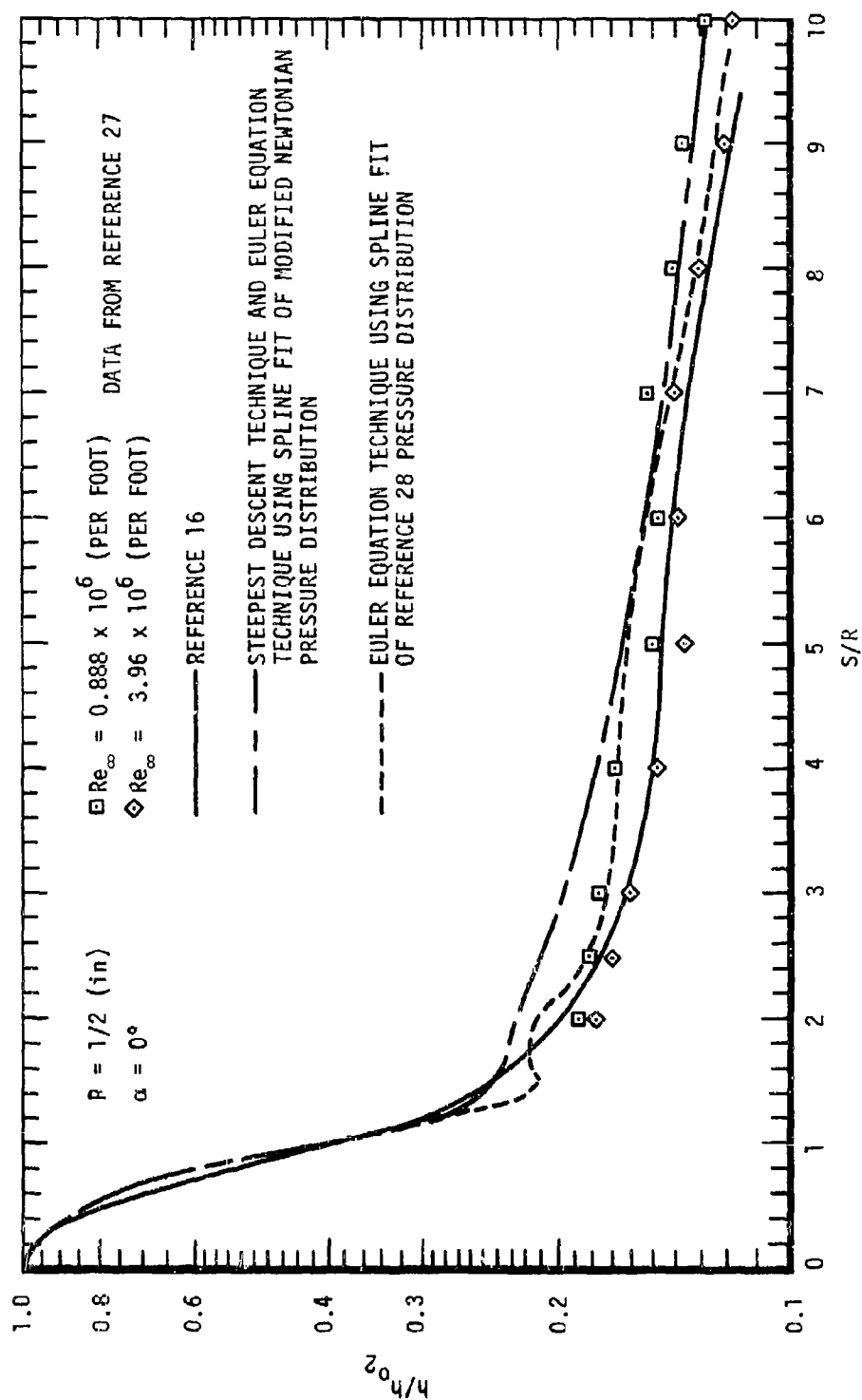


Figure 7. 25° Cone Heat-Transfer Distribution

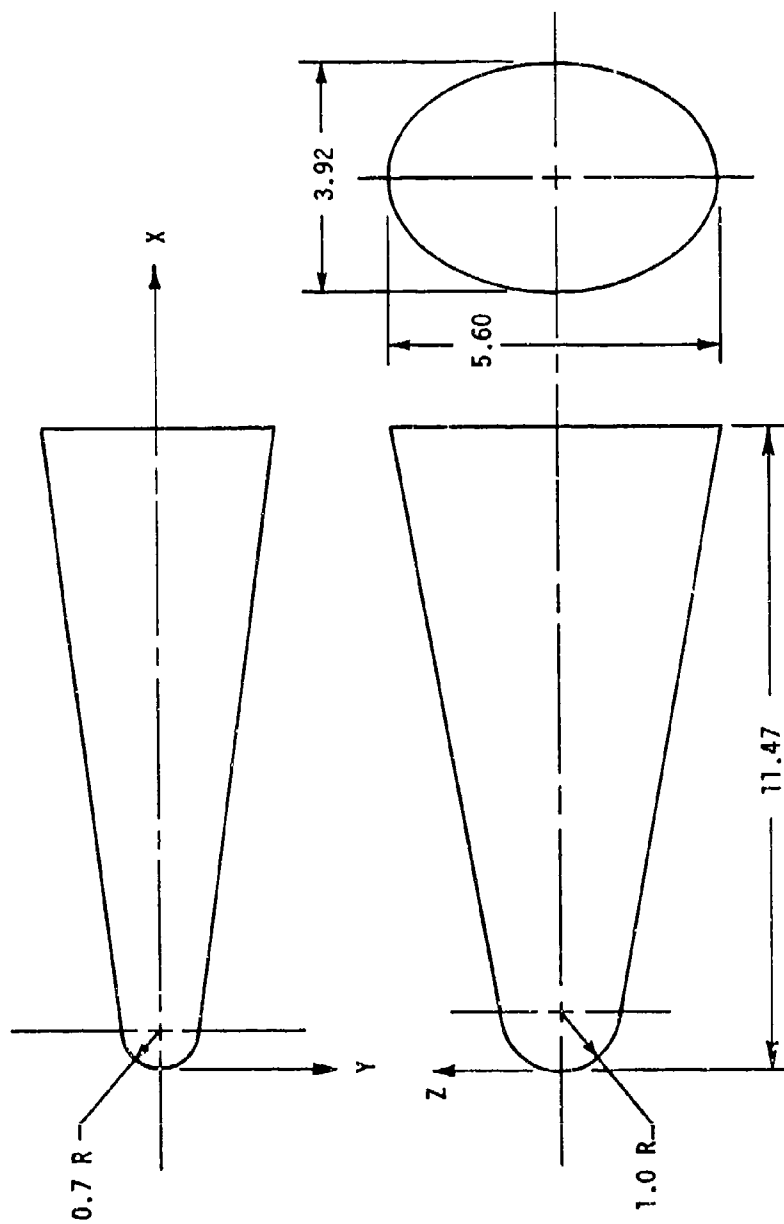


Figure 8. 0.7:1.0 Elliptical Cone Description

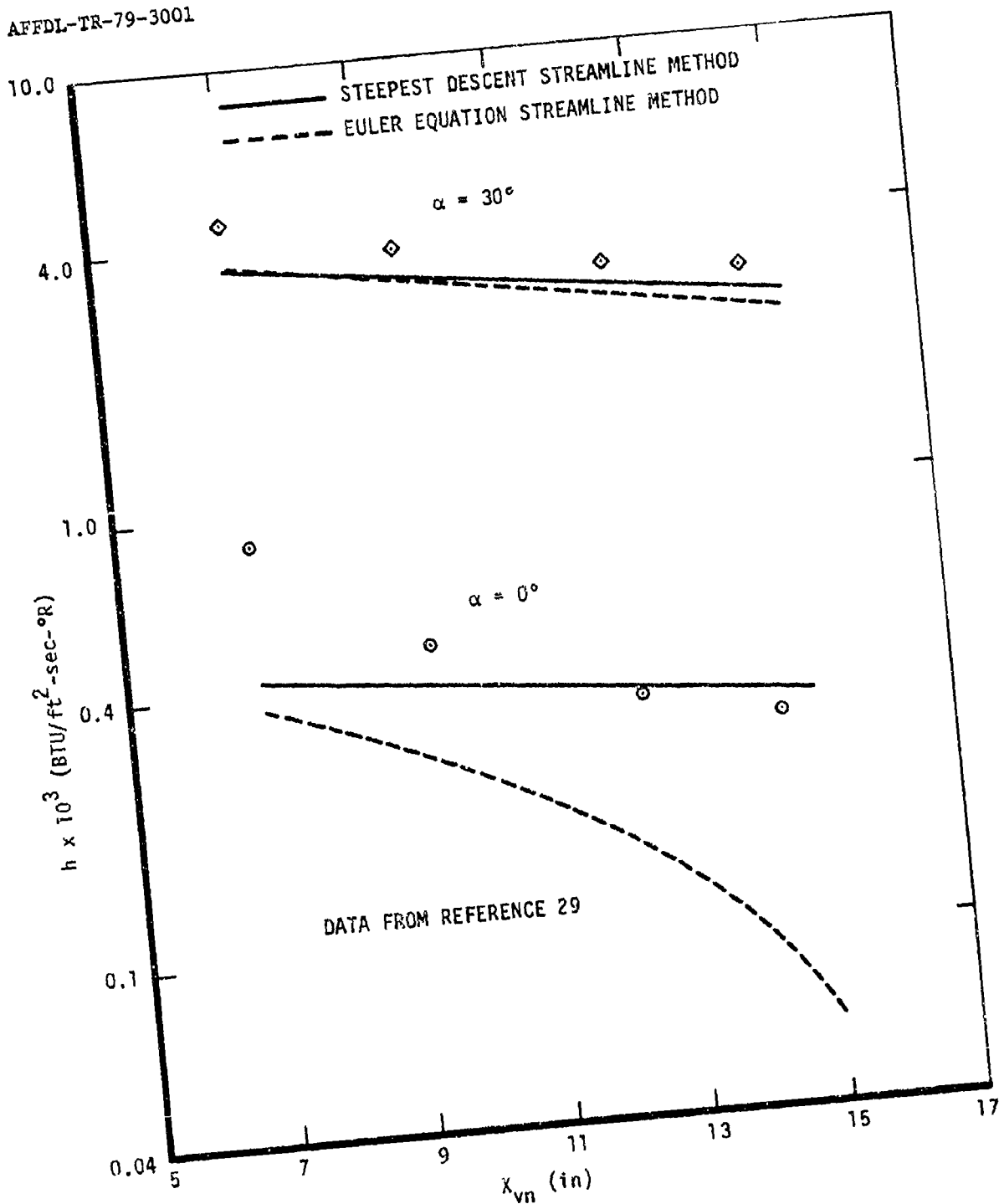


Figure 9. 0.7:1.0 Elliptical Cone Windward Streamline Heat-Transfer Distribution

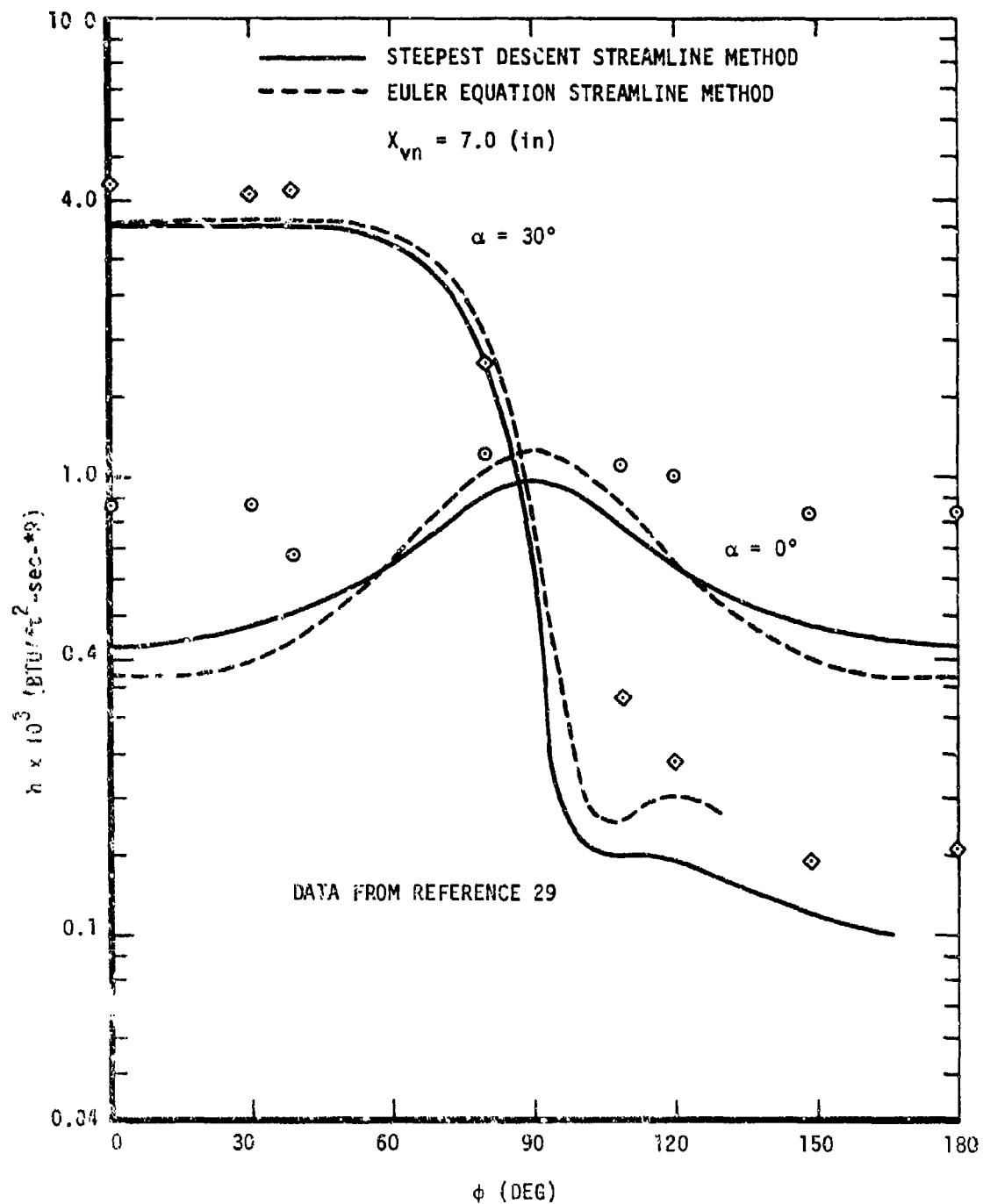


Figure 10. 0.7:1.0 Elliptical Cone Circumferential Heat-Transfer Distribution

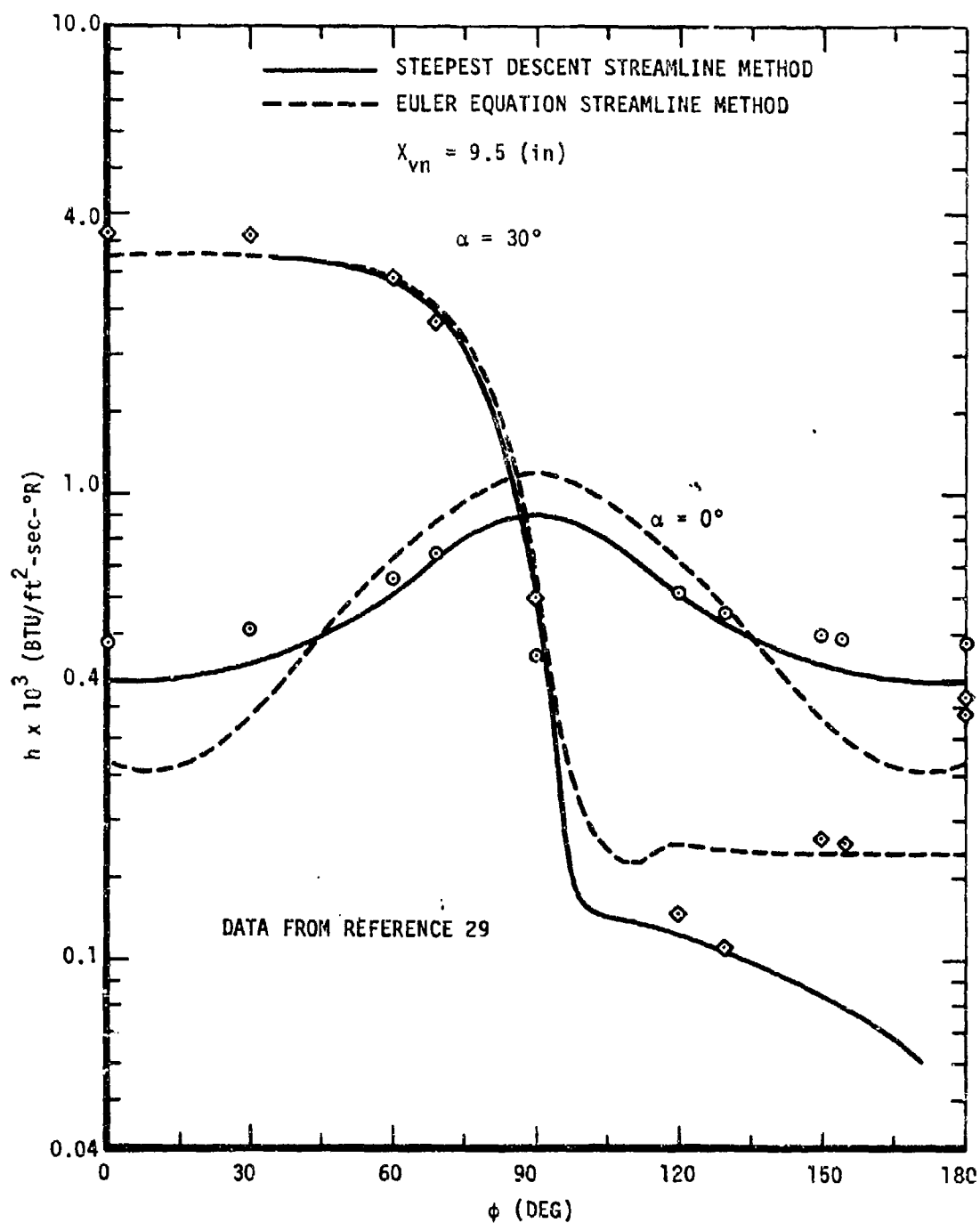


Figure 10. Continued

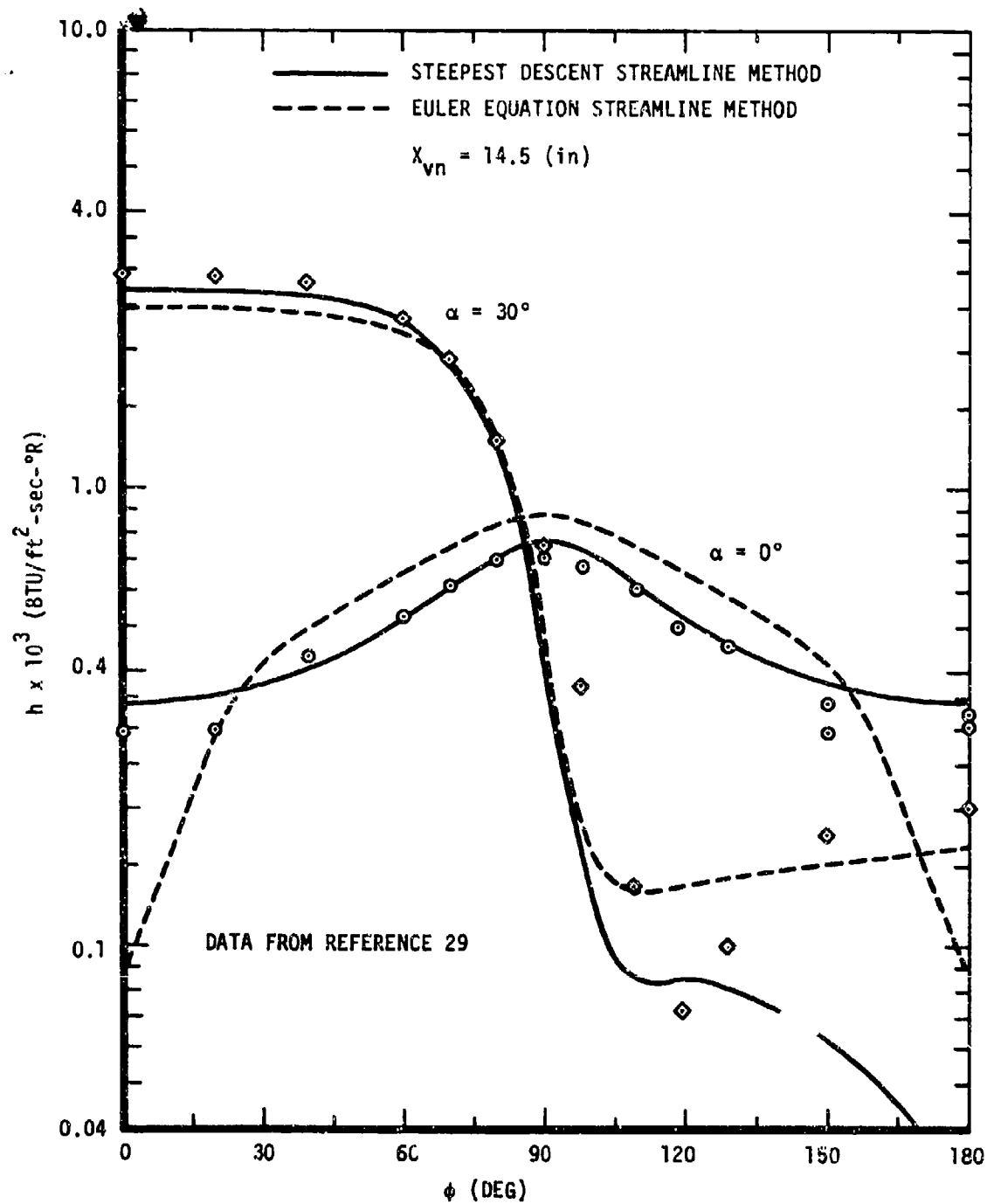


Figure 10. Concluded

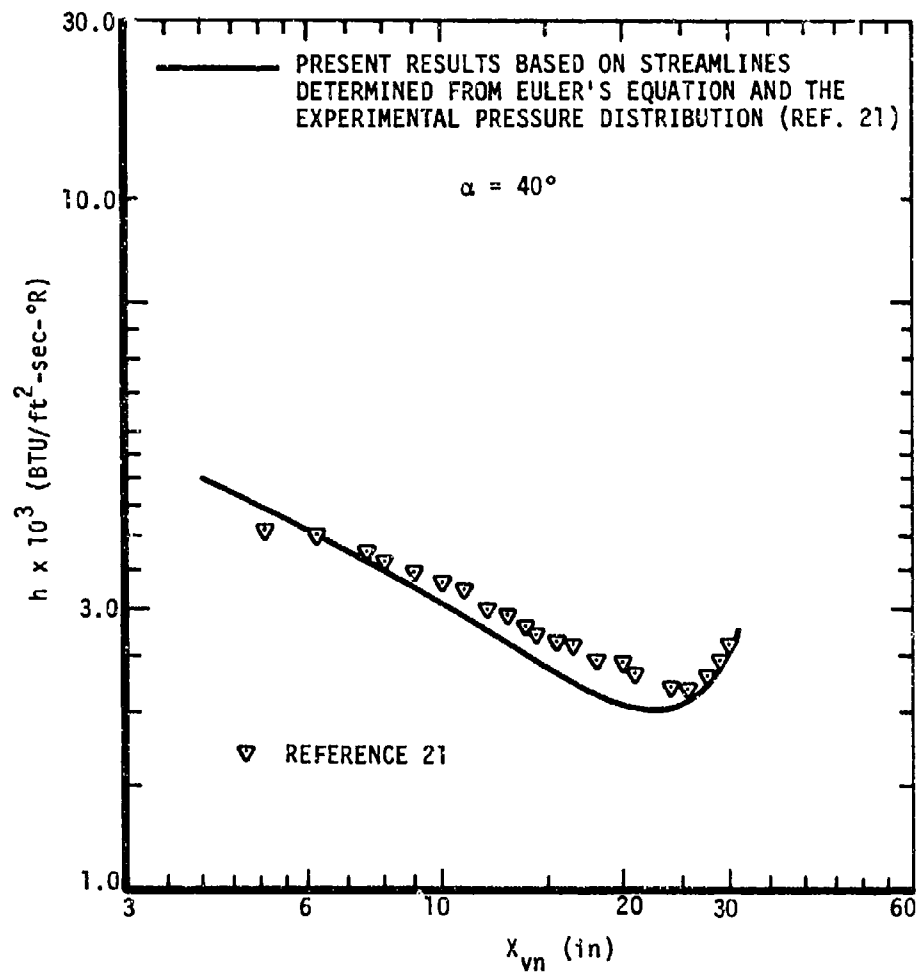


Figure 11. 80° Delta Wing Windward Streamline Heat-Transfer Distribution

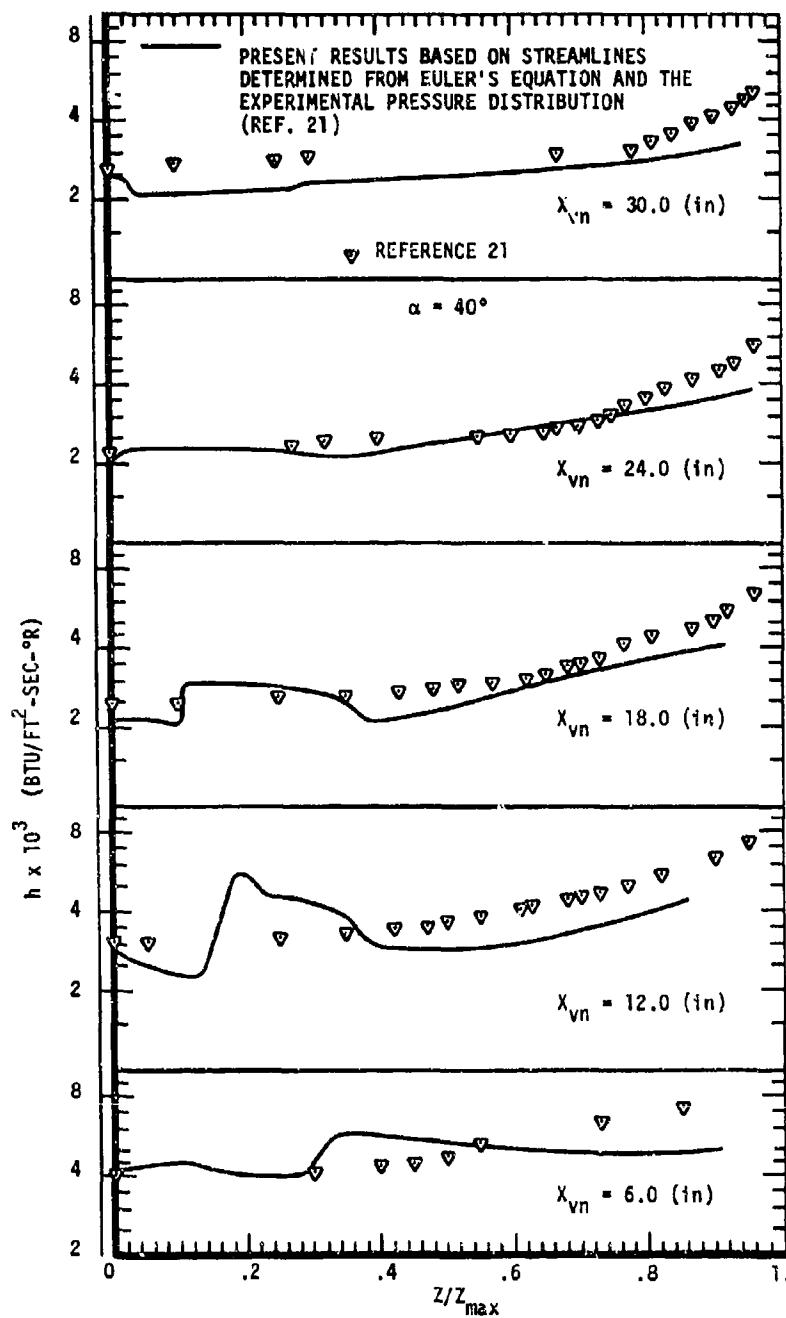


Figure 12. 80° Delta Wing Spanwise Heat-Transfer Distribution

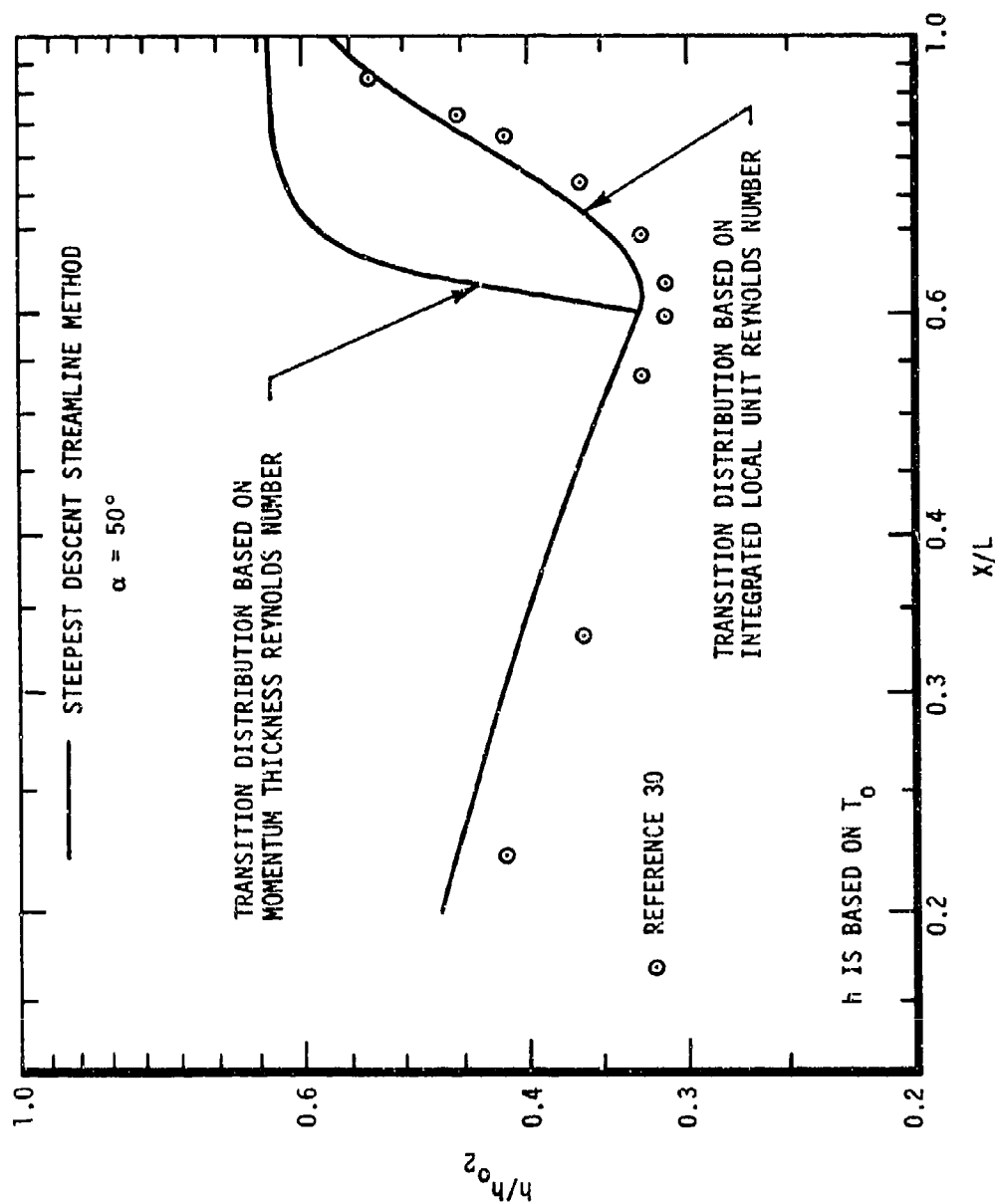
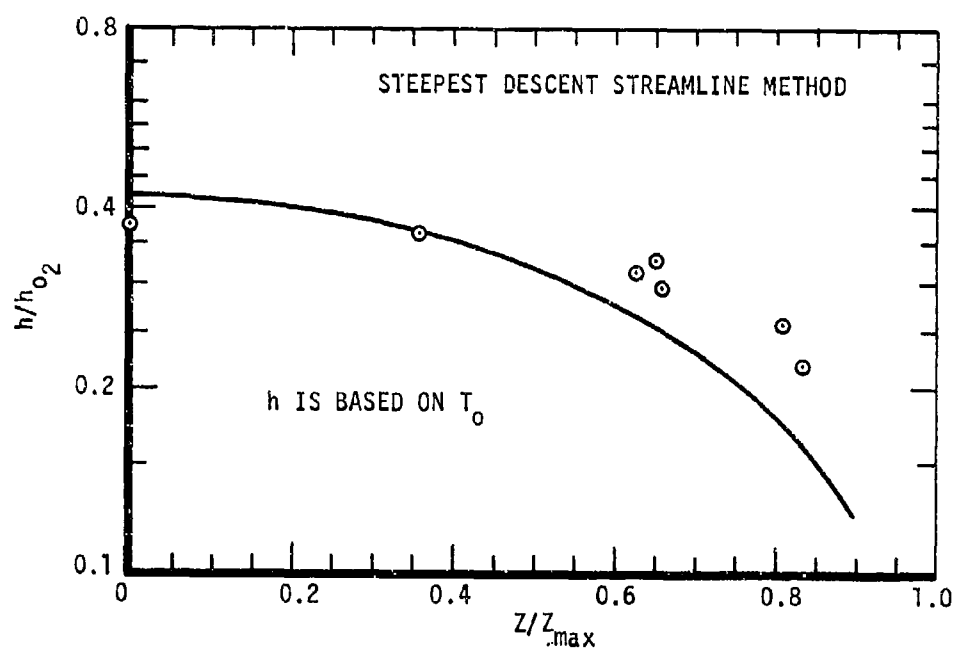
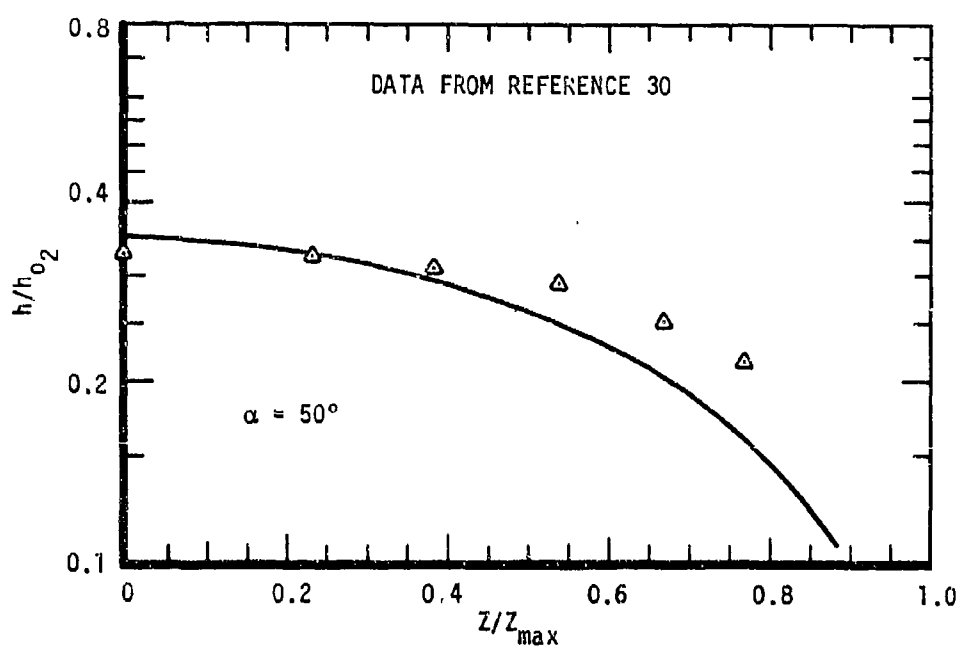


Figure 13. 10° Cone Windward Streamline Heat-Transfer Distribution

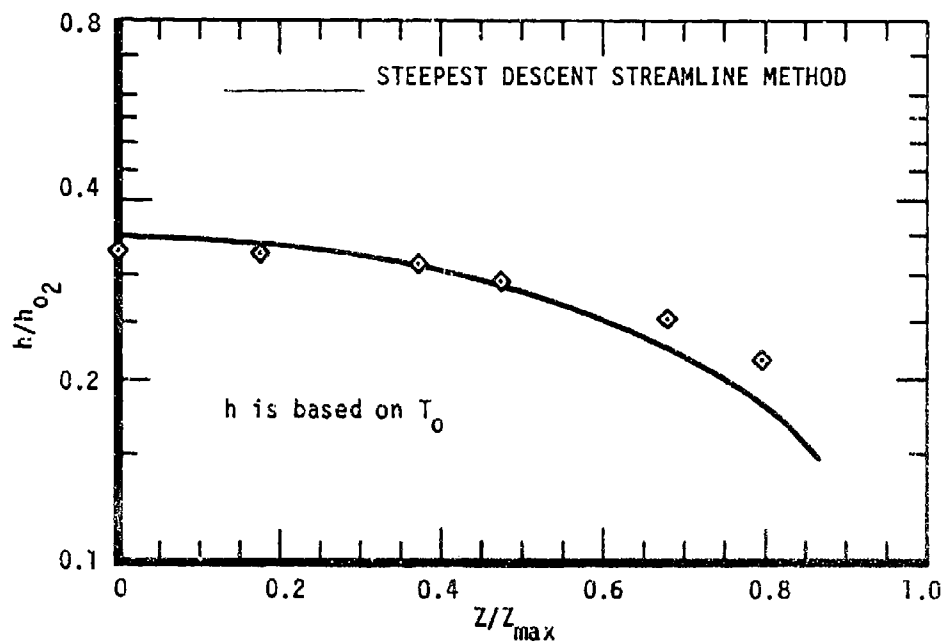


(a) $X/L = 0.3$

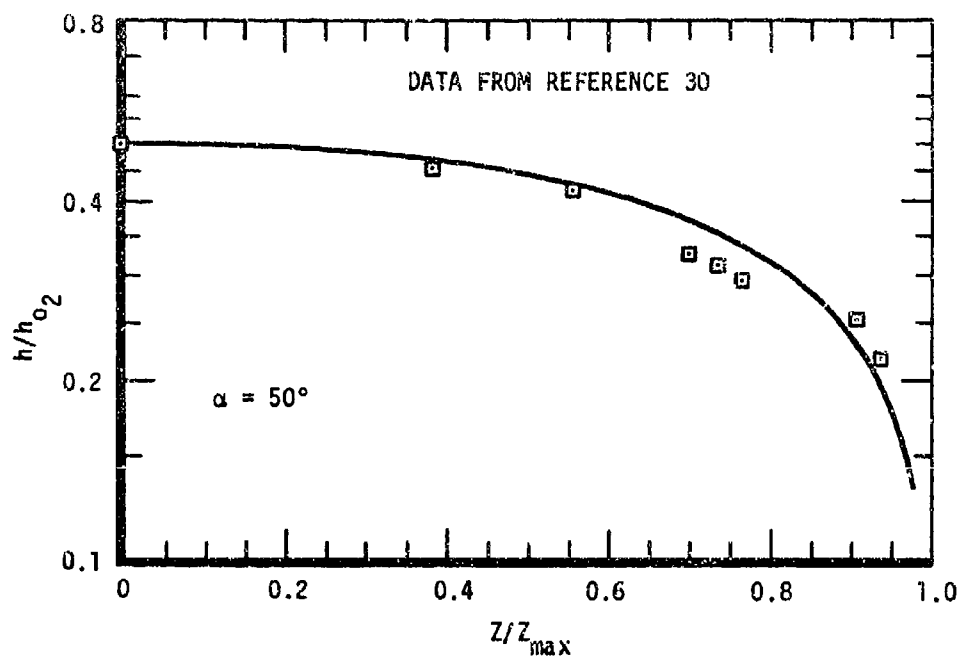


(b) $X/L = 0.5$

Figure 14. 10° Cone Spanwise Heat-Transfer Distribution



(c) $X/L = 0.7$



(d) $X/L = 0.9$

Figure 14. Concluded

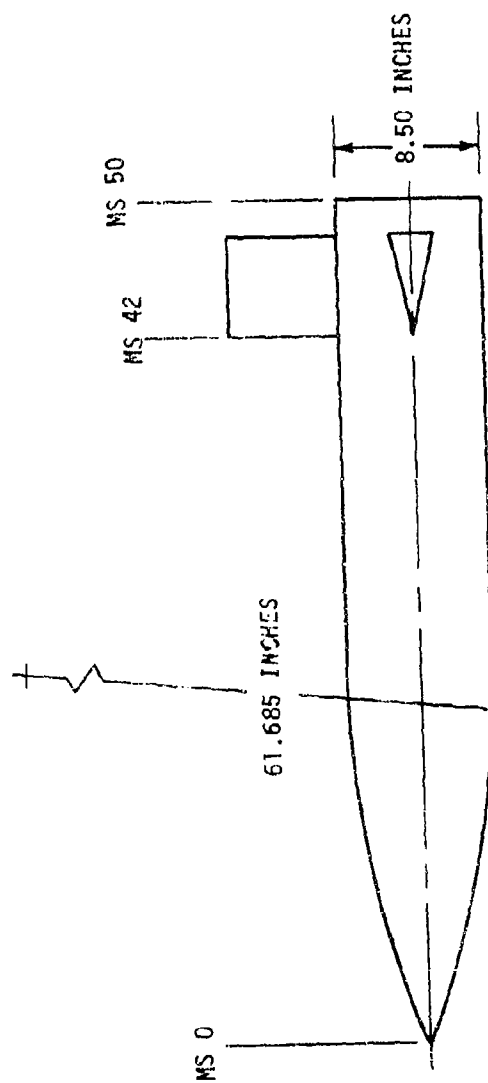
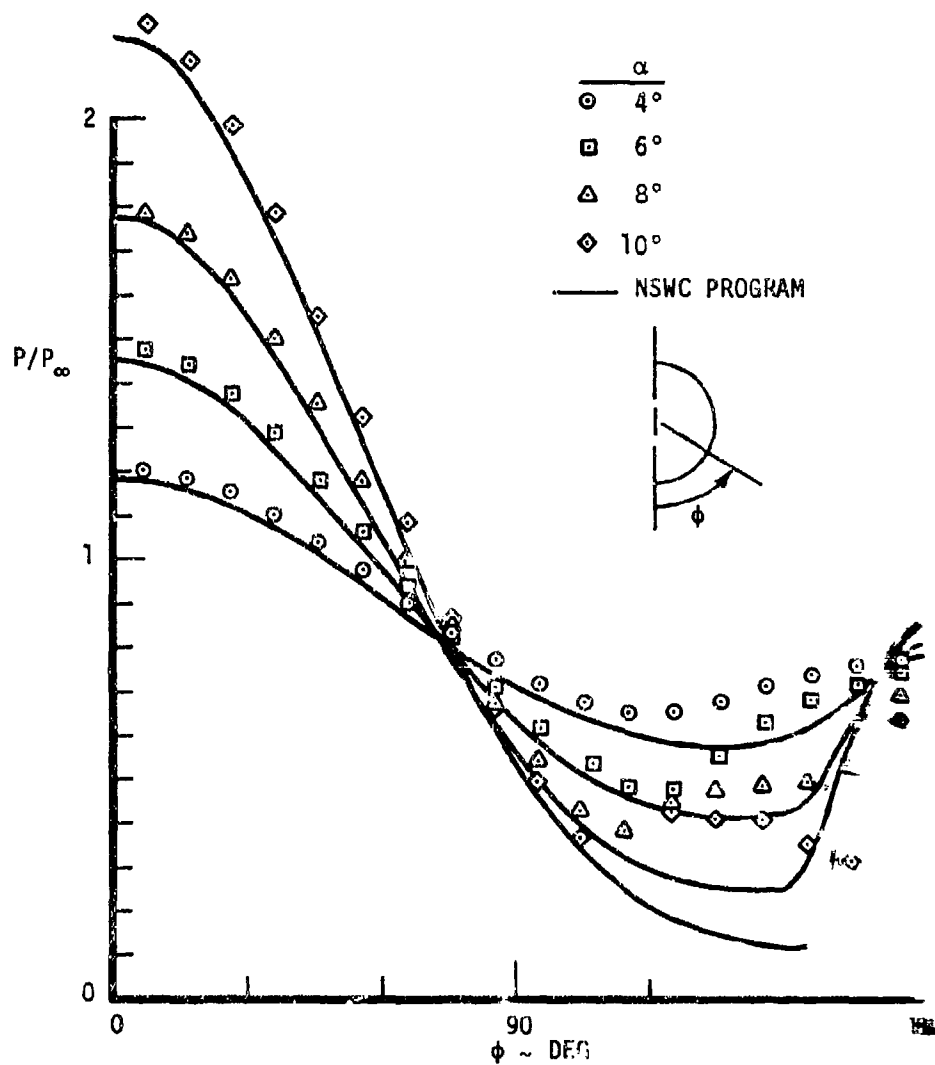


Figure 15. Ogive-Cylinder Geometry

Figure 16. Surface Pressures on Ogive-Cylinder at Model S: $\alpha = 4^\circ, 6^\circ, 8^\circ, 10^\circ$

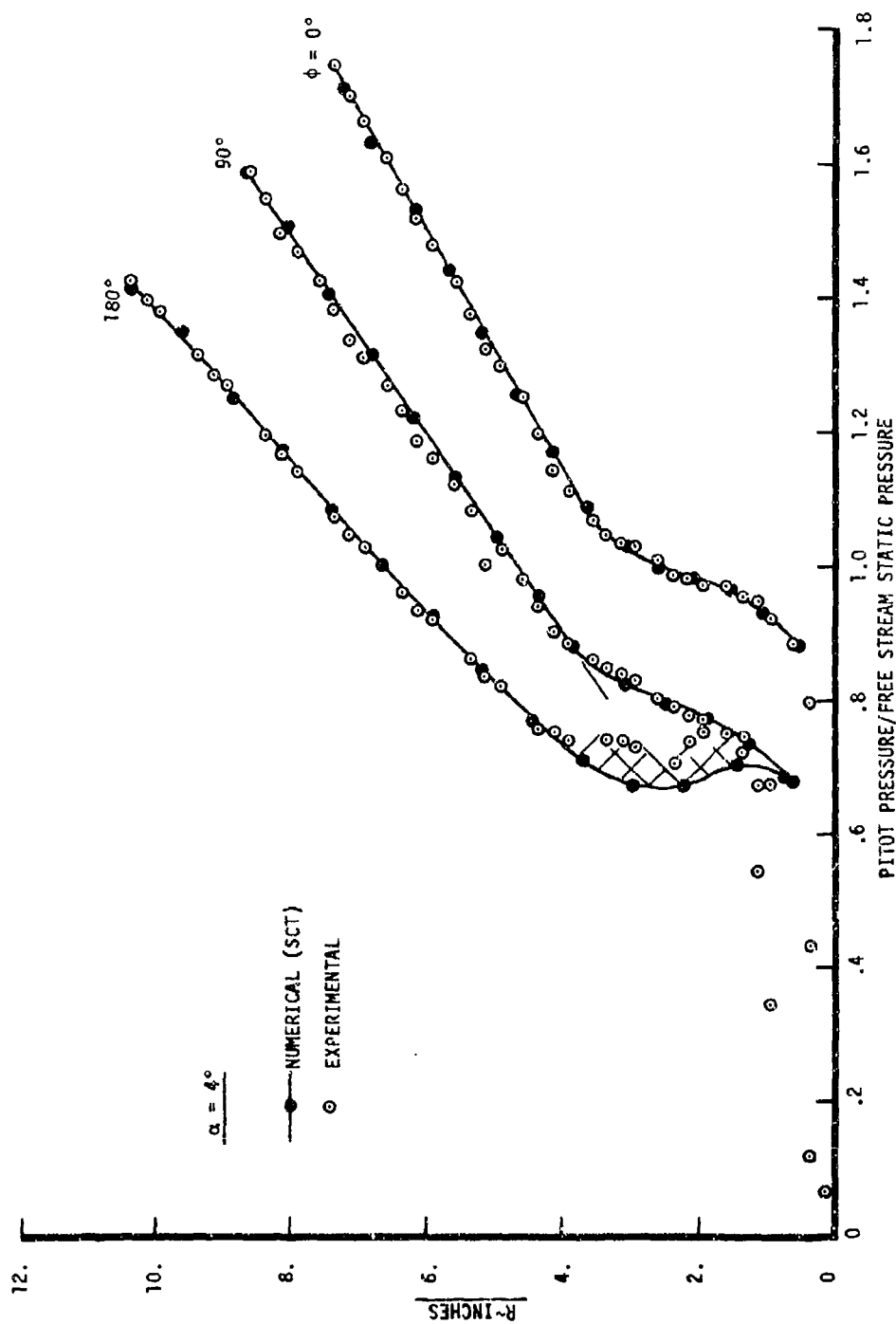


Figure 17. Pitot Pressure Surveys for the Ogive-Cylinder at Model Station 41.7

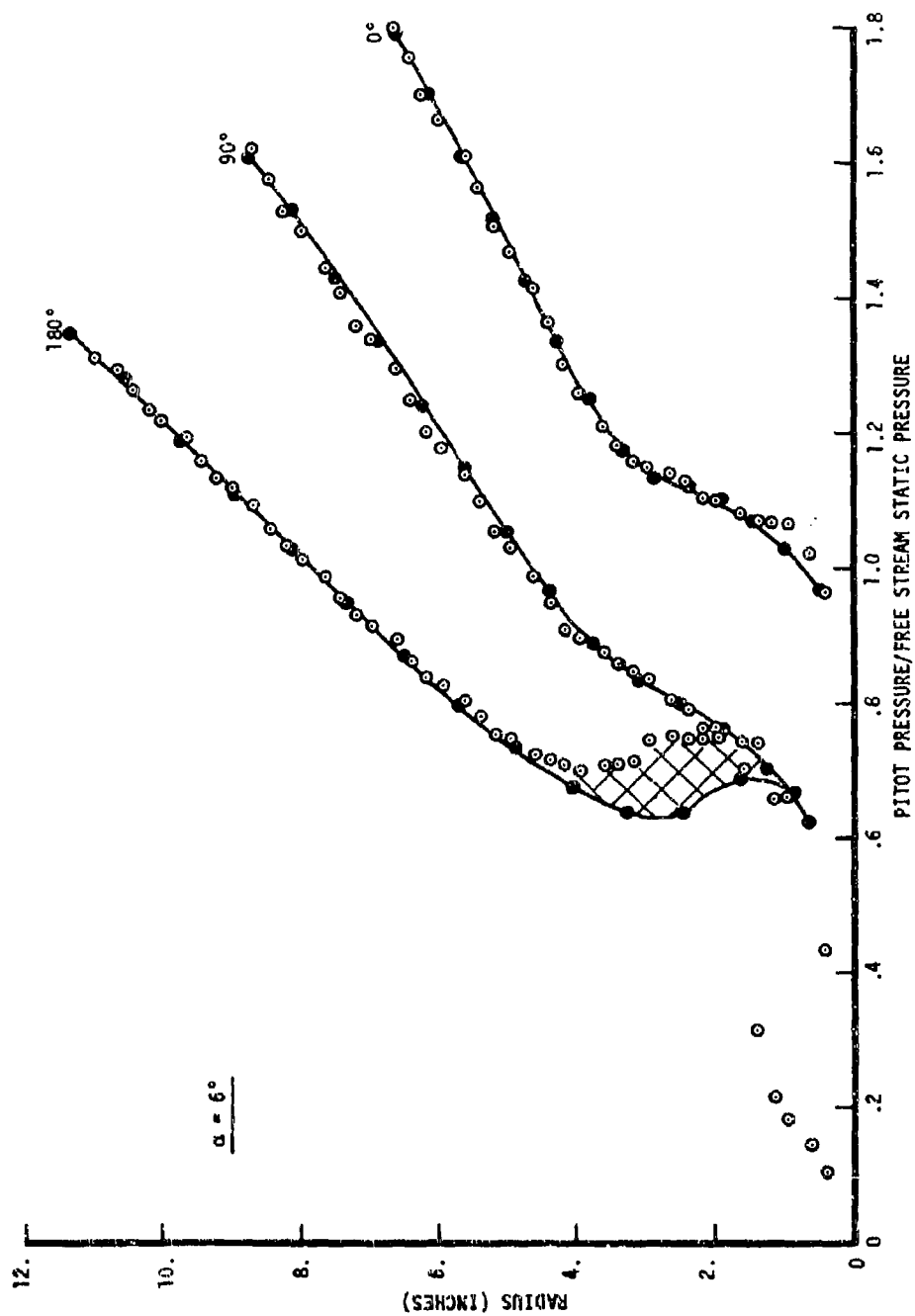


Figure 17. Continued

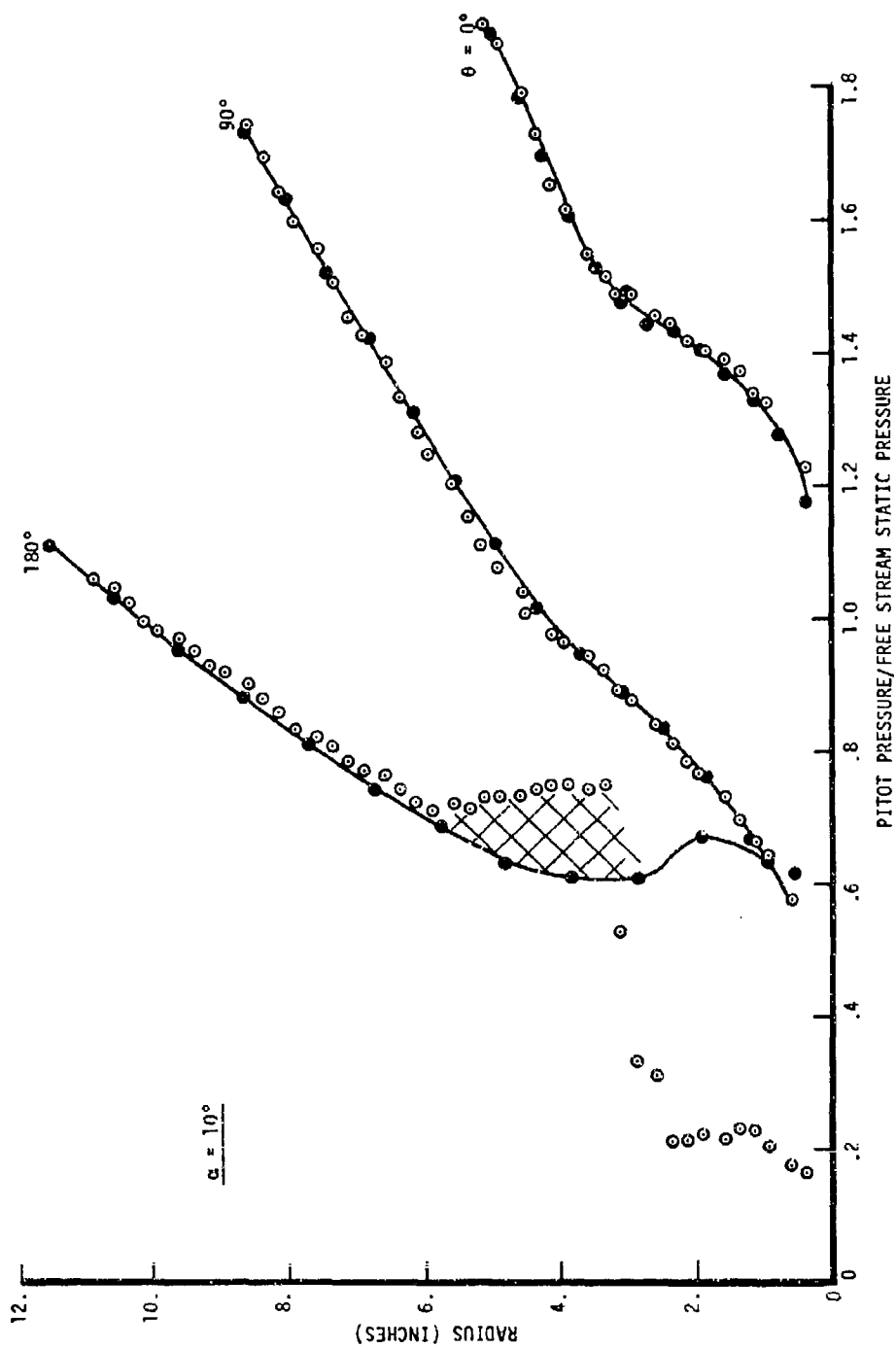


Figure 17. Concluded

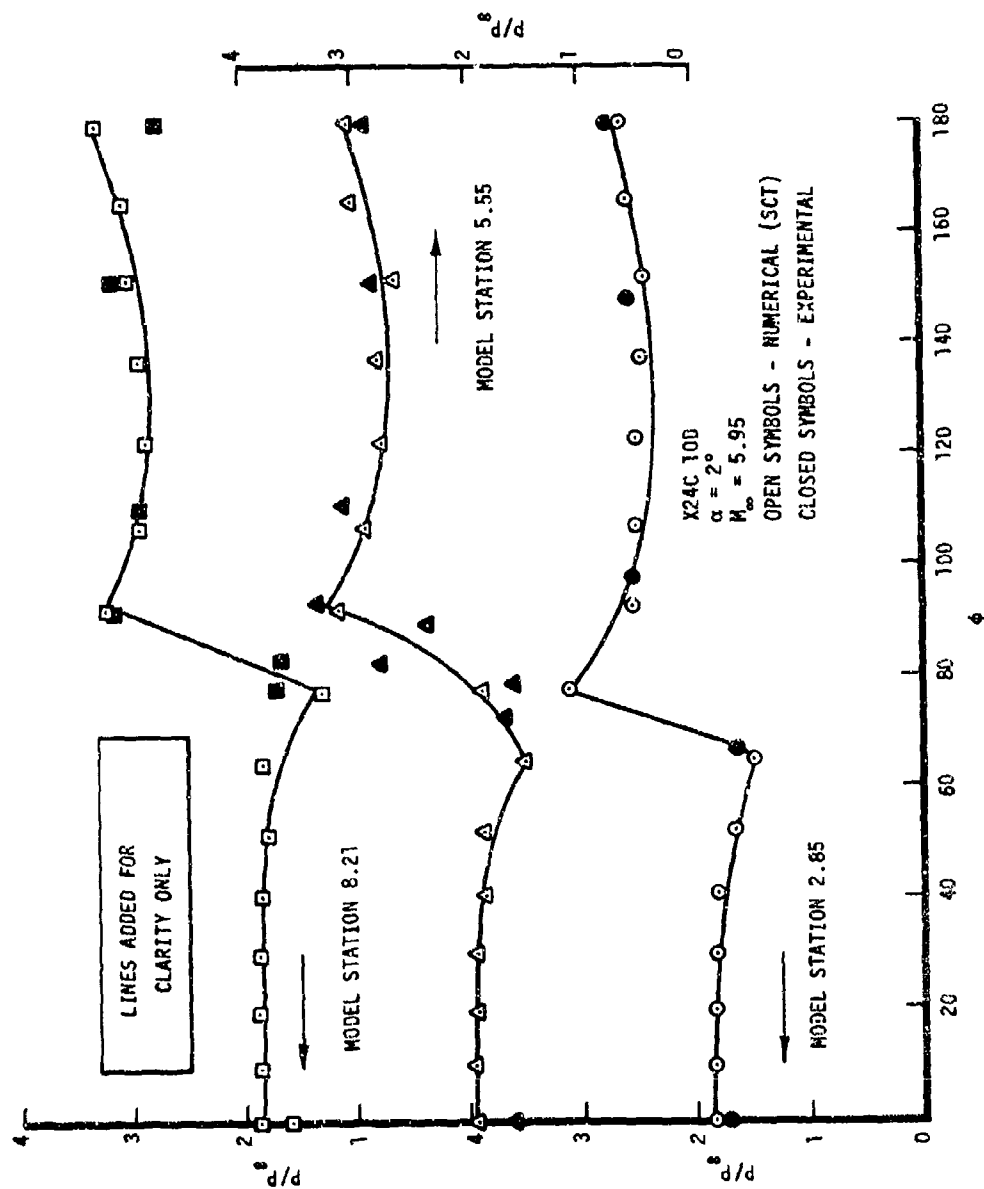


Figure 18. Surface Pressures on the X24C-100 at 2° Angle of Attack

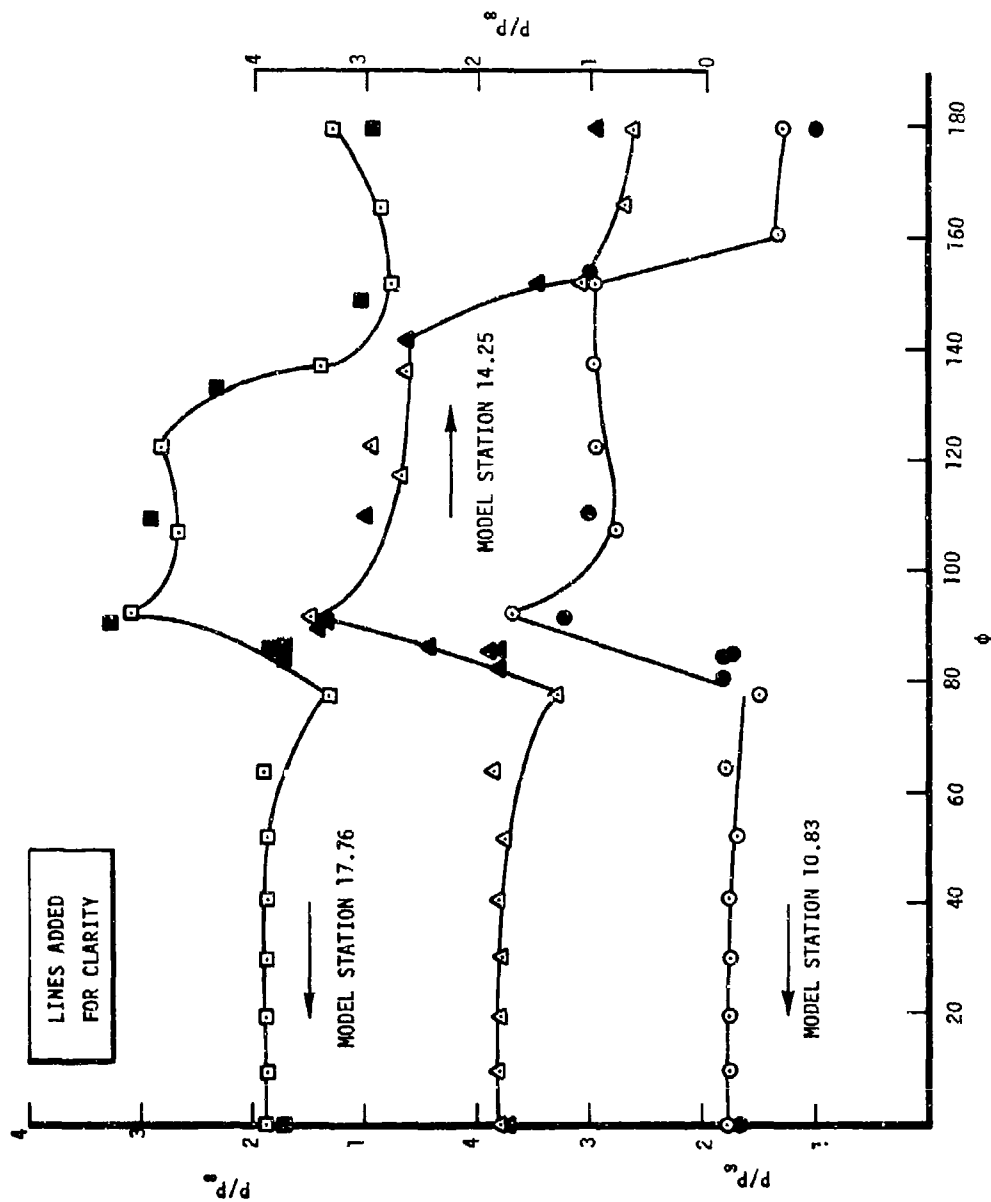


Figure 18. Continued

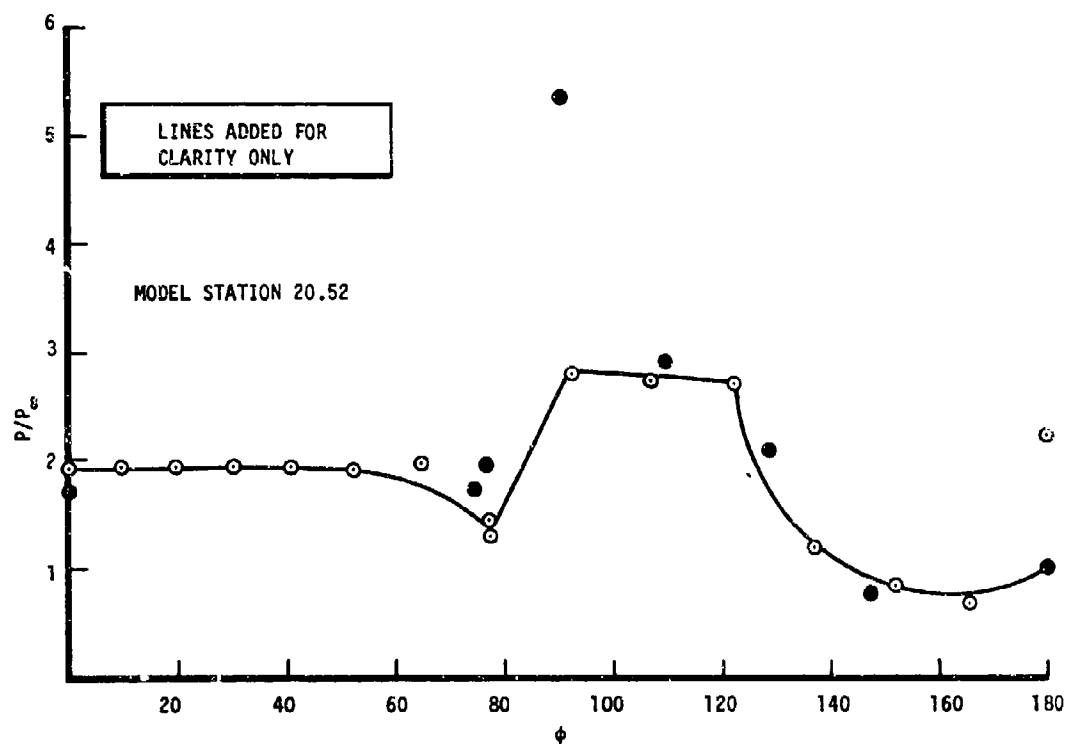


Figure 18. Concluded

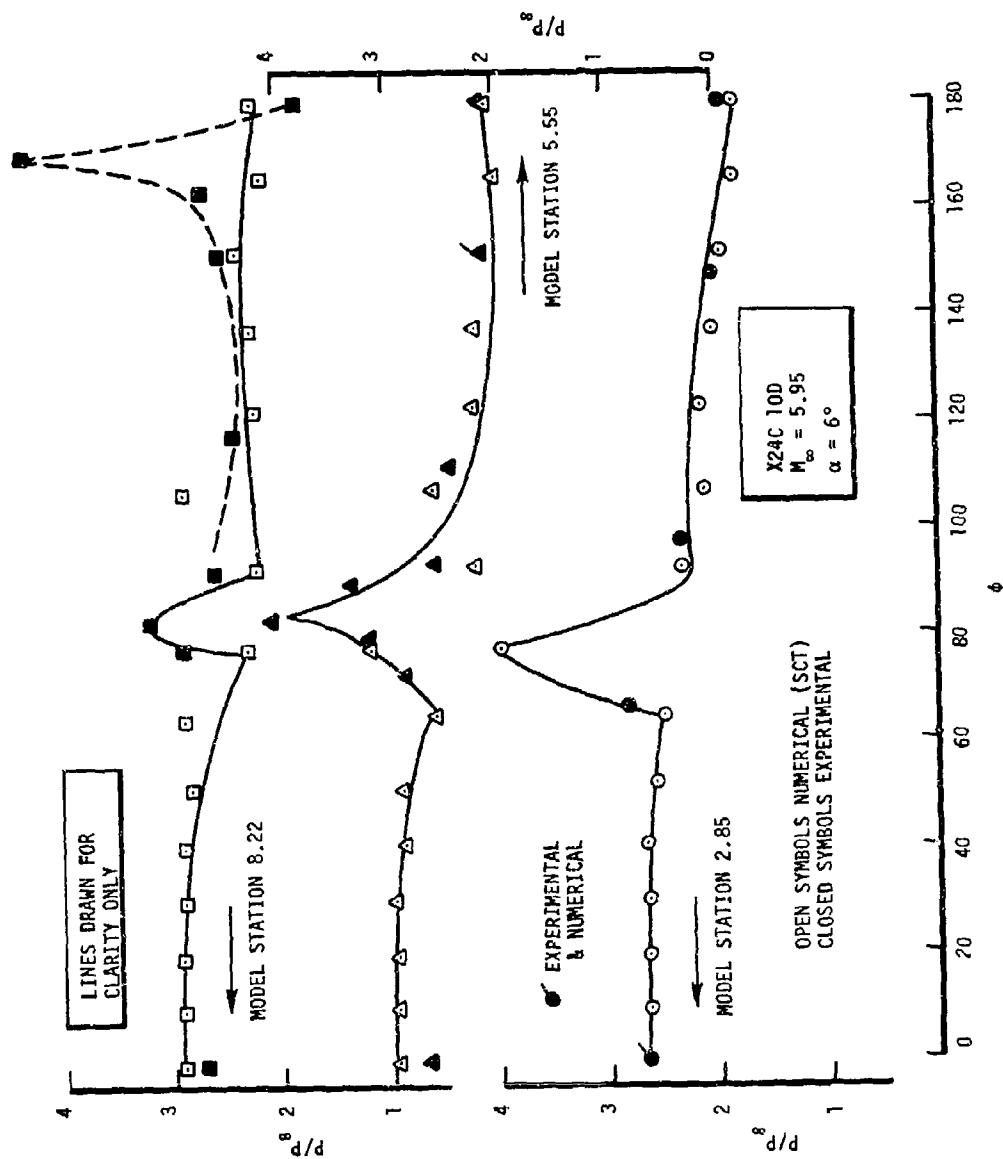


Figure 19. Surface pressures on the X24C-10D at 6° Angle of Attack

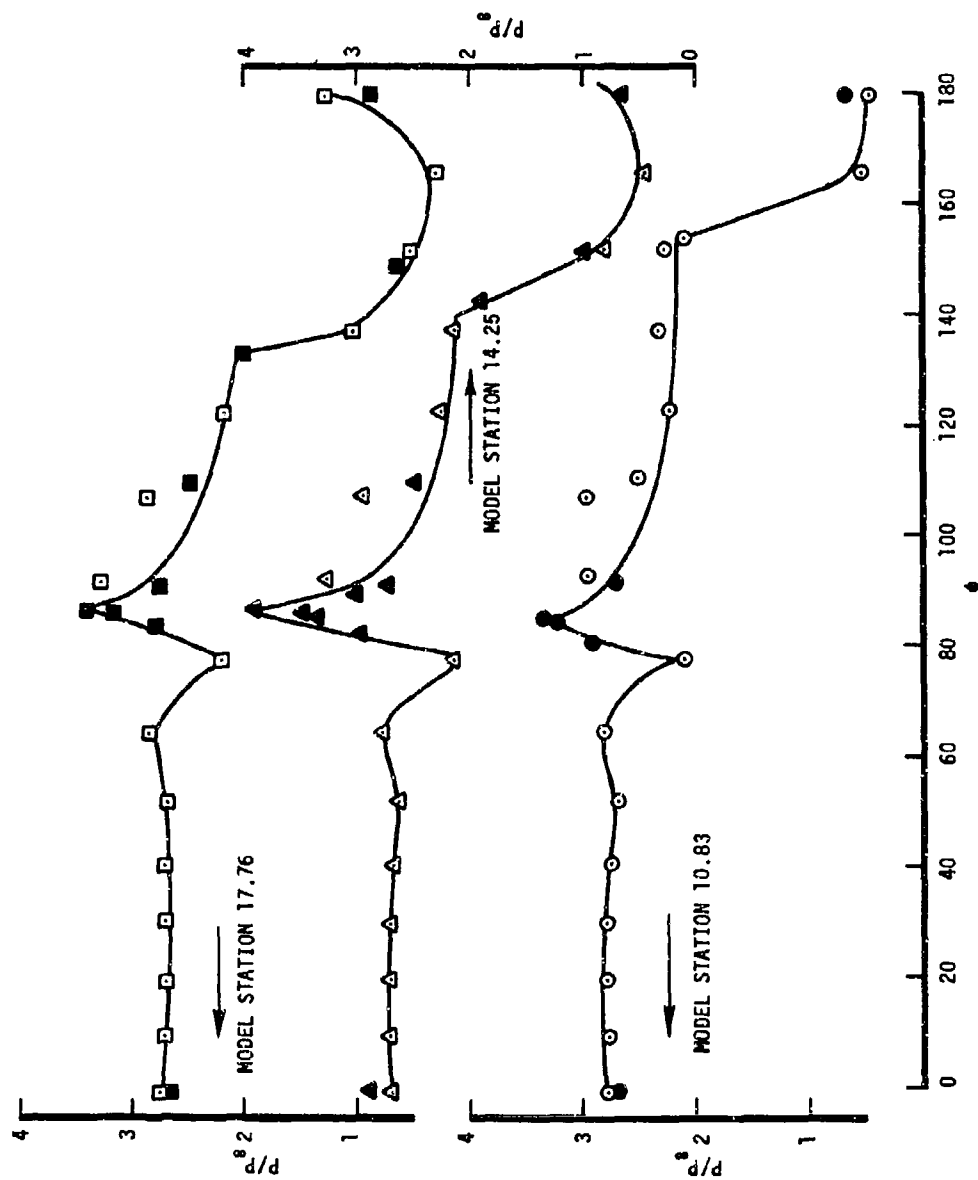


Figure 19. Continued

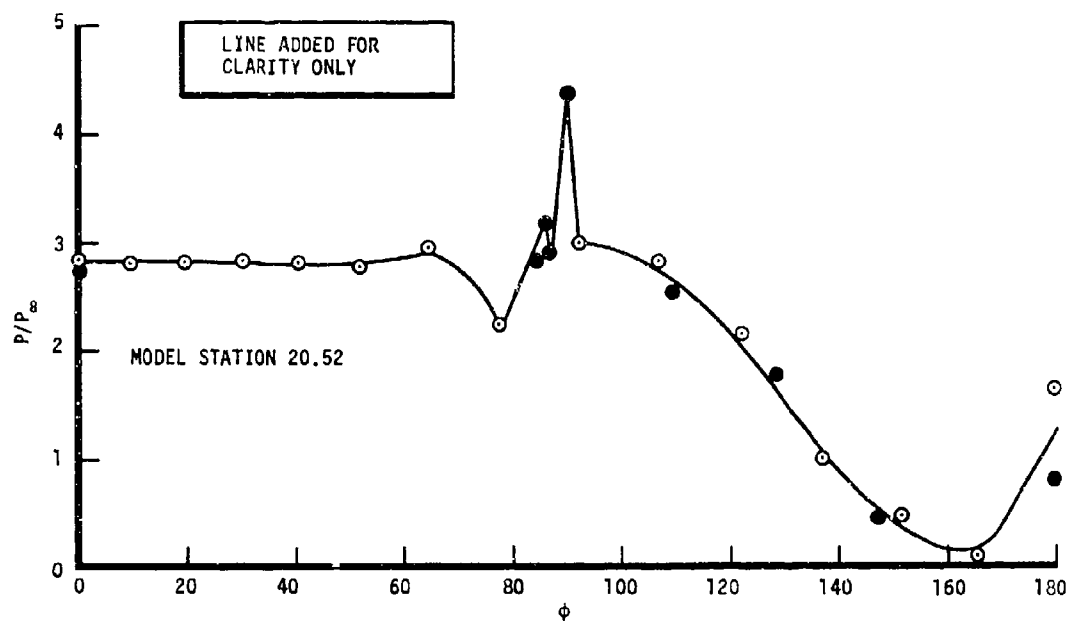


Figure 19. Concluded

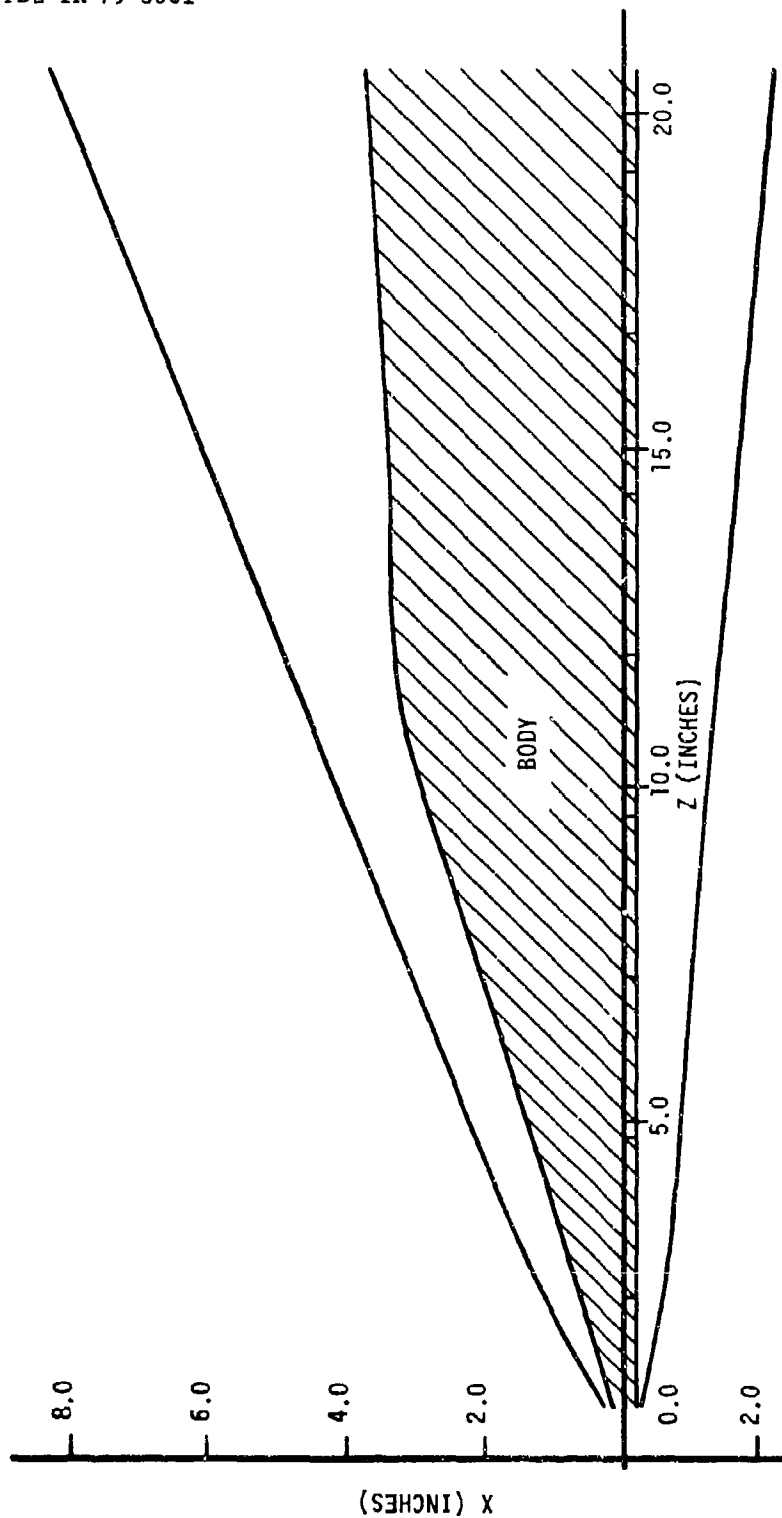


Figure 20. X24C-100 Inviscid Shock Location (Longitudinal Plane)

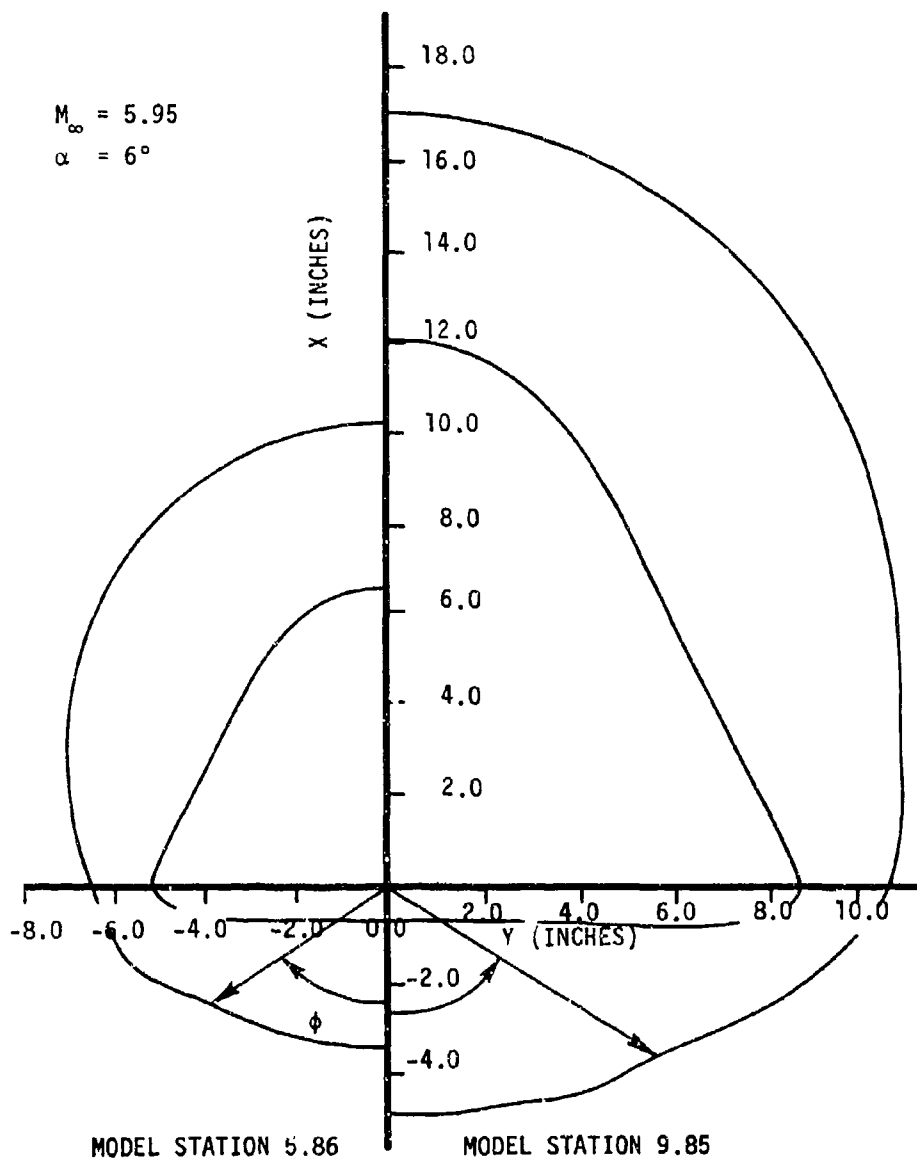


Figure 21. X24C-10D Inviscid Shock Location (Tangential Plane)

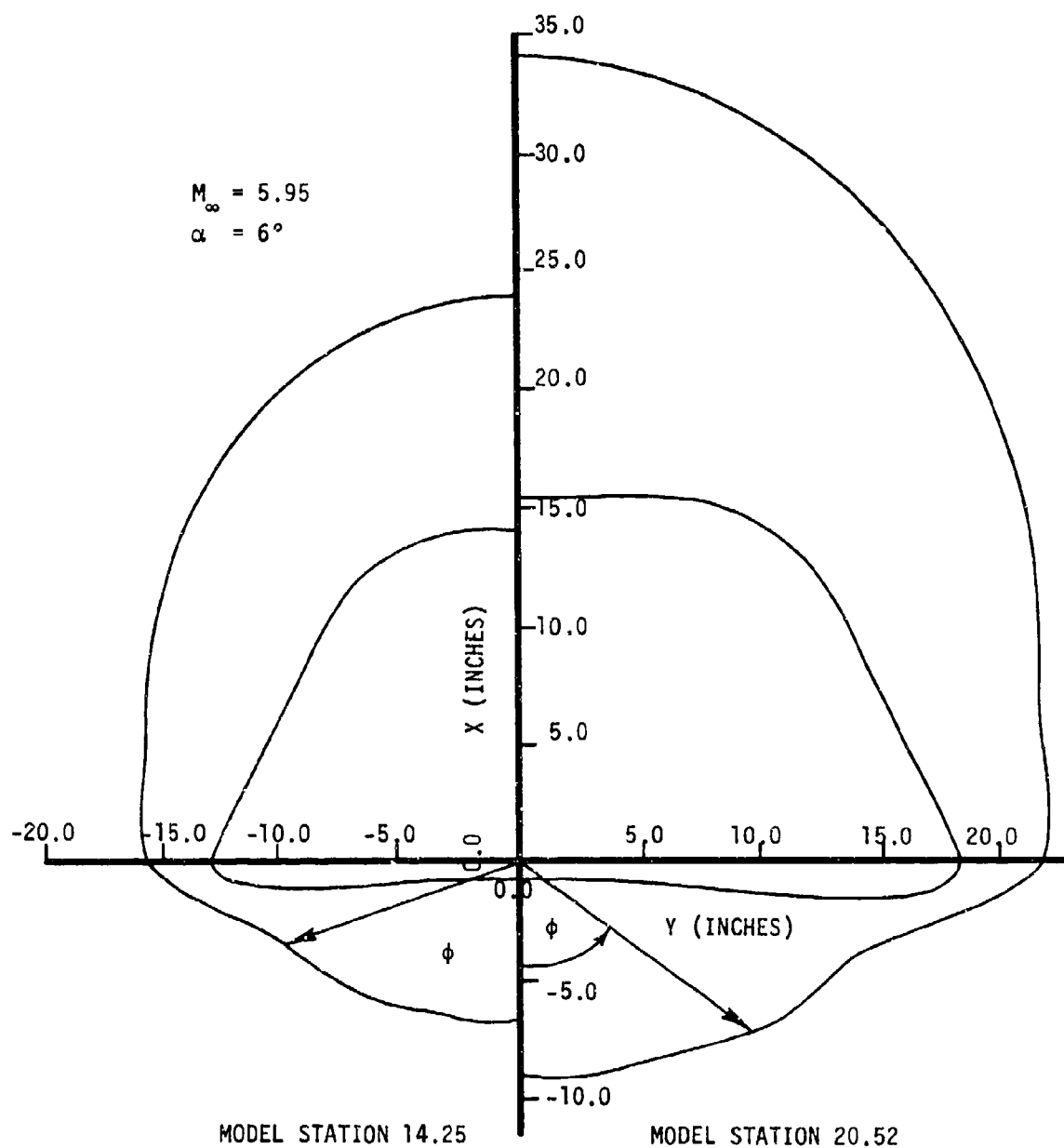


Figure 21. Concluded

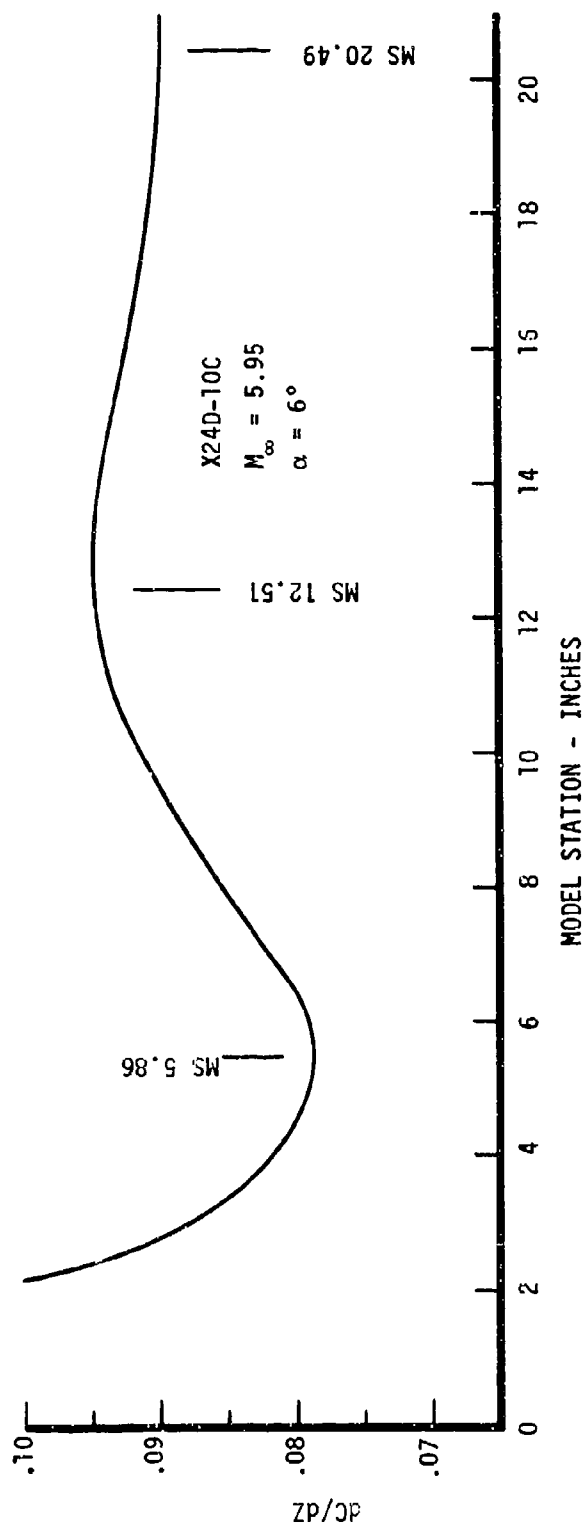


Figure 22. Longitudinal Slope of the Shock Wave at $\phi = 0^\circ$

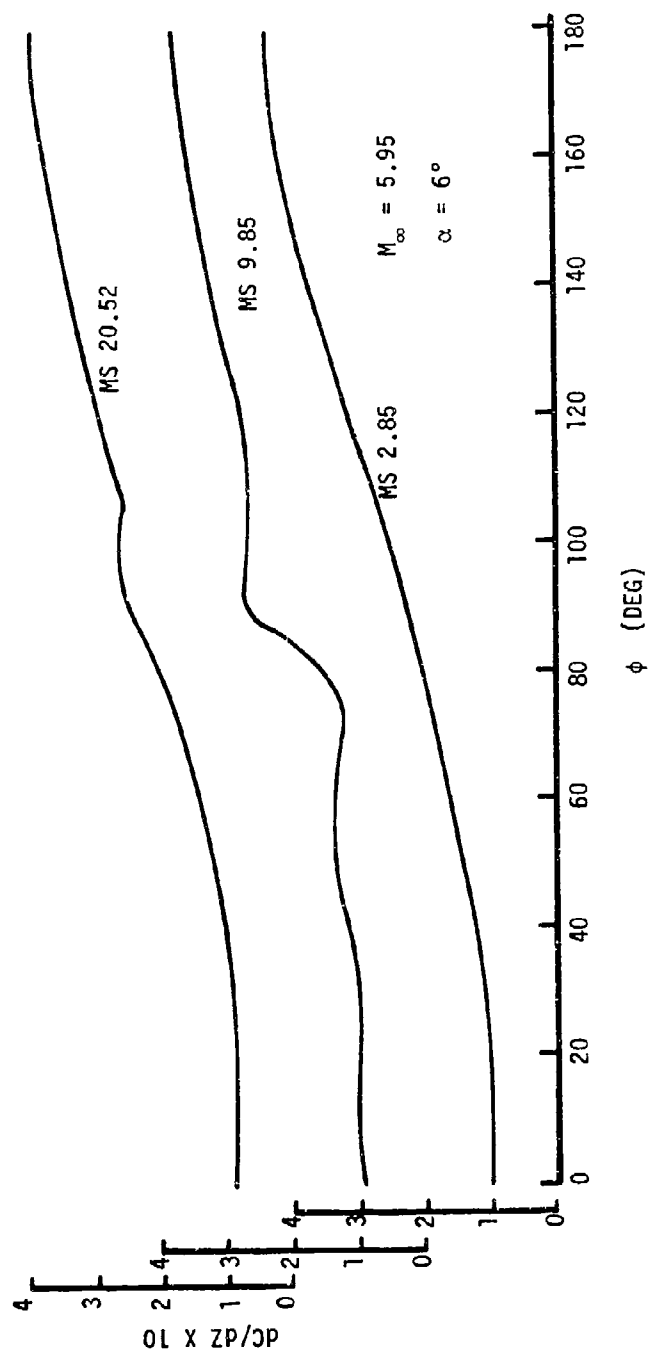


Figure 23. Angular Dependence of the Longitudinal Slope of the Shock at Three Body Stations

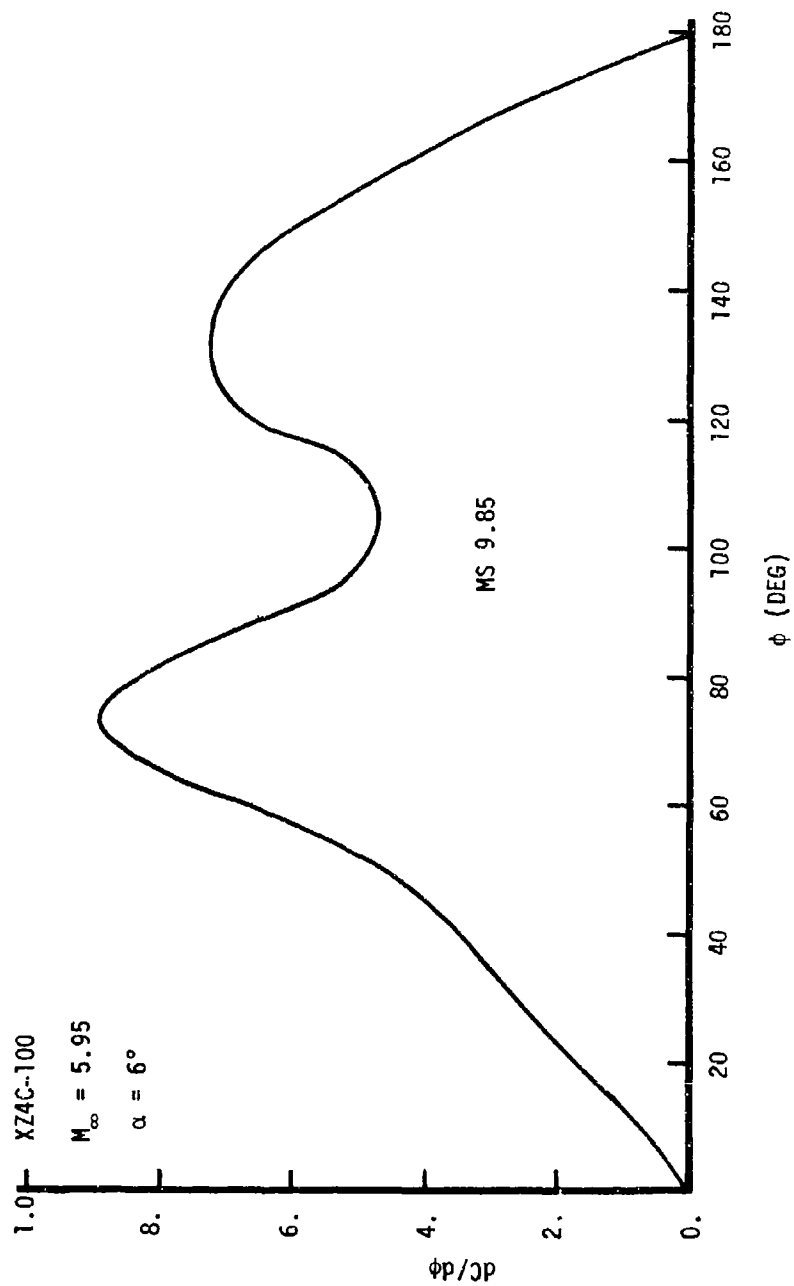


Figure 24. Tangential Slope of the Bow Shock

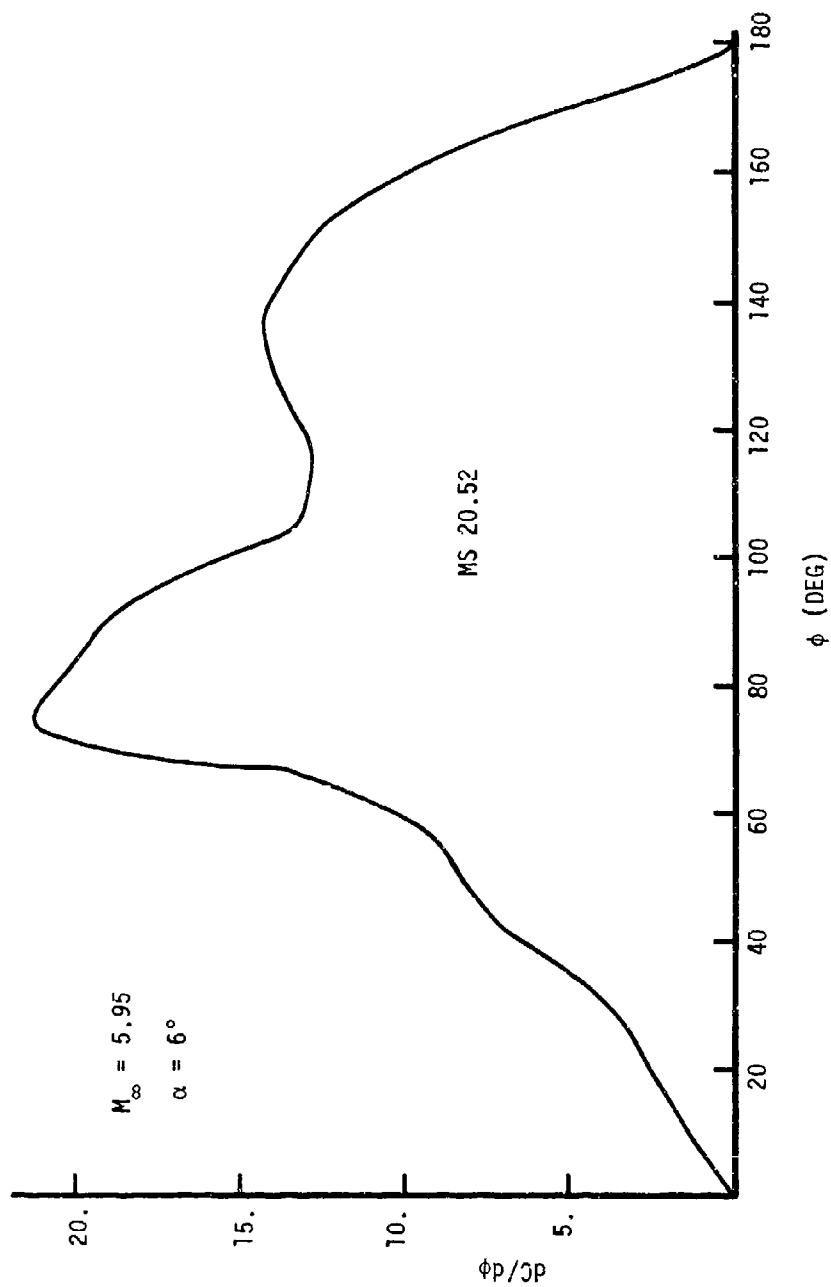


Figure 24. Concluded

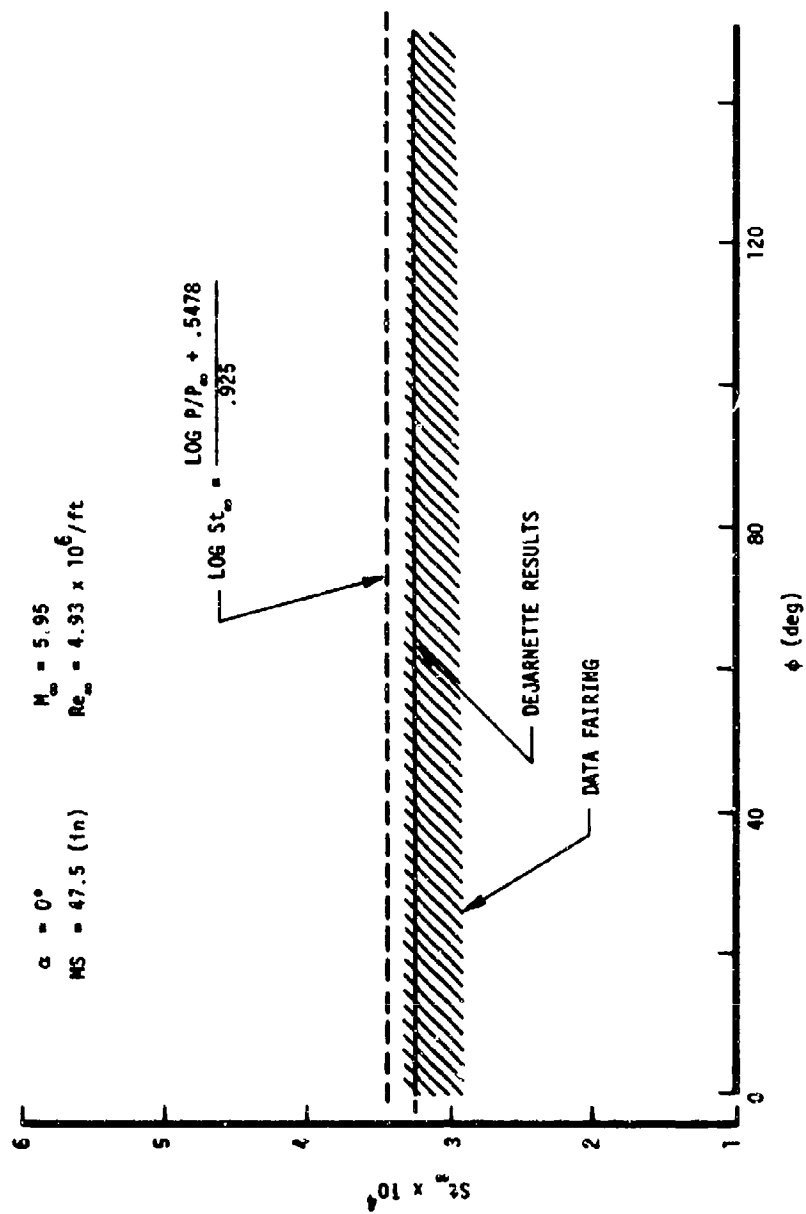


Figure 25. Comparison of Numerical and Experimental Station Numbers on the Ogive-Cylinder

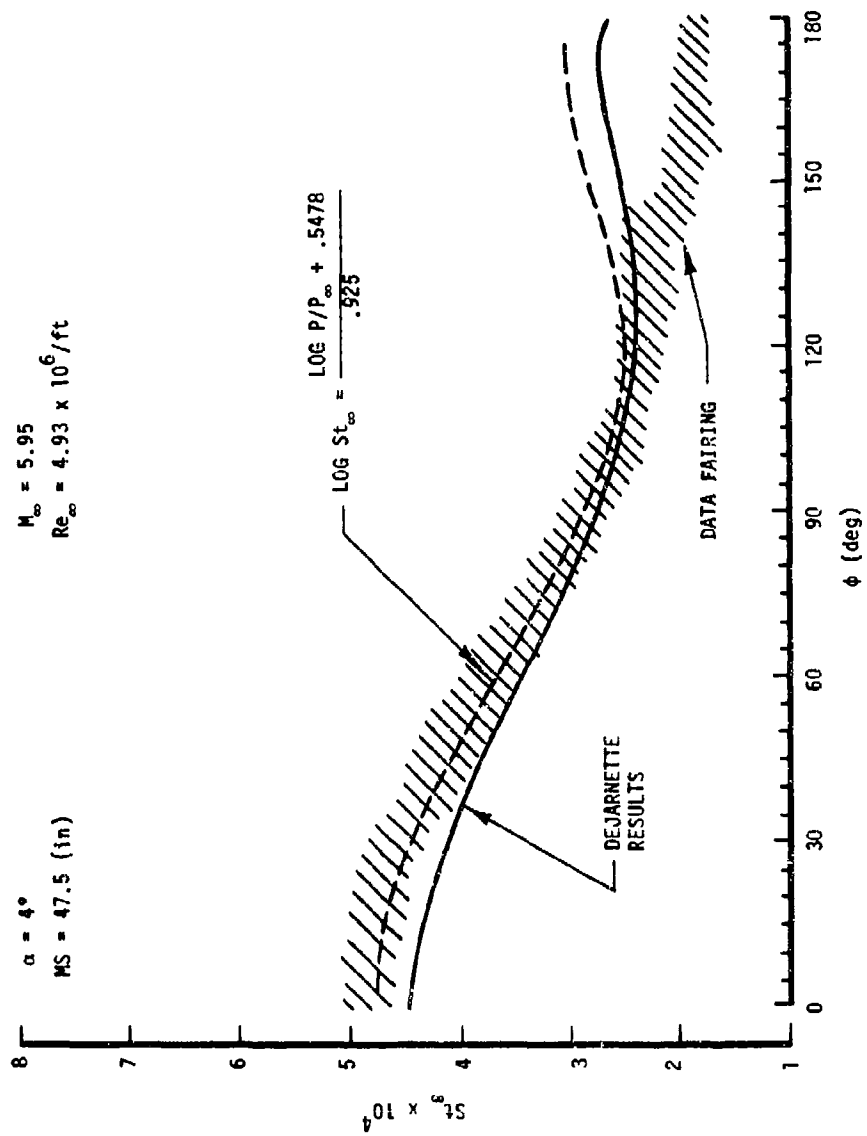


Figure 25. Continued

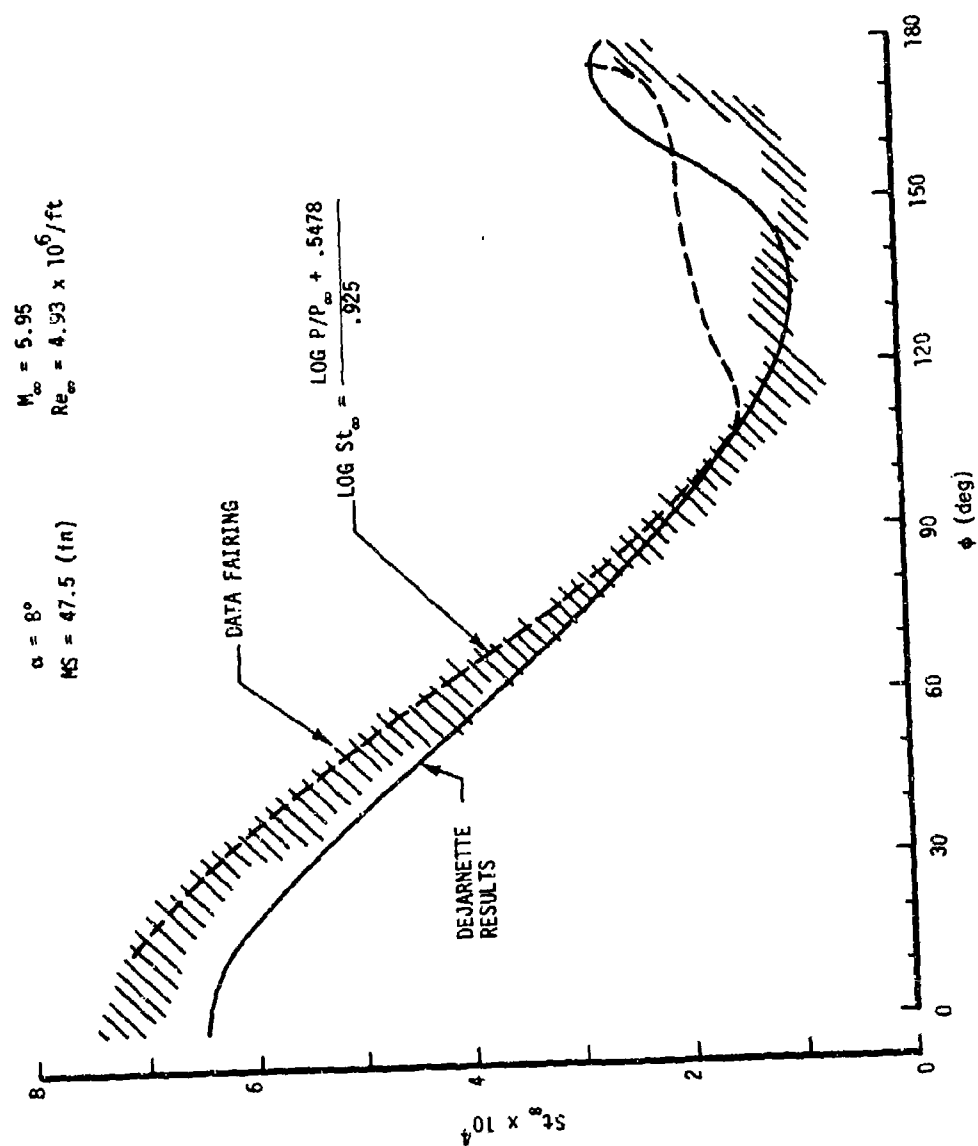


Figure 25. Continued

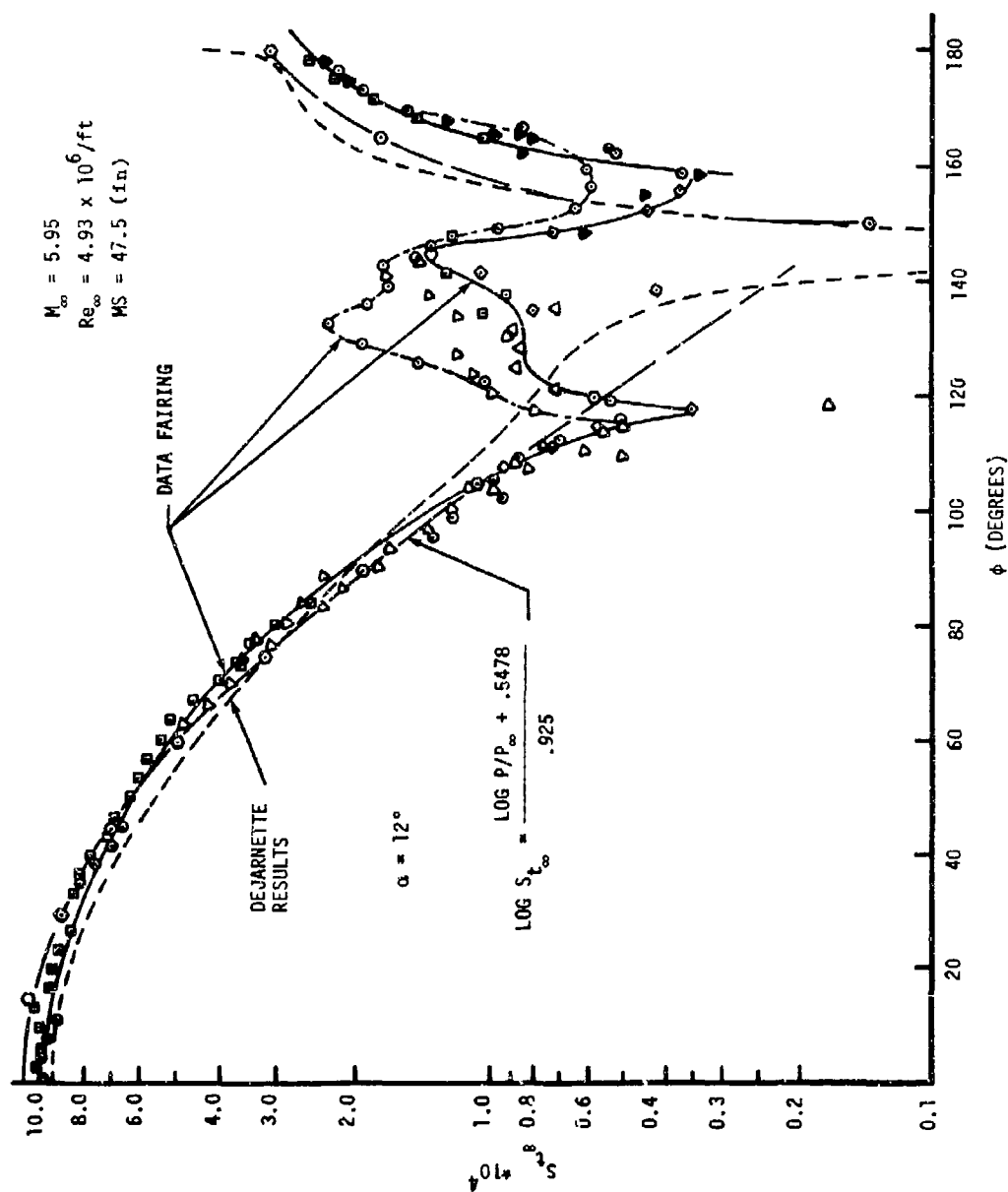


Figure 25. Concluded

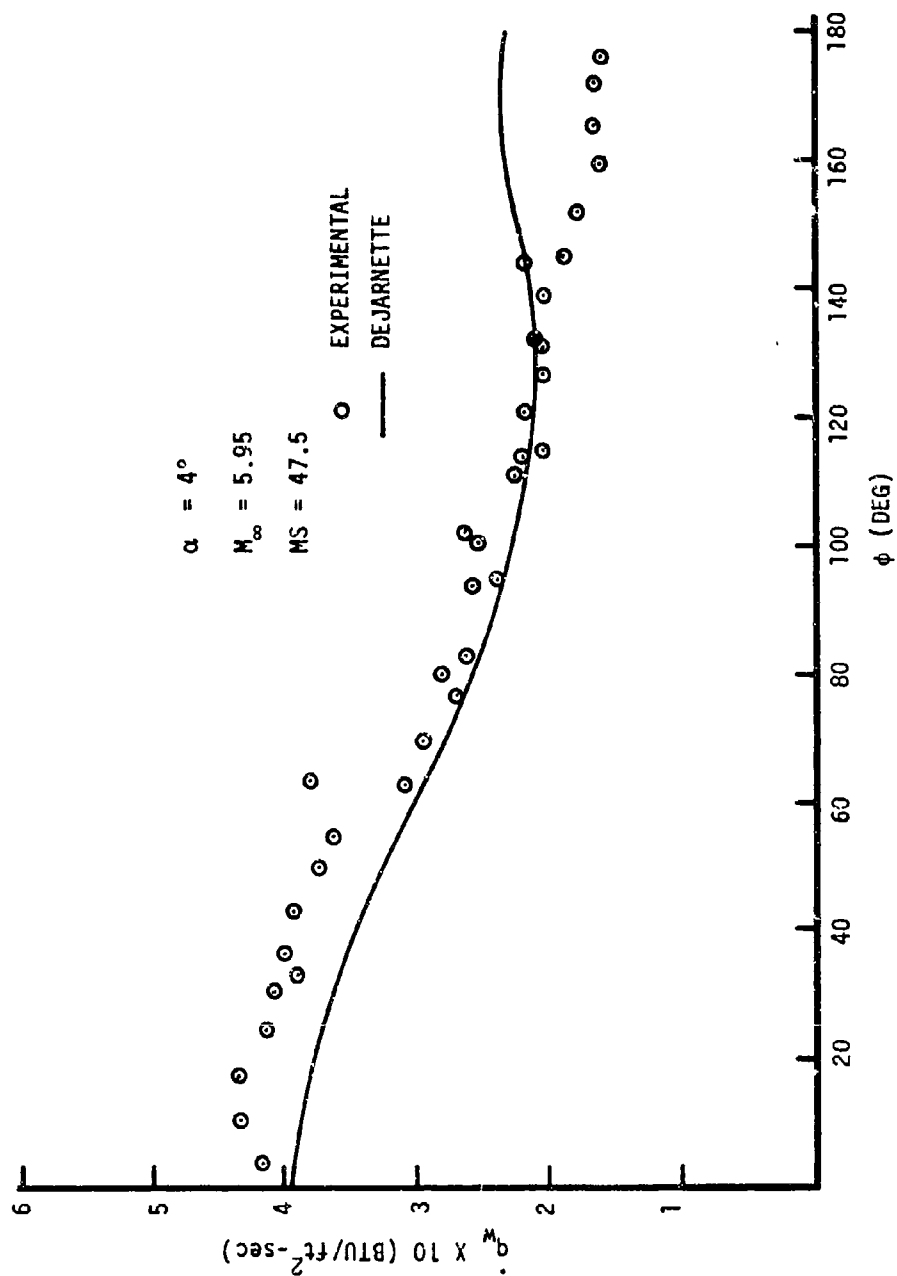


Figure 26. Comparison of Numerical and Experimental Heat Transfer to the Ogive-Cylinder

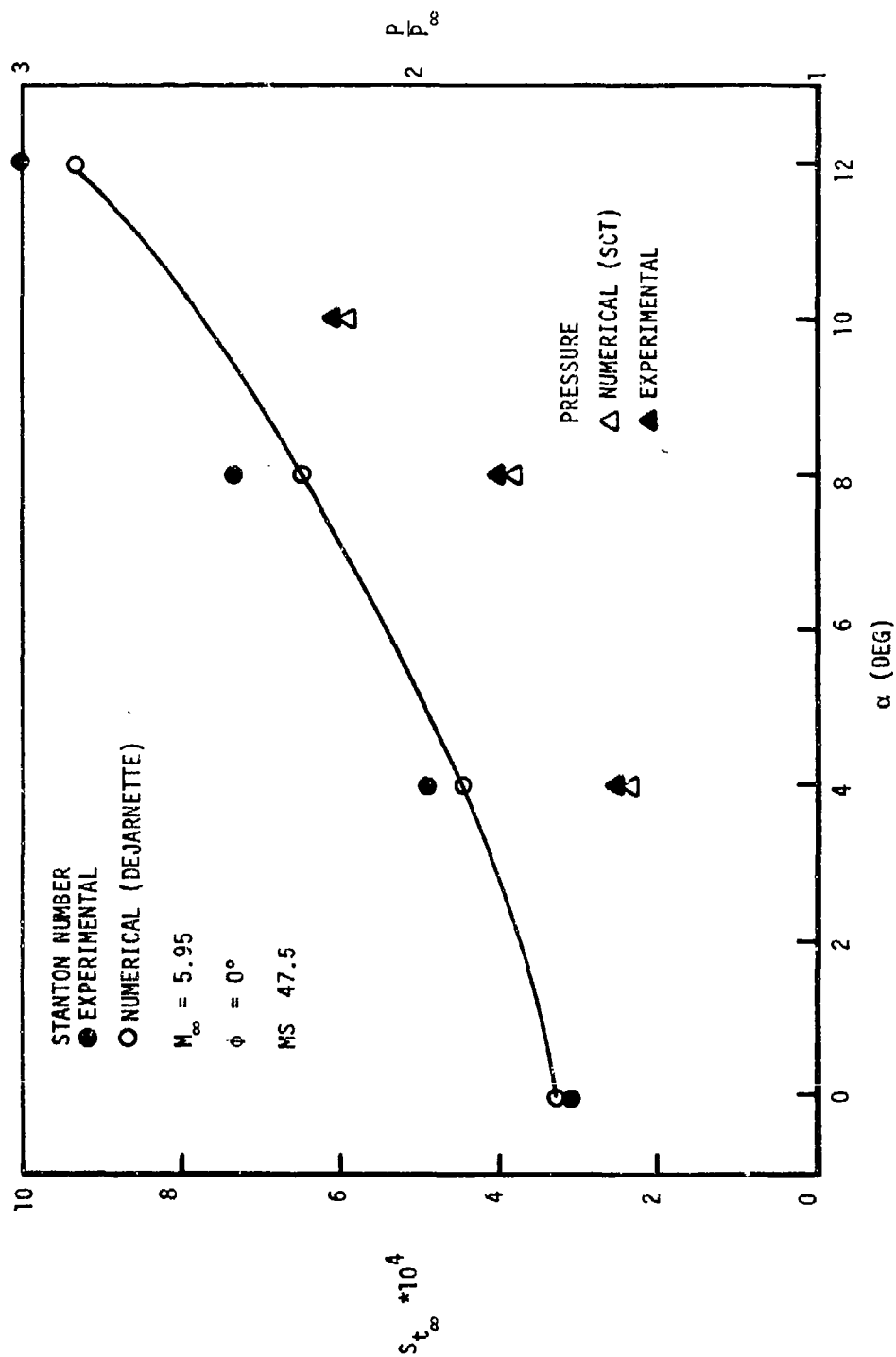


Figure 27. Comparison of Numerical and Experimental Pressures and Stanton Numbers on the Ogive-Cylinder as a Function of Angle of Attack

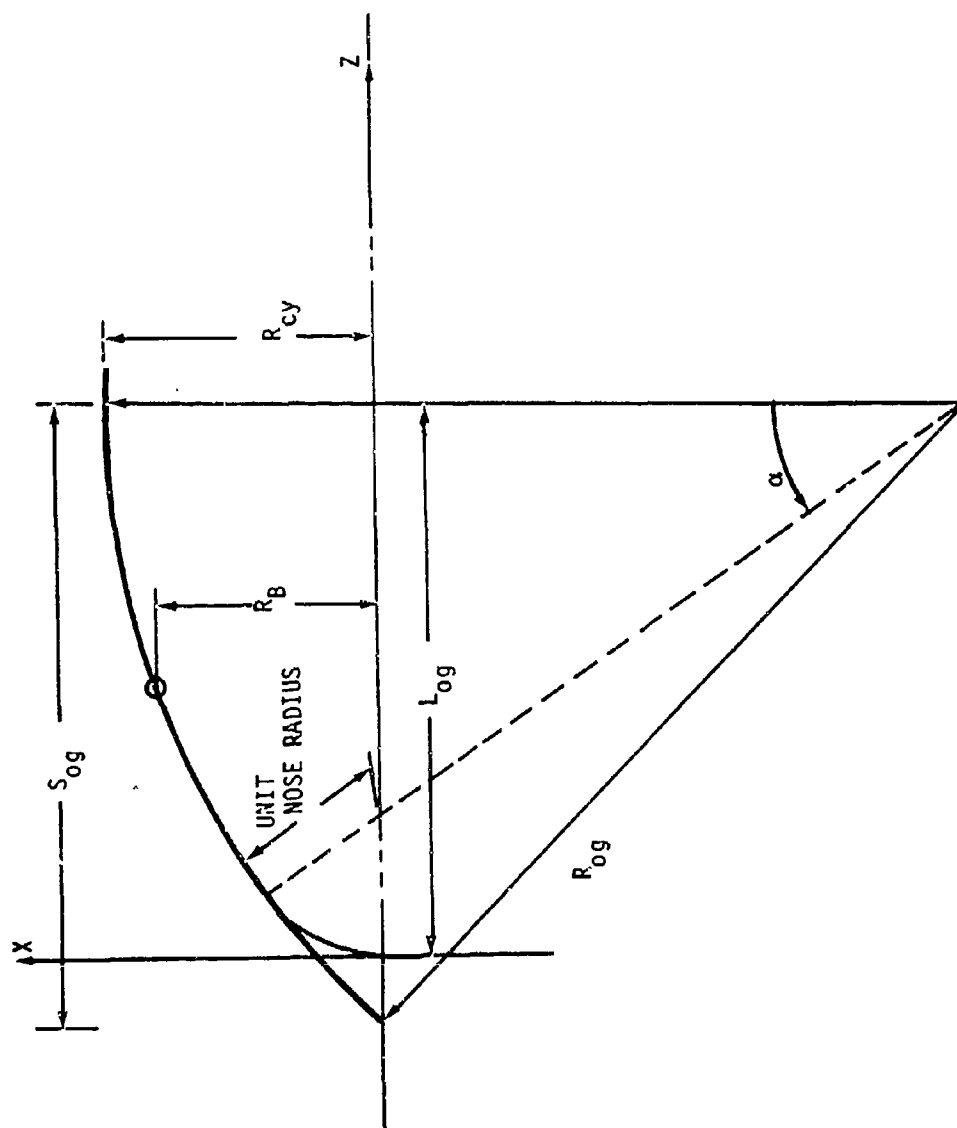


Figure A-1. Construction Used in the Calculation of the Ogive-Cylinder Geometry

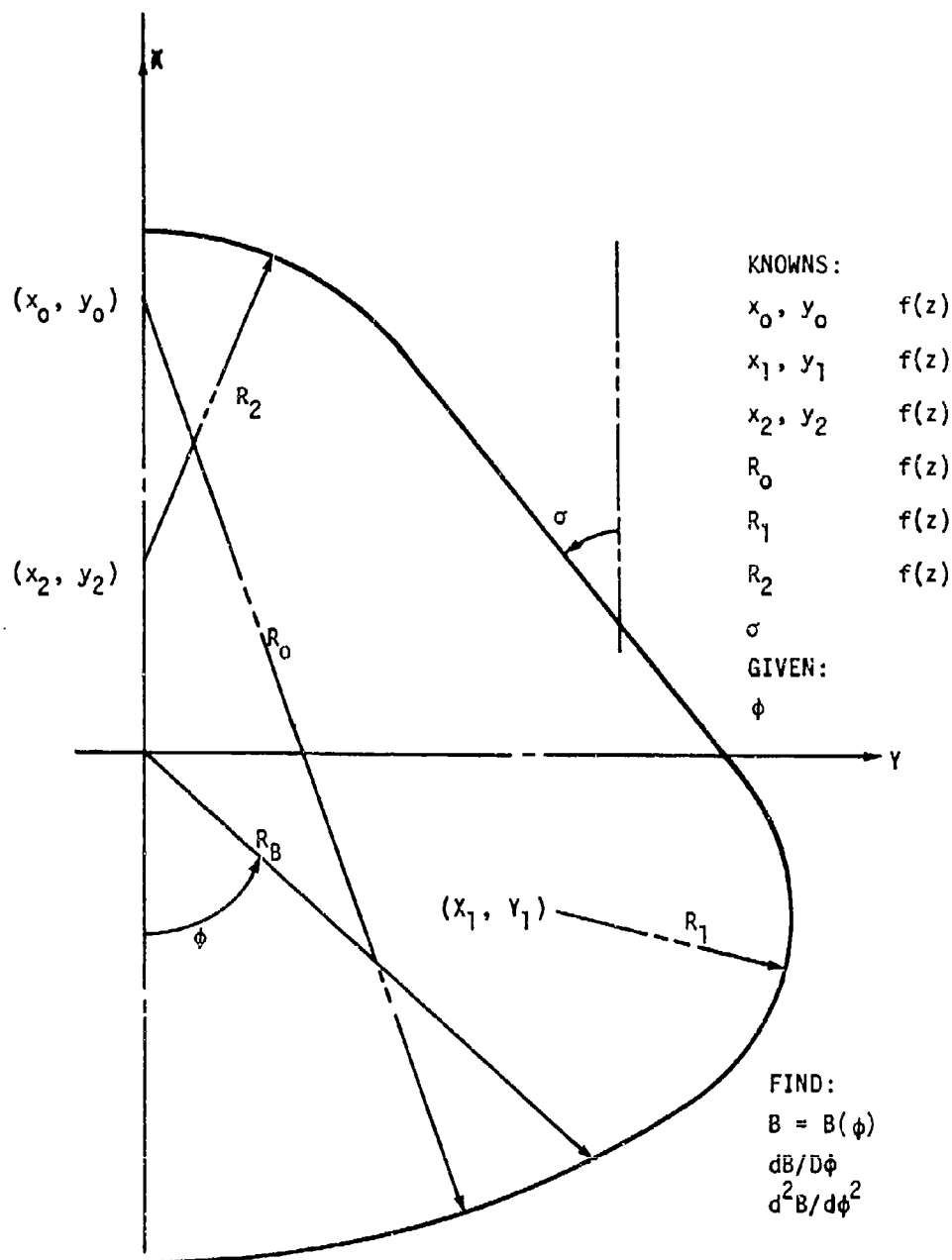


Figure B-1. Typical Cross Section of the X24C-10D

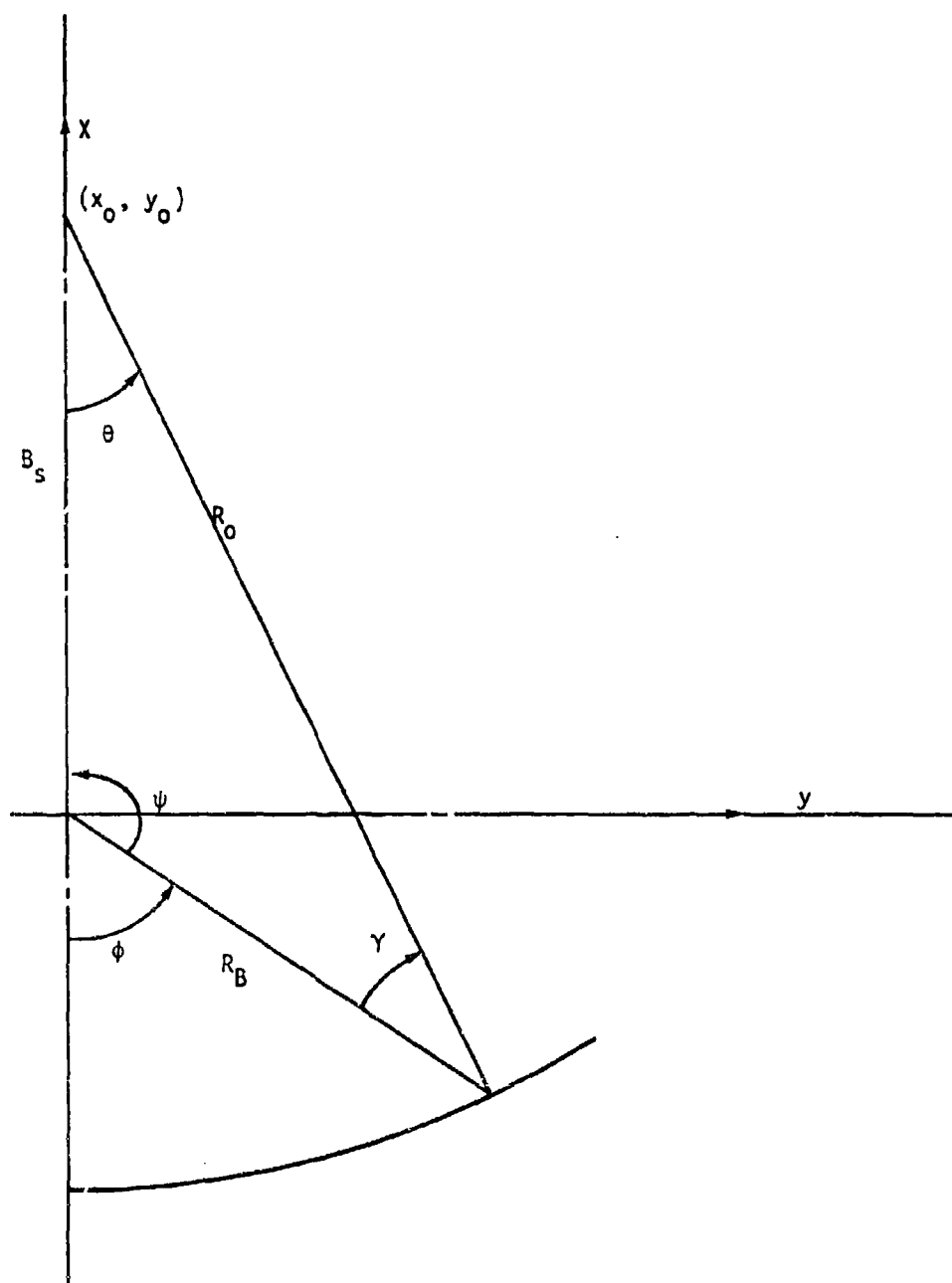


Figure B-2. Construction of the Body Radius for a Circular Bottom

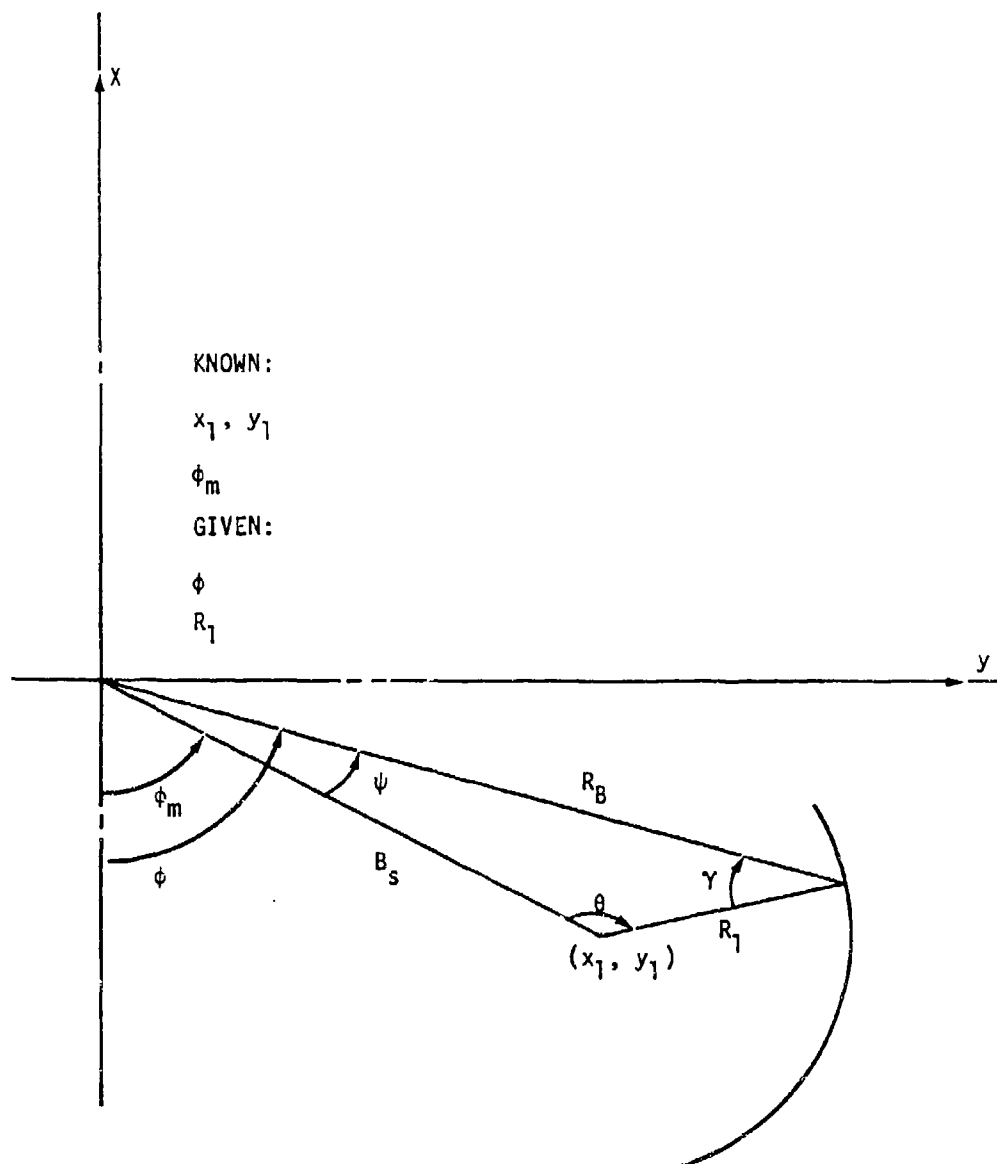


Figure B-3. Construction of the Body Radius for a General Circular Segment

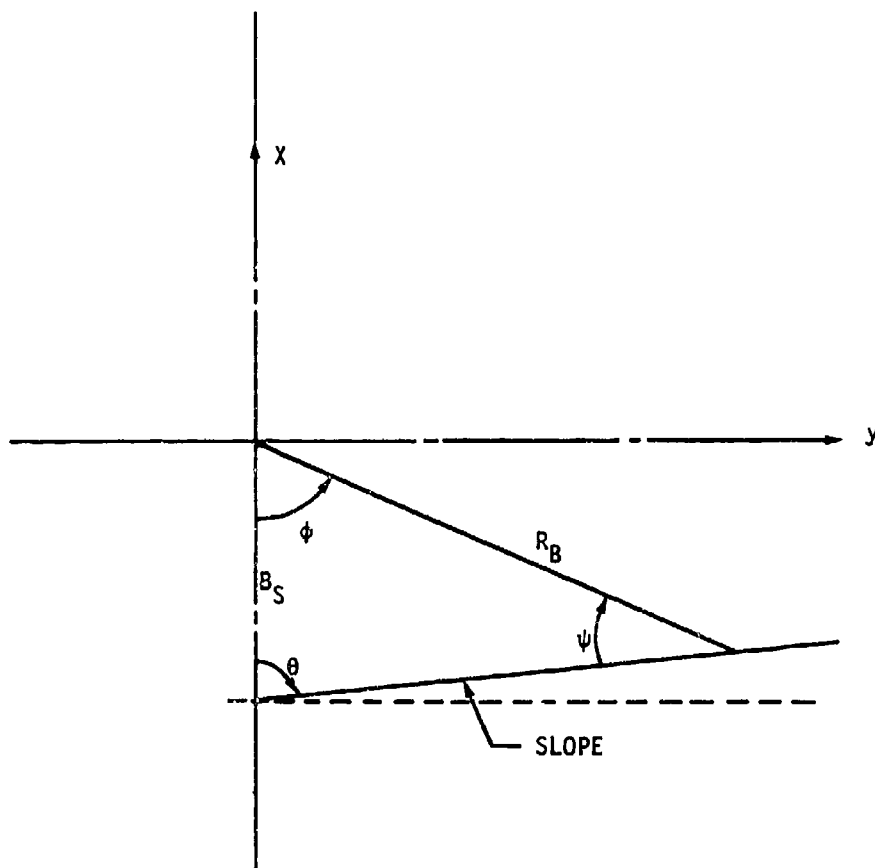


Figure B-4. Construction Used for a Straight Bottom Segment

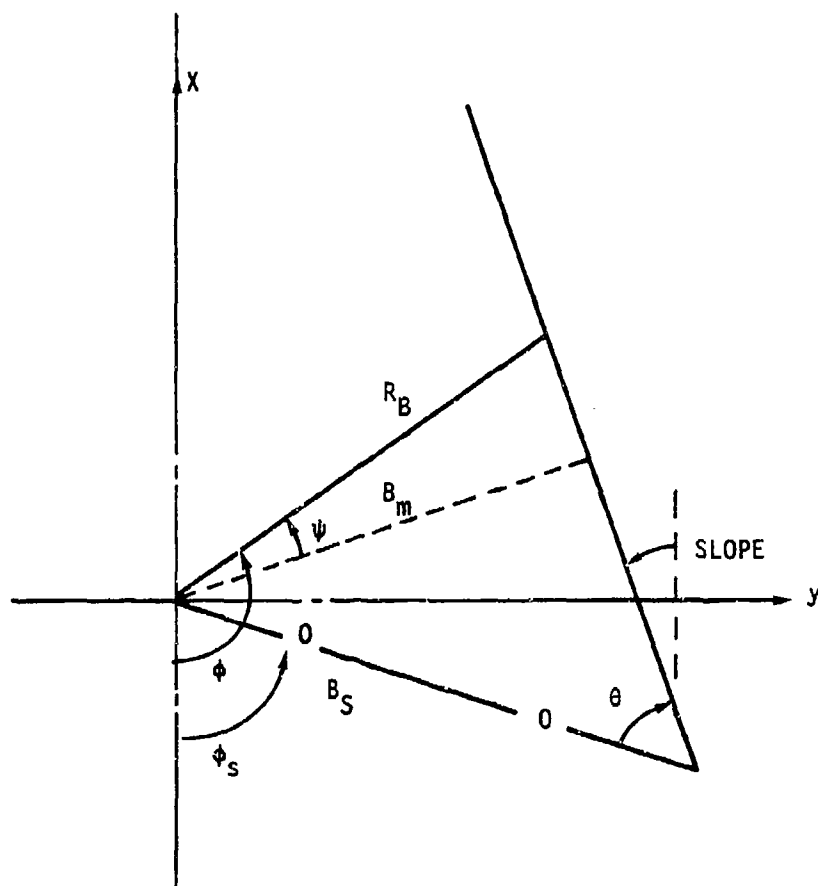


Figure B-5. Construction Used for a General Straight Segment